University of Alberta

Dynamic Modeling of the Periotest® Method

By

Demetrios Kostas Giannitsios

A thesis submitted to the Faculty of Graduate Studies and research in partial fulfillment of the requirements for the degree of Masters of Science.

Department of Mechanical Engineering
&
Department of Biomedical Engineering

Edmonton, Alberta

Spring 2001

National Library of Canada
Acquisitions and Bibliographic Services
395 Wellington Street
Ottawa ON K1A 0N4
Canada

Bibliothèque nationale du Canada
Acquisitions et services bibliographiques
395, rue Wellington
Ottawa ON K1A 0N4
Canada

Your file Votre référence

Our file Notre référence

The author has granted a non-exclusive licence allowing the National Library of Canada to reproduce, loan, distribute or sell copies of this thesis in microform, paper or electronic formats.

The author retains ownership of the copyright in this thesis. Neither the thesis nor substantial extracts from it may be printed or otherwise reproduced without the author's permission.

L'auteur a accordé une licence non exclusive permettant à la Bibliothèque nationale du Canada de reproduire, prêter, distribuer ou vendre des copies de cette thèse sous la forme de microfiche/film, de reproduction sur papier ou sur format électronique.

L'auteur conserve la propriété du droit d'auteur qui protège cette thèse. Ni la thèse ni des extraits substantiels de celle-ci ne doivent être imprimés ou autrement reproduits sans son autorisation.

0-612-60429-2

Canada

University of Alberta

Library Release Form

Name of Author:	**Demetrios Kostas Giannitsios**
Title of Thesis:	**Dynamic Modeling of the Periotest® Method**
Degree:	**Master of Science**
Year this Degree Granted:	**2001**

Permission is hereby granted to the University of Alberta Library to reproduce single copies of this thesis and to lend or sell such copies for private, scholarly or scientific research purposes only.

The author reserves all other publication rights in association with the copyright in the thesis, and except as herein before provided, neither the thesis nor any substantial portion thereof may be printed or otherwise reproduced in any material form whatever without the author's prior written permission.

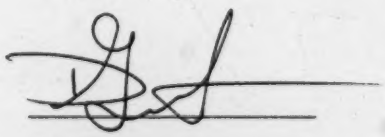

Demetrios Kostas Giannitsios
10 Adrian Place
St Albert, Alberta
T8N 2Z3

Date: January 26/2001

University of Alberta

Faculty of Graduate Studies and Research

The undersigned certify that they have read, and recommend to the Faculty of Graduate Studies and Research for acceptance, a thesis entitled **Dynamic Modeling of the Periotest® Method** submitted by **Demetrios Kostas Giannitsios** in partial fulfillment of the requirements for the degree of **Master of Science.**

Dr. M.G. Faulkner (Supervisor)

Dr. A.W. Lipsett (Co-Supervisor)

Dr. J. Wolfaardt (Co-Supervisor)

Dr. K. Fyfe

Dr. A. E. Elwi

Date: January 26/2001

Τής μητέρας μου τρελλές θεωρίες

καί του πατέρα μού κοινή λογίκη!

Abstract

The use of bone-anchored implants for prosthesis attachment has increased substantially since their introduction over 30 years ago. Unfortunately, little is know of the mechanism responsible for bonding implants to bone and as a result, more failures occur than are desired. A mechanical method known as the Periotest® has been used to assess the degree of bonding by determining the degree of mobility of these implants. Unfortunately, the results of many studies using this device have been controversial due to a lack of understanding of the parameters influencing the instrument.

Dynamic modeling of the mechanical interaction of the Periotest® and the implant system along with an in vitro and in vivo study were all aimed towards attaining a better understanding of these parameters.

What was found was that implant diameter, length of engagement between bone and implant, angulation of Periotest® handpiece, striking height all influenced the output of the Periotest®.

Acknowledgments

I am glad that I can say that the last 2 years (and 4 months) of my life have been my best. I owe a great deal of gratitude to many of the incredible people from the Mechanical Engineering Department, COMPRU and life long friends that have been a part of the scheme of things from the beginning of my studies. Some may have contributed directly towards my research, other to my well being and many to both. Regardless of the roll that they played, be it supervisor, instructor, technical aid, lab-mate, secretary, doctor, teacher, student, or teammate I am proud to consider them all my friends. As a wise old man (my father) once said, "A man is only as strong as the support he has from his family and friends". Thank you.

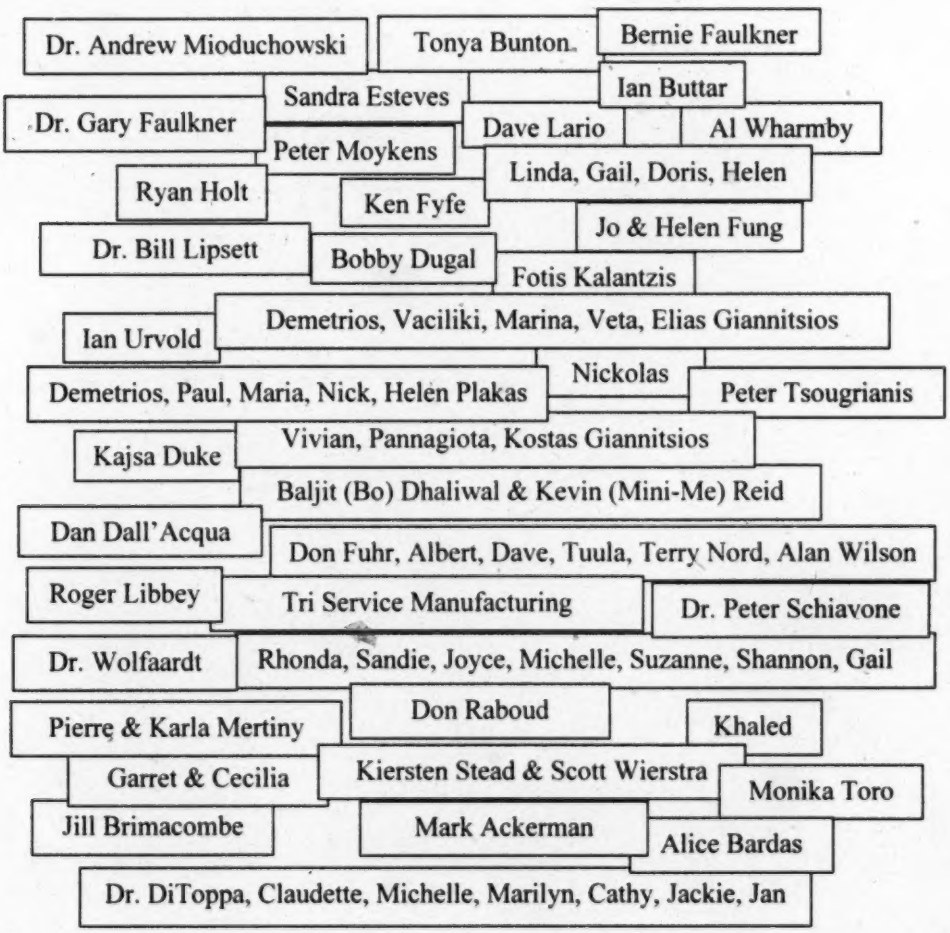

Contents

1 Introduction 1

1.1 Introduction 1

1.2 Periotest® 3
1.2.1 Classical Application 3
1.2.2 Endosseous Implant Application 5

1.3 Review of Literature 7
1.3.1 Parameters Effecting PTV 7
1.3.1.1 Implant Geometry 7
1.3.1.2 Bone Variables 8
1.3.1.3 Testing Procedure/Clinical Variables 11
1.3.2 Modeling of the Periotest® 12
1.3.3 Other Mechanical Methods 15
1.3.3.1 Impedance Head Hammer 15
1.3.3.2 Resonance Frequency Analysis 18

1.4 Outline of Thesis 20

2 Modeling of the Periotest®/Implant System 33

2.1 Introduction 33

2.2 Modeling Considerations 34
2.2.1 Interface Tissue 35
2.2.2 Implant System 36
2.2.3 Periotest® System 38
2.2.4 Datum Point 38

2.3 Free-Body Diagram vs Mass Acceleration Diagram 39

3 Testing Methods and Materials 53

3.1 Introduction 53

3.2 Materials and Methods 54
3.2.1 Periotest® Modified 54
3.2.2 Data Acquisition System 55
3.2.3 Testing Discs 57

3.2.4 Testing Apparatus 58
3.2.5 Testing 60
3.2.6 Strain Gauged Abutment 60
3.2.7 *In Vivo* Testing 61

3.3 Results 62

4 Results & Discussion 71

4.1 Strain Gauge Results 72
4.1.1 Contact Time Validation 72
4.1.2 Damping Behaviour of FRB-10 72

4.2 *In Vitro* Testing Results 73

4.3 Validation of the Dynamic Model using *In Vitro* Testing 74
4.3.1 The *In Vitro* Theoretical Model 74
4.3.2 Discussion of Supporting Tissue Quality 75
4.3.2.1 Sensitivity to Supporting Tissue Type /Stiffness 75
4.3.2.2 Sensitivity to Supporting Tissue Length of Engagement 76

4.3.3 Sensitivity to Implant Diameter 78
4.3.4 Discussion of Testing Protocol 79
4.3.4.1 Sensitivity to Striking Height 79
4.3.4.2 Sensitivity to Handpiece Angulation 79
4.3.4.3 Comparing Kaneko's Rotational Model (1994) with *In Vitro* Data 80

4.4 Periotest® Calibration and Resolution 81
4.4.1 Calibration 81
4.4.2 Resolution of the Periotest® 82

4.5 *In Vivo* Results 83

5 Conclusions 97

5.1 Summary 97

5.2 Future Considerations 99
5.2.1 Model with Multi-Layered Supporting Tissue 99
5.2.2 Calibration Device 100
5.2.3 Increase the Precision of the Periotest® Output 101

5.2.4 Investigating of the Damping of Bone *In Vivo* 101
5.2.5 Assessment of Bone Height During Surgery or CT Scan 101

References **103**

Appendices

A Analytical Model of the Periotest method **107**
B *In Vivo* Data **118**
C Clinical Protocol for Periotest® Testing **130**

List of Tables

1-1	Range of Implant Fequencies due to Interface Bone	17
2-1	Material Properties	37
4-1	The Relationship Between Contact Time, Periotest® Value and Degrees of Mobility	82

List of Figures

1-1	Schematic Diagram of the Periotest® Device	21
1-2	Degrees of Mobility Determined from the Periotest® Deceleration Signal	22
1-3	Illustration of the Physical Interaction Between the Periotest® (PT) and the Implant System (IS)	23
1-4	Geometric Similarities Between Intraoral Implants and Teeth	24
1-5	Mandible Cross-section	24
1-6	Single Degree of Freedom Model of Periotest®/Implant System with No Viscous Damping (Modified from Kaneko 1993)	25
1-7	Single Degree of Freedom Model of Periotest®/Implant System with Viscous Damping (Modified from Kaneko 1993)	25
1-8	Rotational Single Degree of Freedom Model of Periotest®/Implant System with No Viscous Damping (Modified from Kaneko 1994)	26
1-9	Impedance Head Hammer (Modified from Elias et al. 1996)	27
1-10	Theoretical Force Curve for an Impedance Head Hammer Dynamic Test (Modified from Elias et al. 1996)	28
1-11	Typical Force Curve from a Lateral Impact with the Impedance Head hammer (Modified from Elias et al. 1996)	29
1-12	Schematic of Resonance Frequency Analysis Transducer (Modified from Meredith 1997)	30
1-13	Schematic of Resonance Frequency Analysis Transducer and Response Curve	31
1-14	The Relative Size of the Resonance Frequency Analysis Transducer Compared with the Oral Cavity for Intraoral Testing	32
2-1	Schematic of Periotest® and Implant System	46
2-2	Proposed Mathematical Model of Periotest® and Implant System	47
2-3	Typical 4mm Brånemark Flanged Implant Detail	48
2-4	Typical 5.5mm Brånemark Abutment	49
2-5	Typical Brånemark Abutment Screw	50
2-6	a) Free Body Diagram and b) Mass-Acceleration Diagram	51
2-7	Generalized Co-ordinates of the System	52
3-1	Periotest® Modification for Data Acquisition System Connection	63
3-2	Periotest® Accelerometer Signal Displayed	63
3-3	Typical Periotest® Accelerometer Signal	64
3-4	Machine Drawing of the *In Vitro* Testing Discs	65
3-5	*In Vitro* Testing Discs	66
3-6	*In Vitro* Testing Equipment	67

3-7	Cathetometer	68
3-8	Strain Gauged 10mm Abutment	69
3-9	Surgical Location for BAHA® Implant Placement	70
4-1	Comparison of the Periotest® Accelerometer Signal with the Strain Gauged Abutment Signal	85
4-2	Numerical Modeling and the *In Vitro* Results	86
4-3	The Numerical Model Predicting the PTV Response for a Doubling of the Supporting Tissue Stiffness for an Implant with 3.83mm of Anchorage	87
4-4	The Numerical Model Predicting the PTV Response due to a Change in the Ratio of Vertical to Horizontal Supporting Tissue Stiffness for an Implant with 3.83mm of Anchorage	88
4-5	The Numerical Model Predicting the PTV Response for Longer Tissue/Implant Engagement Levels	89
4-6	Change in Length of Tissue/Implant Engagement and Striking Height due to Marginal Loss of Supporting Tissue	90
4-7	The Numerical Model Predicting the PTV Response for a 0.5mm Marginal Loss of Supporting Tissue	91
4-8	The Numerical Model Predicting the PTV Response for Both 3.75mm and 5mm Diameter Implants with an Anchorage Length of 2.78mm	92
4-9	Effect of Angulation of the Periotest® on Striking Height	93
4-10	*In Vitro* Testing Results Compared with the Rotational Kaneko Model (1994)	94
4-11	Comparison of the Standard Periotest® Output with the Digitally Acquired Periotest® Output	95
4-12	*In Vivo* Testing Data for Patient # 00895	96
A-1	a) Free Body Diagram and b) Mass Acceleration Diagram	116
A-2	Deflection of the System for Determining the Force in the Vertical Springs	117
B-1	*In Vivo* Testing Data for Patient #00845	119
B-2	*In Vivo* Testing Data for Patient #00874	120
B-3	*In Vivo* Testing Data for Patient #00895	121
B-4	*In Vivo* Testing Data for Patient #00896	122
B-5	*In Vivo* Testing Data for Patient #00897	123
B-6	*In Vivo* Testing Data for Patient #00909	124
B-7	*In Vivo* Testing Data for Patient #00913	125
B-8	*In Vivo* Testing Data for Patient #00914	126
B-9	*In Vivo* Testing Data for Patient #00927	127
B-10	*In Vivo* Testing Data for Patient #00930	128
B-11	*In Vivo* Testing Data for Patient #00931	129

Chapter 1

Introduction

1.1 Introduction

The use of bone-anchored (endosseous) implants has revolutionized the development of prostheses both within the oral cavity as well as for craniofacial applications. Within the mouth, implants provide a stable foundation for individual and multiple tooth replacements while extraoral implants are used to help individuals with facial defects regain quality of life. In the latter case they can have a tremendously positive effect upon an individual suffering from some form of facial trauma requiring a prosthetic appliance. Aside from the potentially beneficial psychological effects, an endosseous implant system is a structurally superior system providing a stable support for prosthesis retention. This mechanical enhancement alleviates concern that the patient

might have of an untimely failure of retention of the prosthesis. In addition, the prosthesis can be constructed with enhanced esthetic features such as having very fine edges that allow it to blend into the surrounding natural tissue. This is a major advancement over a thick edged prosthesis, which were typically anchored to a set of eyeglasses or with skin adhesives. While success rates of craniofacial implants are high, (up to 97.5% and 94.5% for nonirradiated and irradiated patients, Wolfaardt et al. 1993), the potential for implant failure still exists. The occurrence of these failures can be as early as 3-4 months post-operatively due to factors such as tissue overheating from high speed drilling/tapping (Wilkes and Wolfaardt 1998), and poor initial stability or even bacterial infection (Nishimura et al. 1997). As a result, a method is required for clinically assessing the implant-bone interface. It is at the interface where structural and functional bonding of living ordered bone to the endosseous implant, termed osseointegration, (Brånemark et al. 1985) occurs.

Unfortunately the mechanisms of osseointegration are still not completely understood (Meredith et al. 1998). To this end, various non-mechanical methods such as radiography have been implemented in hopes of developing a better understanding of the mechanism of osseointegration. However, information from imaging by high quality radiographs is considered to be of limited value, costly and carry the risk of radiation exposure (van Steenberghe and Quirynen 1993). An alternative is the implementation of mechanical methods such as the Resonance Frequency Analysis (RFA)(Meredith 1997), the Impedance Head Hammer (IHH)(Elias et al. 1996), and the Periotest® (Siemens AG, Bensheim, Germany 1983) to assess the mobility of implants and thereby develop a

correlation to the degree of osseointegration. These methods, which are discussed in detail below, all use a dynamic mechanical technique to assess the bond while at the same time being noninvasive, relatively rapid, and relatively inexpensive. The most widely used of these, the Periotest®, has led to controversial findings by many authors and as a result the device has been considered unreliable. Ultimately, the aim of this thesis is to provide a solid theoretical model of the Periotest® dynamics, which will provide a better understanding of how the Periotest® responds to variations in the geometric and clinical parameters. This model is applied to both experimental *in vitro* and *in vivo* situations.

1.2 Periotest®

1.2.1 Classical Application

The Periotest® was originally designed to assess the health of the periodontal ligaments of natural teeth through measurements of their dynamic mobility. It is a self-contained unit consisting of a stainless steel handpiece connected to a microcomputer (Figure 1-1). The handpiece contains an impacting rod with mass of 8.4 grams (Kaneko 1993), supported on low friction bearings, with a small accelerometer attached to the non-contact end. Two induction coils are incased within the handpiece. One coil acts as a propulsion coil and the second as the measuring coil. Depressing the button on the handpiece accelerates the impact rod towards the target while the internal measuring coil restricts the rod to travel at a constant speed of 0.2m/s. A single test requires 4 seconds

and during this time, a total of 16 impacts will occur between the rod and the target. The rod will deliver an average load of 15N per test (Teerlinck et al. 1991) however, the magnitude has been found to vary depending upon the resistance/stiffness of the system. The accelerometer signal, processed by a microcomputer unit which performs signal amplification and conditioning, determines a contact time and finally outputs an integer value known as a Periotest® value (PTV) within the range of -8 to 50PTV. Figure 1-2 shows various Periotest® signals for different degrees of tooth mobility. As the mobility of the tooth increases, the contact time will also increase, which corresponds to an increase in PTV.

A closer look at a typical accelerometer signal is shown in Figure 1-3 illustrating the corresponding physical interaction of the Periotest® and implant system. It is important to note that the duration of the impact is in the order of a tenth of a millisecond. The contact time (CT) is the portion of the curve where the Periotest® rod is decelerating due to the resistance of the implant system. Point A (Figure 1-3A) is the point of initial contact (zero displacement and acceleration, but maximum velocity of V the constant velocity of the Periotest®), Point B (Figure 1-3B) is the point where the acceleration of the system is at a maximum and the velocity is zero. This corresponds to a position of maximum deflection. The system then begins returning to the undeformed state (Point C) (Figure 1-3C), while all the time the system is in a state of deceleration. Once at Point C, the Periotest® rod separates from the implant system and is retracted by the handpiece (portion D) (Figure 1-3D). Portion D of Figure 1-3 illustrates how the internal propulsion

system acts as an electronic brake by bringing the acceleration of the impacting rod to zero to prepare for the next strike.

The PTV is a function (Equation 1.1) of the contact time, CT (Lukas and Schulte 1990):

$$PTV = 50 * CT - 21.3 \tag{1.1}$$

where the contact time is in milliseconds. Equation (1.1) is linear and is to be used for PTVs from –8 to +13. For PTV > 13, the relationship between PTV and CT is nonlinear and is

$$PTV = 10\left[\sqrt{\left(\frac{CT}{0.06ms} - 8.493\right)}\right] - 4.17. \tag{1.2}$$

1.2.2 Endosseous Implant Application

While originally developed to assess the mobility of natural dentition, more recently, the Periotest® has been used as a means for determining the state of health of the bone/implant interface for both intra- and extraoral implants. This application has produced varied results with some authors referring to the Periotest® as a diagnostic tool that lacks sensitivity or resolution and thus are distrustful of it, while others consider it a

viable tool for this application. This is in contrast to the use of the Periotest® to detect natural tooth mobility where confidence in the technique is high.

The application of the Periotest® for assessment of implant mobility has shown potential in studies by Olivé and Aparicio (1990), Haas et al. (1995), Cranin et al. (1998), and Drago (2000). Of the implants studied, the oral implants seemed to be the most logical considering the geometric similarities such as root lengths and supra-alveolar lengths they share with the natural teeth that they replace (Figure 1-4). Unfortunately, bonding of implants to bone is not accomplished by the same supporting mechanism that connects teeth to the alveolar process. Teeth are connected to bone via periodontal ligaments whereas implants bond to bone by osseointegration. As a result, there is a difference between the Periotest® response for both cases. Natural teeth have Periotest® values in the 0 to +50 range while implants have PTV values in the more reduced range of -8 to 0 (Isidor 1998). These results indicate a significant difference between the stiffness of natural dentition and osseointegrated implants. However, aside from the variations in PTV range, it would seem possible that the Periotest® should still function well for both intra- and extraoral implants.

1.3 Review of Literature

1.3.1 Parameters Affecting PTV

1.3.1.1 Implant Geometry

There exists a plethora of intraoral implants on the market today designed with variations in lengths, diameters, surface textures and thread styles that are touted to provide better integration. However, how do these parameters affect the response of the Periotest® and ultimately, can the Periotest® detect the geometric variations for any or all of them? Chavez et al. (1993) and Salonen et al. (1997) found a varied range of PTV for dental implants and implant systems respectively. These studies implied that the Periotest® does discriminate between implant systems, however, it is not clear as to which parameter or if all parameters affect the PTV. When considering only one geometric parameter, the studies seem to contradict one another. For example, the study by Cranin et al. (1998) showed that there was no distinct trend for implant diameter and mobility using the Periotest® device. In contrast, Ochi et al. (1994) as well as Aparicio and Orozco (1998) compared the PTV for different diameter implants. The studies showed that larger diameter implants typically have lower PTVs. Drago (2000) hypothesized that larger diameter implants have more surface area in contact with the bone and therefore the PTV should be lower. Other contradictory findings (Teerlinck et al. 1991; Carr et al. 1995; Tricio 1995) showed that implant lengths and coatings do not influence PTV whereas in other studies embedding depth or implant length has influenced PTV (Derhami et al. 1995; Haas et al. 1995; Haas et al. 1999; Drago 2000).

They found that the PTV decreased as the length of implant anchoring increased and reasoned that this was a result of an increased amount of surface area of bone in contact with the implant. One finding which seemed consistent throughout most studies was the relationship between striking height/position on the abutment and PTV. As the striking height above the surface of the coronal plane of the implant was increased, the PTV increases (Teerlinck et al. 1991; Derhami et al. 1995; Meredith 1998; Haas et al. 1999; Drago 2000). Derhami et al. (1995) noted a change of 1.5PTV for every 1mm change in striking position.

1.3.1.2 Bone Variables

Another parameter that is believed to affect PTV is the quality of bone tissue in which an implant system is anchored (Olivé and Aparicio 1990; Salonen et al. 1993; Salonen et al. 1997). Ultimately, the better the quality of bone, the higher the likelihood of successful osseointegration, which results in a lower PTV. Typically, cortical bone is considered to be good bone for implant placement and cancellous and fibrous tissue are not as ideal. As a result, variation in the proportions of cortical and cancellous bone lead to variation in bone density, which leads to variation in PTV as found by Tricio et al. (1995). Variations in bone density can be found throughout the body in the different types of bone and, therefore, the anatomical location of implantation provides another indication of how the bone quality affects PTV. There have been extensive studies of the testing of intraoral implants placed into both the mandible (lower jaw) and maxilla (upper jaw) of patients with the Periotest®. What was found when these implants were tested

for mobility with the Periotest®, was a lower PTV in the mandible than for the maxilla (Olivé and Aparicio 1990; Salonen et al. 1993; Haas et al. 1995; Cranin et al. 1998; Drago 2000;). These results seem logical due to the function of the mandible and its resulting loading. The bone in the maxilla is not as dense as it is in the mandible (Salonen et al. 1997). Under closer examination, a typical mandible cross-section (Figure 1-5) reveals an inner area of cancellous bone surrounded by a layer of cortical bone. Bicortical placement of an implant would result in a very stiff foundation and a low PTV. It is this cortical bone that influences PTV (van Steenberghe et al. 1995). Derhami et al. (1995) also showed how the PTV varies in different craniofacial regions in a cadaver. All four implants were placed in the mastoid process of the skull with three of the four having a PTV of -4. The fourth implant was connected to a BAHA and gave a higher PTV of -2. From the same study, implants located in the orbital had a range of PTV from 2 to 3.

Bone density at the implant interface can be affected by the presence of fibrous scar tissue, which increases mobility. In the study by Haas et al. (1999), it was found that fibrous encapsulation of an implant will influence the PTV. Other studies by Tricio et al. (1995), Salonen et al. (1997), Cranin et al. (1998), Isidor (1998), and Drago (2000) confirm the ability of the Periotest® to assess a large degree mobility of an implant incased in fibrous scar tissue. These implants tend to be the ones that ultimately fail. An apparent advantage of the Periotest® is its ability to discriminate between different degrees of osseointegration which could be due to the amount of bone at the interface. For example, the study by Cranin et al. (1998) considers the Periotest® results compared

with radiographic results. It concluded that the Periotest® was effective at determining bone loss from around the endosseous implant. Although studies have shown that the Periotest® can assess the quality of bone and mobility, other studies suggest that it can only detect large changes in the interface bone height (Isidor 1998). Others (Olivé and Aparicio 1990; Haas et al. 1995; Salonen et al. 1997; Cranin et al. 1998) found no indication that increasing or decreasing the length of osseointegration would affect PTV. Bone density is also known to vary with gender. Studies by Olivé and Aparicio (1990) and Drago (2000) confirm that gender affects the PTV. Typically, males are proportionally larger than females and hence have greater cortical bone thickness for a given type of bone than do females. Ultimately, this results in longer lengths of tissue/implant engagement and lower PTV values. As well, Olivé and Aparicio (1990) believe that the density of bone will tend to change throughout the healing process and they found that over time the PTV would decrease thus showing healing of the interface. In contrast, Isidor (1998) did not find any evidence that PTV decreases over time.

The biological parameters such as location and type of supporting tissue, the length of tissue/implant contact, and gender seem to influence the density and quality of supporting tissue for implants. Ultimately, it is the quality and quantity of supporting tissue in contact with the implant that determines the mobility of the Periotest®/implant system. However, it is difficult to monitor these parameters *in vivo* and this could account for the conflicting data.

1.3.1.3 Testing Procedure/Clinical Variables

Testing procedure and equipment limitations of the Periotest® have been considered as potential factors influencing PTV. Studies by Chai et al. (1993) and Derhami et al. (1995) considered interoperator variability. None was found in either study. The variability in measurements of one Periotest® instrument to another was evaluated by Manz et al. (1992), Derhami et al. (1995) and Haas et al. (1999). It was determined that specific instrument variability had no influence. However, Haas et al. (1999) found that previous studies used different striking points with different implant systems resulting in varying PTV and thus making any comparisons difficult. He recommended that a standardized measuring point be used. Derhami et al. (1995) also made the same recommendation.

Derhami et al. (1995) considered the effect of horizontal distance of the Periotest® handpiece from implant having an effect on PTV. A distance indicator was mounted to the tip of the Periotest® handpiece so that the holding distance was maintained between 1.5 to 2.0mm from the implant. The Periotest® would produce repeatable results when kept within the range. Another concern of researchers has been the affect that handpiece angulation has on PTV (Lukas and Schulte 1990; Derhami et al. 1995; Meredith et al. 1998). Meredith stated that angulation is one of the clinical variables which limits the sensitivity of the Periotest® and Derhami noted that this concern has been considered by the manufacturer and that an audible warning signal is produced when the handpiece is rotated outside an acceptable range.

Another concern has been the consistent application of torque preload for the abutment. Drago (2000) believes that a protocol is required and that a preload torque driver be used versus the conventional hand driver. This allows for a consistent preload of the abutment to the implant resulting in a consistent rigidity. If there were any loosening of the abutment screw, the Periotest® has been shown to be able to differentiate the loosening before it was clinically detected (Faulkner et al. 1999). A loose abutment screw would lead to a higher PTV than expected. Finally, maintaining the same lateral striking direction for all longitudinal tests would eliminate the possibility of the different mobility being measured (Ichikawa et al. 1994). This is typically due to the inhomogeneous nature of bone structure resulting in a different effective stiffness in different lateral striking directions.

Ultimately, a standardized testing protocol for the Periotest® is required and in order to establish it, a clearer understanding of its mechanics is required. This can be done by theoretically modeling the dynamics of the Periotest®/implant system and assessing the response of the system to changing geometric and clinical parameters discussed above. This is the goal of the present work.

1.3.2 Modeling of the Periotest®

To better understand the dynamics of the Periotest®, theoretical models have been developed. One of the earliest Periotest® models was developed Kaneko (1993). Figure 1-6 illustrates the single degree of freedom model used to describe the motion of the implant and Periotest®. Motion is allowed only in one direction, in this case lateral to

the long axis of the implant system. The Periotest® impacting rod is modeled as a particle with mass M traveling at a constant velocity V towards the implant system. The implant and the surrounding cortical bone are lumped together and modeled as a particle but with a mass m that is supported by the interface having a stiffness k, or as he refers to this mechanical property as compliance c, where $k=1/c$. The interface is the major link between the bone and implant and is considered to be the least stiff component of the modeled system and, therefore, it is the stiffness of the interface that dominates the stiffness of the entire system. The effects of damping are neglected in this model. The solution of this model is

$$x = x_o \sin \omega t \qquad 0 \le t \le \tau \tag{1.3}$$

where x is the displacement of the Periotest®/implant system, x_o is the amplitude of displacement which is initially unknown, t is the time after impact and τ is the contact time. The solution predicts that the response of the Periotest® striking the implant system will be sinusoidal.

Ultimately, Kaneko (1993) theoretically determined the resolution of the Periotest® from the model and the input of numerical data from clinical studies. From the literature, the mass M of the Periotest® is 8.4 grams traveling at a velocity V of 20 (cm s^{-1}). The mass of the dental implant and the effective mass of the cortical bone are assumed to be 0.4 grams and 2.4 grams respectively. The theory predicted that the magnitude of the Periotest®/implant system mobility to be in the range of 15 to 43 (μm)

for a corresponding -8 to 13 PTV range respectively, which is better than that of 100(μm) for radiography. Kaneko also suggested a single degree of freedom model (Figure 1-7) incorporating the effect of viscous damping. He concluded by stating that by measuring the area under the force-time signal, the damping of the system could be measured. A study by Faulkner et al. (1999) produced the complete solution for the single degree of freedom model with damping effects posed by Kaneko (1993).

A second paper by Kaneko (1994) hypothesized another single degree of freedom model of the Periotest® (Figure 1-8). Again the effective mass of the implant and Periotest® rod are given by m and M respectively. However, this model allows for fixed rotational motion. The implant system was modeled with a pinned connection at the apical point of the implant thus allowing for rotation about this point. The effective stiffness of the interface k was modeled as a spring located a distance h' from the point of rotation and a distance h from the point of impact. The effect of viscous damping was ignored to simplify the model. What he found was that the effective stiffness k_{eff} depended on the tapping point and thus PTV varies appropriately. The following equations show the correlation of k_{eff} and PTV with k, h, h', and m.

$$k_{eff} = k\left[\frac{h'}{h+h'}\right]^2 \tag{1.4}$$

$$\text{PTV} = \left[5\pi\left(1+\frac{h}{h'}\right)\sqrt{\frac{8.4+m}{k}}\right] - 21.3 \tag{1.5}$$

For the scenario where the striking height h increases, the equations show that the effective stiffness k_{eff} decreases and the PTV increases. Also, as the implant length h' increases, the k_{eff} will increase slightly resulting in a decrease in PTV. This is an example of the effect of length of bone-implant contact on PTV.

The above model is limited by the assumption that the implant rotates about a pinned point located at the apical point of the implant

1.3.3 Other Mechanical Methods

The Periotest® is not the only dynamic method to determine implant mobility. Other mechanical methods have been proposed and are described here. They are the impedance head hammer and the resonance frequency analysis methods.

1.3.3.1 Impedance Head Hammer

In a study by Elias et al. (1996) a dynamic modal testing technique was developed to assess the implant-bone continuum of an endosseous implant. The technique used a PCB Piezotronics® (model 086080, Buffalo NY) impedance head hammer (IHH) with a modified brass tip used to laterally impact the dental implant (Figure 1-9). The device is hinged at the non-contact end so allowing the hammer to swing with a pendulum-like motion.

The output of the impedance head is a voltage signal that is proportional to the force at the hammer tip upon impact. Figure 1-10 illustrates an ideal impact where the area under the curve is the impulse and the interval T_c is the time for which the hammer and the implant remain in contact and measured in milliseconds. The magnitude of the contact time depends upon the damping and stiffness of the impacted system. The total stiffness of the system is very much dependant upon the least stiff component whereas the total damping is dependant upon the component with the largest damping potential. They considered the interface of the implant and bone to be the least stiff.

They found that the peak force occurs at the maximum displacement and that zero force at the initial position indicates disengagement of the hammer's head. A less stiff interface would flatten out the force curve but physically there is also the possibility that the implant may bounce off the hammer producing high frequency oscillations superimposed on the low-frequency rotation. Therefore relative motion between the hammer and the implant is possible and consequently *f(t)* is not perfectly sinusoidal (Figure 1-11).

Within this study, two *in vitro* tests were conducted. The first test assessed the hammer's ability to distinguish between eight ϕ3.75mm x 7mm long Brånemark implants installed in cortical and trabecular bone. The impulses where kept constant by constraining them to an acceptable range of 292-313 μNs. The resulting frequencies are shown in Table 1-1.

Table 1-1: Range of Implant Frequencies due to Interface Bone

Cortical (hard bone)	4.17 - 6.15 kHz
Cancellous (spongy bone)	2.27 - 3.72 kHz

This is not surprising as it is well known, that cancellous bone is generally more flexible than cortical bone.

The second *in vitro* study used the same implanted cancellous bone samples but this time the implants were cemented into the cancellous bone specimens. The purpose of this testing was to judge the hammer's ability to clearly identify the distinct levels of stiffness of drying cement. They found that the stiffness increased as the cement cured and that the results approached the stiffness of cortical bone after curing had completed.

It was concluded that dynamic modal analysis testing specifically assesses the structural characteristics of the interfacial tissue within 1mm of the implant and the level of fixation between the implant and the surrounding bone.

Although the IHH seems to be a good method for assessing the mobility of implants, a more convenient dynamic testing device is required in order for it to be used clinically. This is primarily due to the inherent geometry, size and method of the IHH, which limits the testing of implants to extraoral implants an anterior oral implants. Testing of some extraoral implant may require the repositioning of the patient instead of the device. Another limitation of the IHH is the difficulty in reproducing the impulse magnitudes. Ultimately, the IHH appears to be a good *in vitro* method but with limitations for *in vivo* testing.

1.3.3.2 Resonance Frequency Analysis

The resonance frequency analysis (RFA) method was developed to specifically assess the status of the implant-bone interface by measuring the frequency response of the system with 2 peizo-ceramic transducers. The RFA transducer system is shown in Figure 1-12 and is made from stainless steel or commercially pure titanium in the form of an L shaped cantilever beam. On the vertical portion of the beam there are two peizo-ceramic crystals, one on each side. Each element is about 3mm x 7mm and is bonded using an epoxy. The transducer is excited using an alternating current signal at various frequencies through one crystal of the transducer until steady state is reached. Once steady state is reached, the frequency of the excitation signal is increased and the process is repeated until an entire sweep of frequencies is made. The excitation signal is a swept sine wave and is varied from 5 to 15 kHz at maximum amplitude of 1 volt. The RFA performs 2 sweeps of the frequency spectrum within the 5 kHz to 15 kHz range. The initial sweep is coarse, consisting of 100 Hz steps, in order to bracket the resonance frequency of the system. The second sweep produces greater resolution of the signal with fine increments of 5 Hz above and below the resonance. The second crystal, which is mounted on the opposite side of the offset cantilever beam, detects the frequency response of the transducer/implant system. Figure 1-13 illustrates a typical frequency response of the RFA transducer when testing the different interfaces that may exist around an implant. A sharp high frequency peak is expected when anchored to an osseointegrated implant. When marginal bone resorption occurs, there is less implant to bone contact therefore reducing the effective stiffness of the interface which causes a

drop in resonant frequency. For an implant encapsulated by fibrous connective tissue, no distinct amplitude can be detected from the frequency response of the RFA indicating reduced stiffness and high damping from the interface.

The RFA assesses the health of the interface by comparing the effective length of the combined transducer and implant engagement length. For the cantilever, the resonant frequency is

$$R_f \propto \frac{1}{(L+\delta L)^2} \tag{1.9}$$

where R_f is the resonance frequency, L is the length of the beam, and δL is the change in the effective length of the beam. This change could be due to a change in bone stiffness or a marginal loss of bone.

Overall the RFA is an excellent mechanical method for distinguishing the quality of the interface. However, there is a major concern about the size of the RFA (Figure 1-14), which limits its application for testing oral implants, especially those located posteriorly in the mouth. Another possible limitation the RFA system is the emerging predominance of non-retrievable restorative systems for osseointegrated implants. These systems use cemented restoration and so have no abutment screw for attachment of the RFA transducer.

1.4 Outline of Thesis

Chapter 2 presents the development of a new theoretical dynamic model of the Periotest® as a 2 degree of freedom system. Modeling considerations are presented as well as the development of the equations of motion. Only the highlights are presented in this chapter with a more complete development presented in Appendix A.

In Chapter 3, the materials and methods used for testing craniofacial implants both *in vitro* and *in vivo* are developed. This includes an explanation of how the Periotest® was modified so that the accelerometer signal could be captured along with sampling information and specifications for the data acquisition. Finally, a brief discussion of the testing apparatus, samples and finally the testing procedure for both the *in vitro* and *in vivo* studies is provided.

Chapter 4 is a presentation of the results of both the *in vitro* and *in vivo* studies and a discussion of their results. A comparison of the *in vitro* results to the model is discussed in hopes of validating the theory. Finally, a sensitivity analysis of the theoretical model is performed to assess the resolution of the model and compare it to the earlier models presented.

Chapter 5 summarizes the thesis work and presents recommendations for further work.

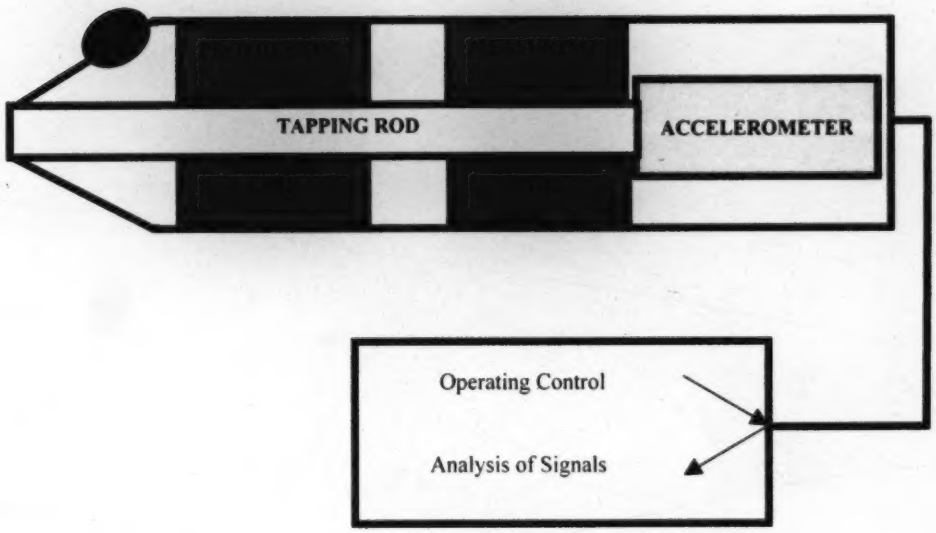

FIGURE 1-1: Schematic Diagram of the Periotest® Device

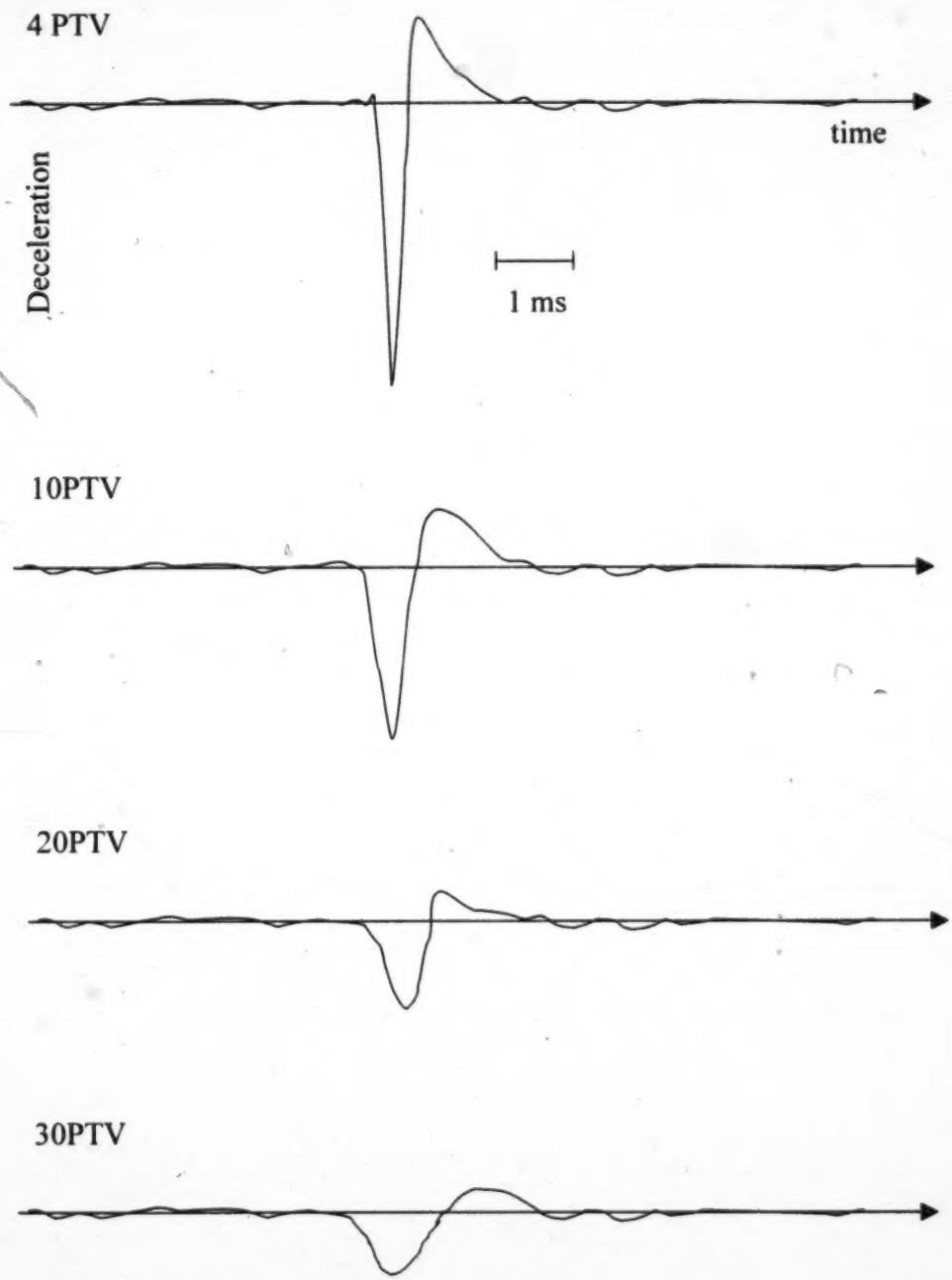

FIGURE 1-2: Degrees of Mobility Determined from the Periotest® Deceleration Signal

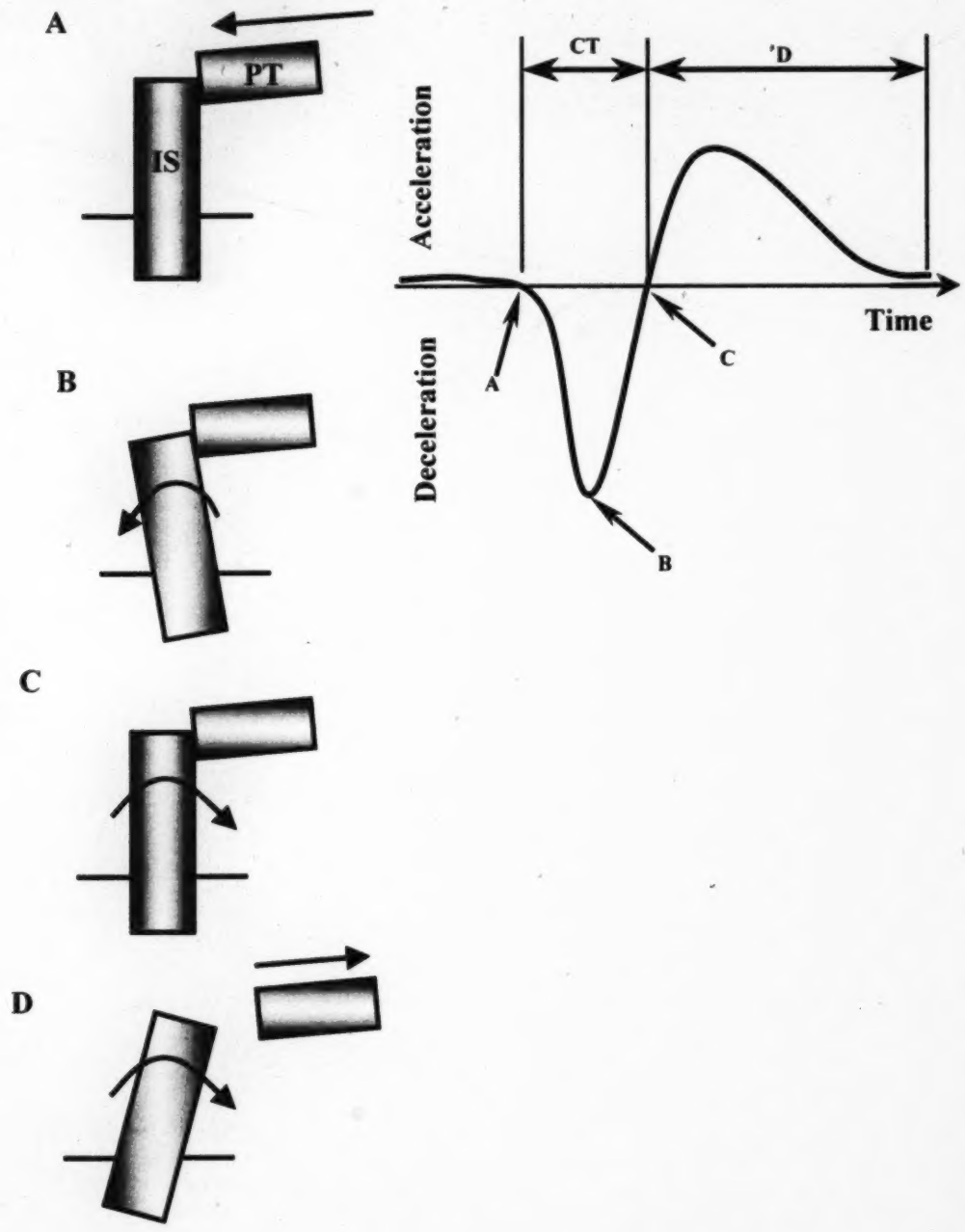

FIGURE 1-3: Illustration of the Physical Interaction Between the Periotest® (PT) and the Implant System (IS)

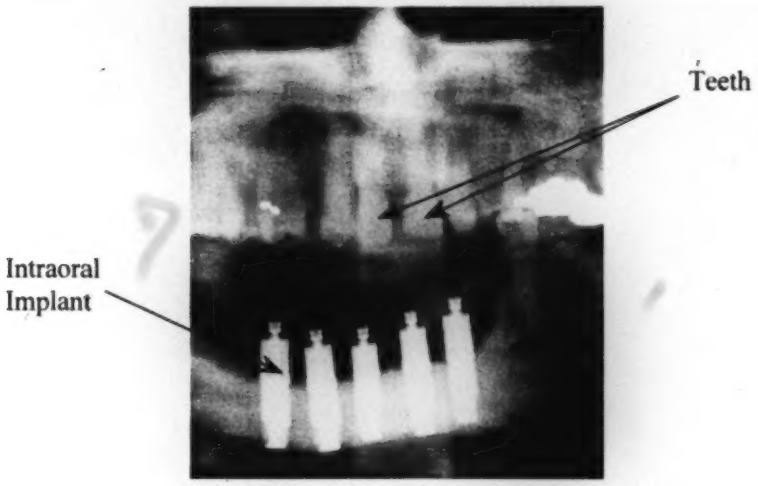

FIGURE 1-4: Geometric Similarities Between Intraoral Implants and Teeth

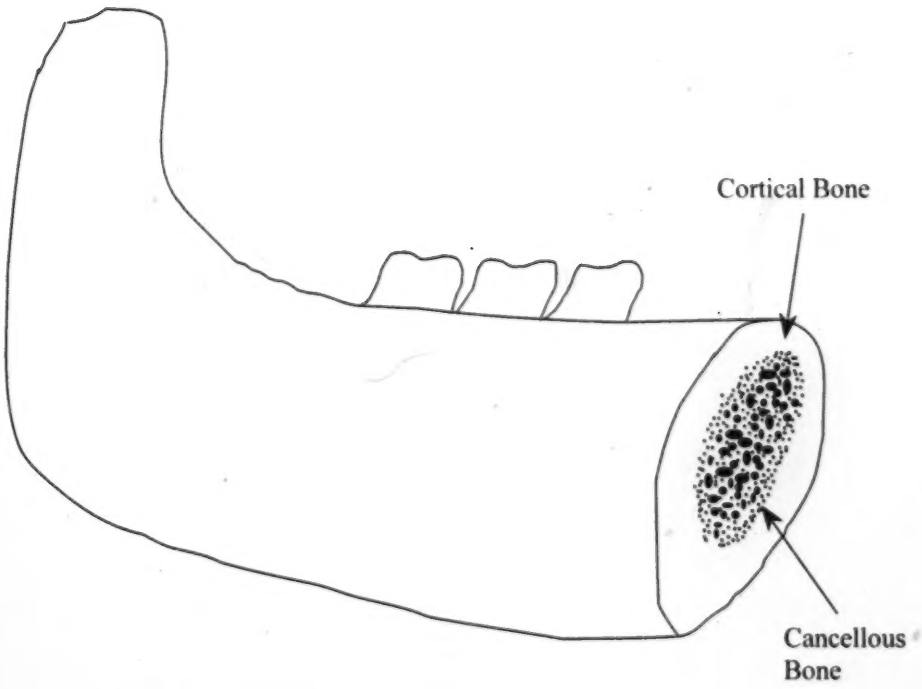

FIGURE 1-5: Mandible Cross-section

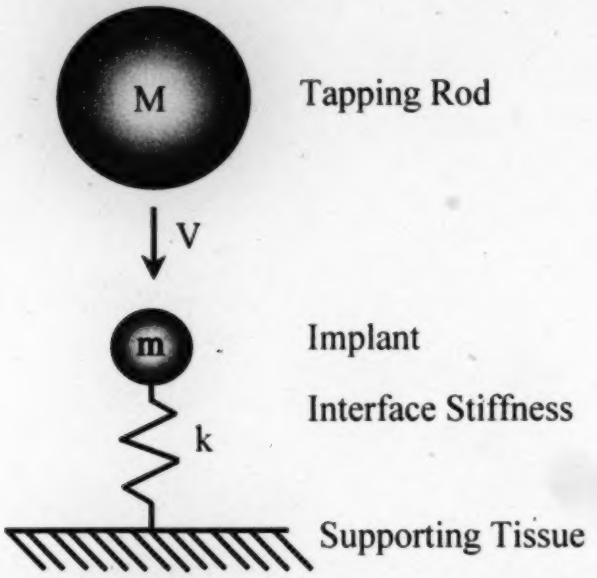

FIGURE 1-6: Single Degree of Freedom Model of Periotest®/Implant System with No Viscous Damping (Modified from Kaneko 1993)

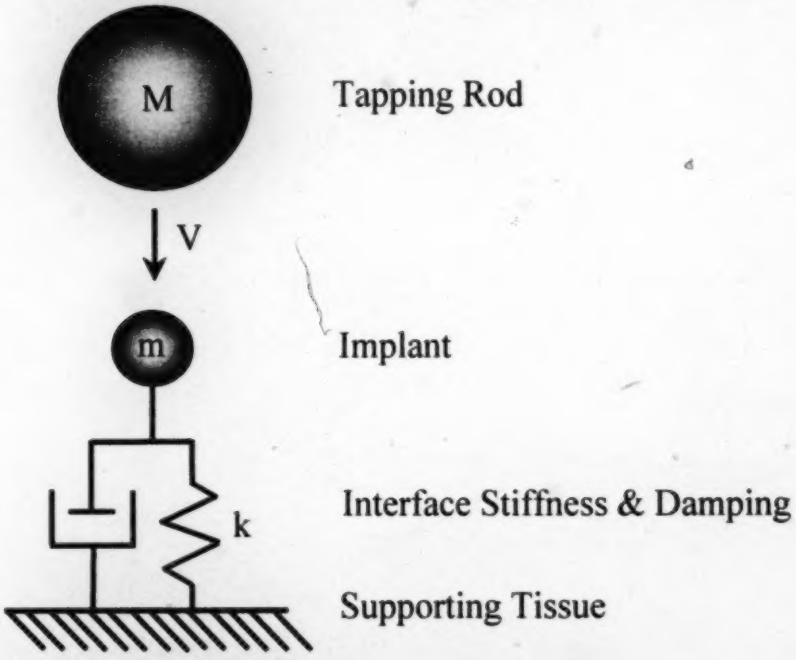

FIGURE 1-7: Single Degree of Freedom Model of Periotest®/Implant System with Viscous Damping (Modified from Kaneko 1993)

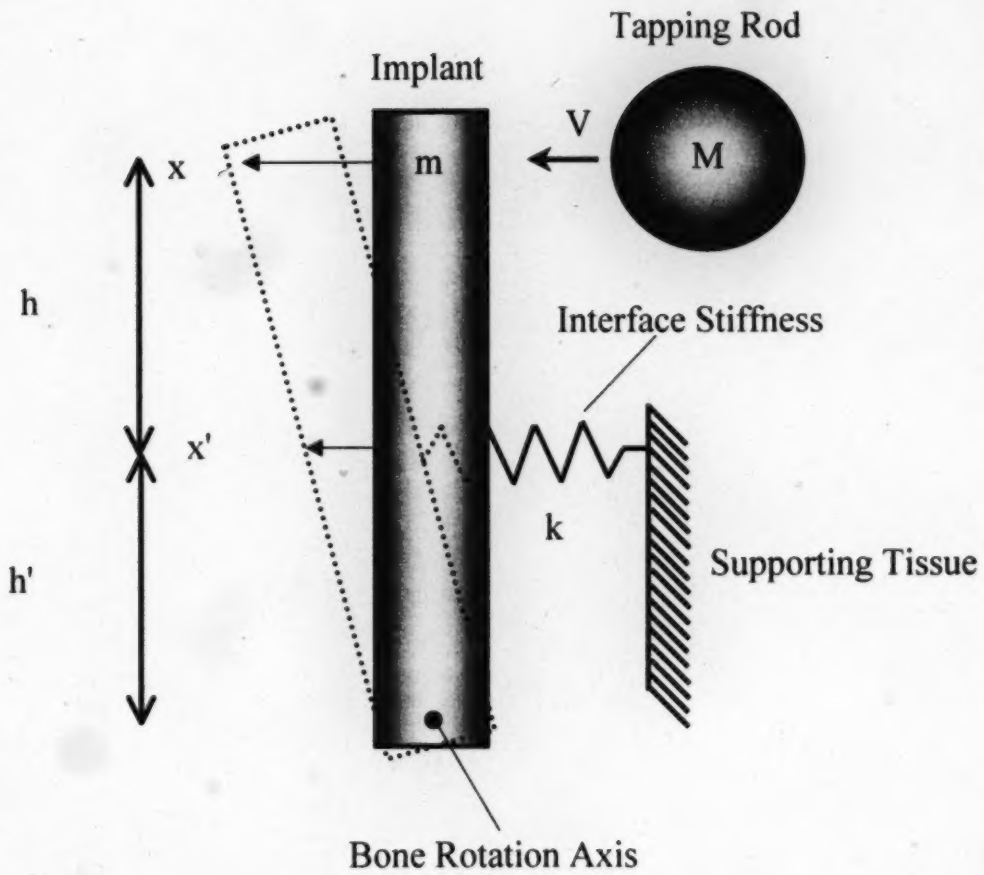

FIGURE 1-8: Rotational Single Degree of Freedom Model of Periotest®/Implant System with No Viscous Damping (Modified from Kaneko 1994)

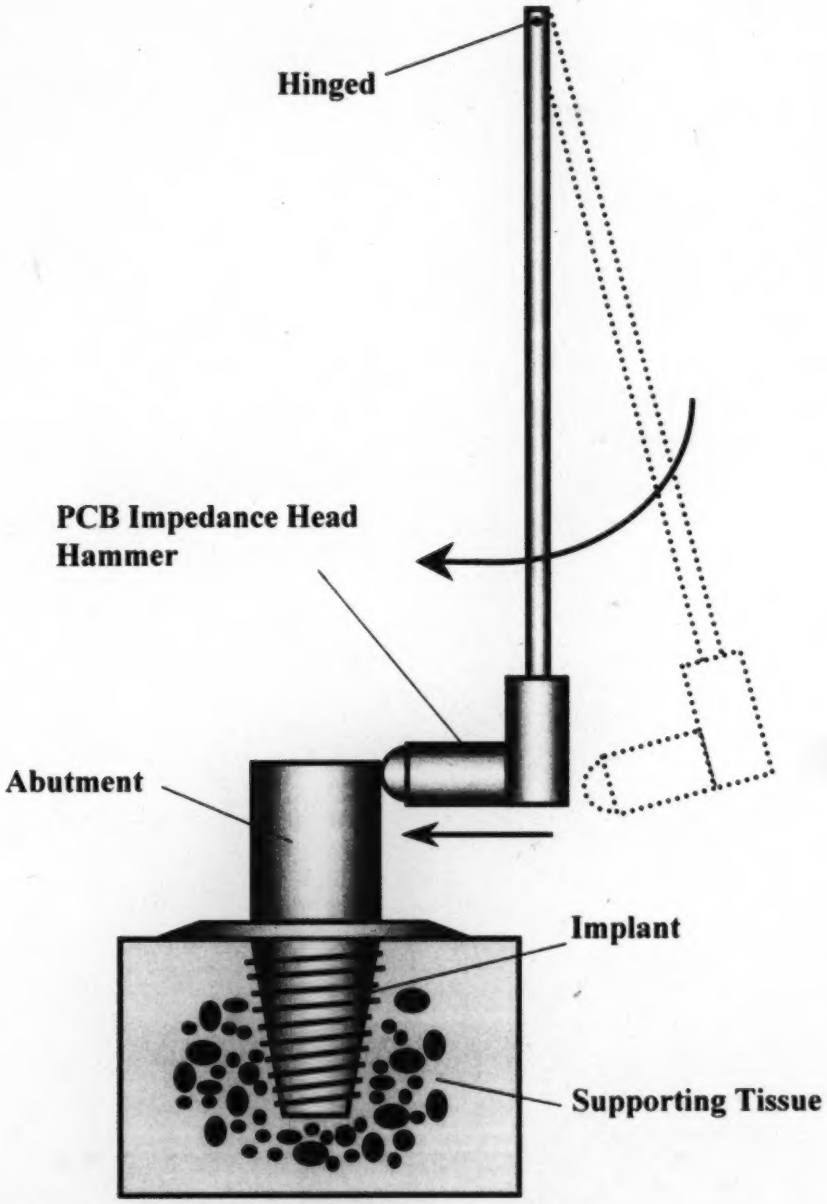

FIGURE 1-9: Schematic of the Impedance Head Hammer
(Modified from Elias et al. 1996)

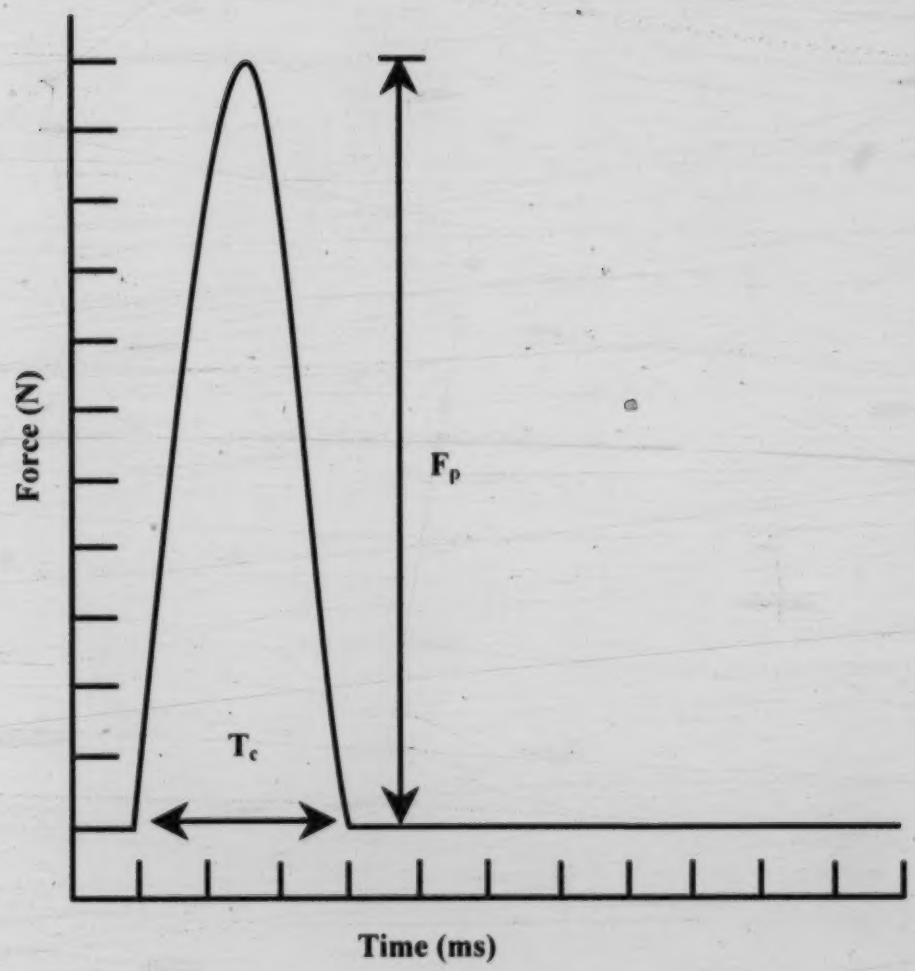

FIGURE 1-10: Theoretical Force Curve for an Impedance Head Hammer Dynamic Test (Modified from Elias et al. 1996)

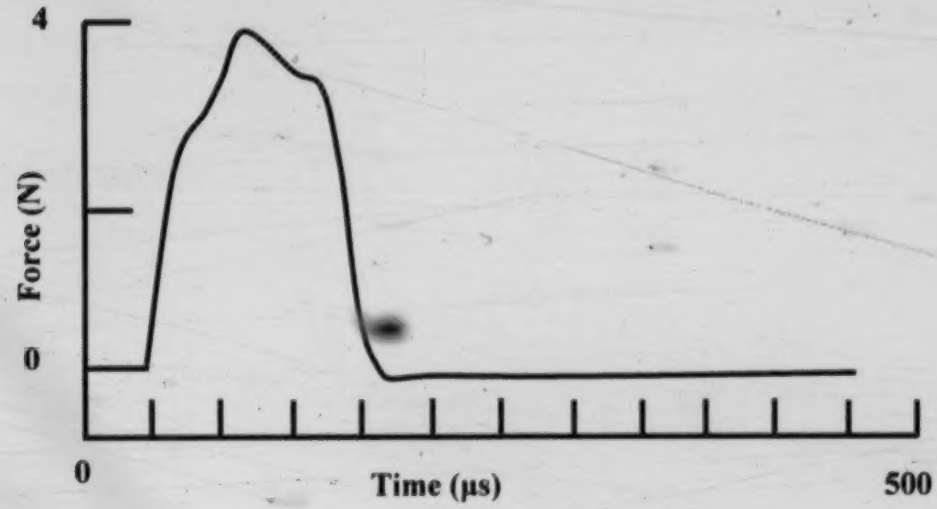

FIGURE 1-11: Typical Force Curve from a Lateral Impact with the Impedance Head Hammer (Modified from Elias et al. 1996)

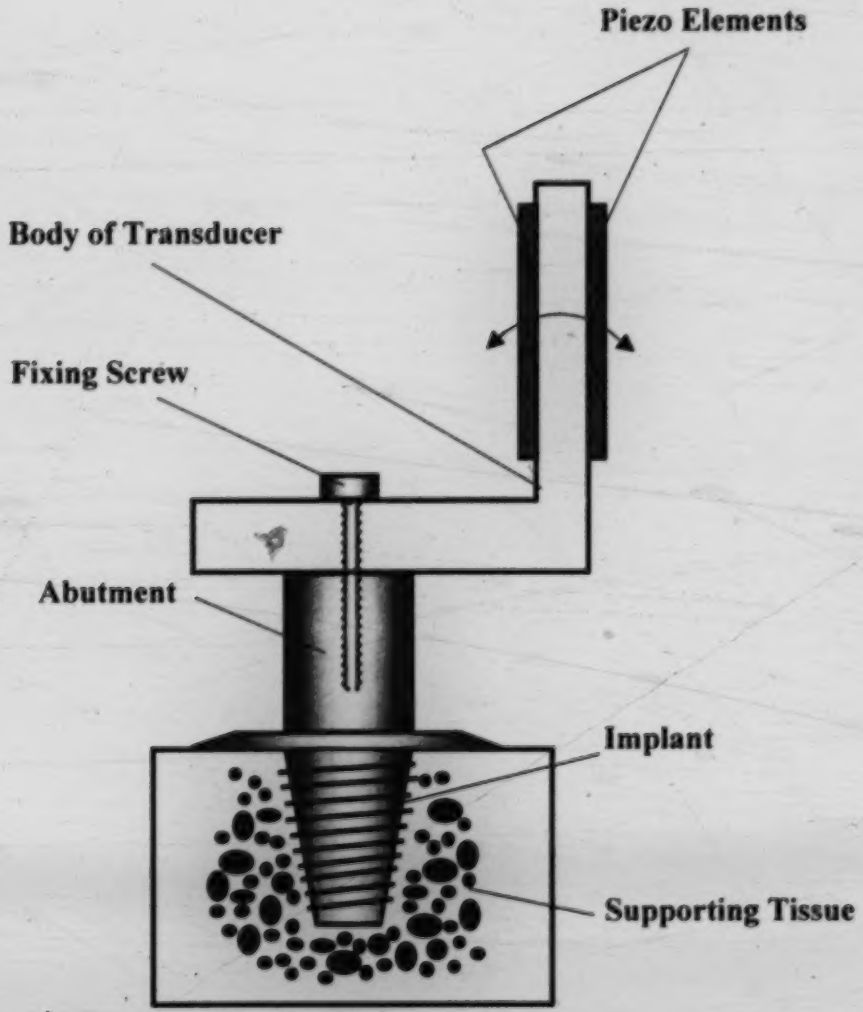

FIGURE 1-12: Schematic of Resonance Frequency Analysis Transducer (Modified from Meredith 1997)

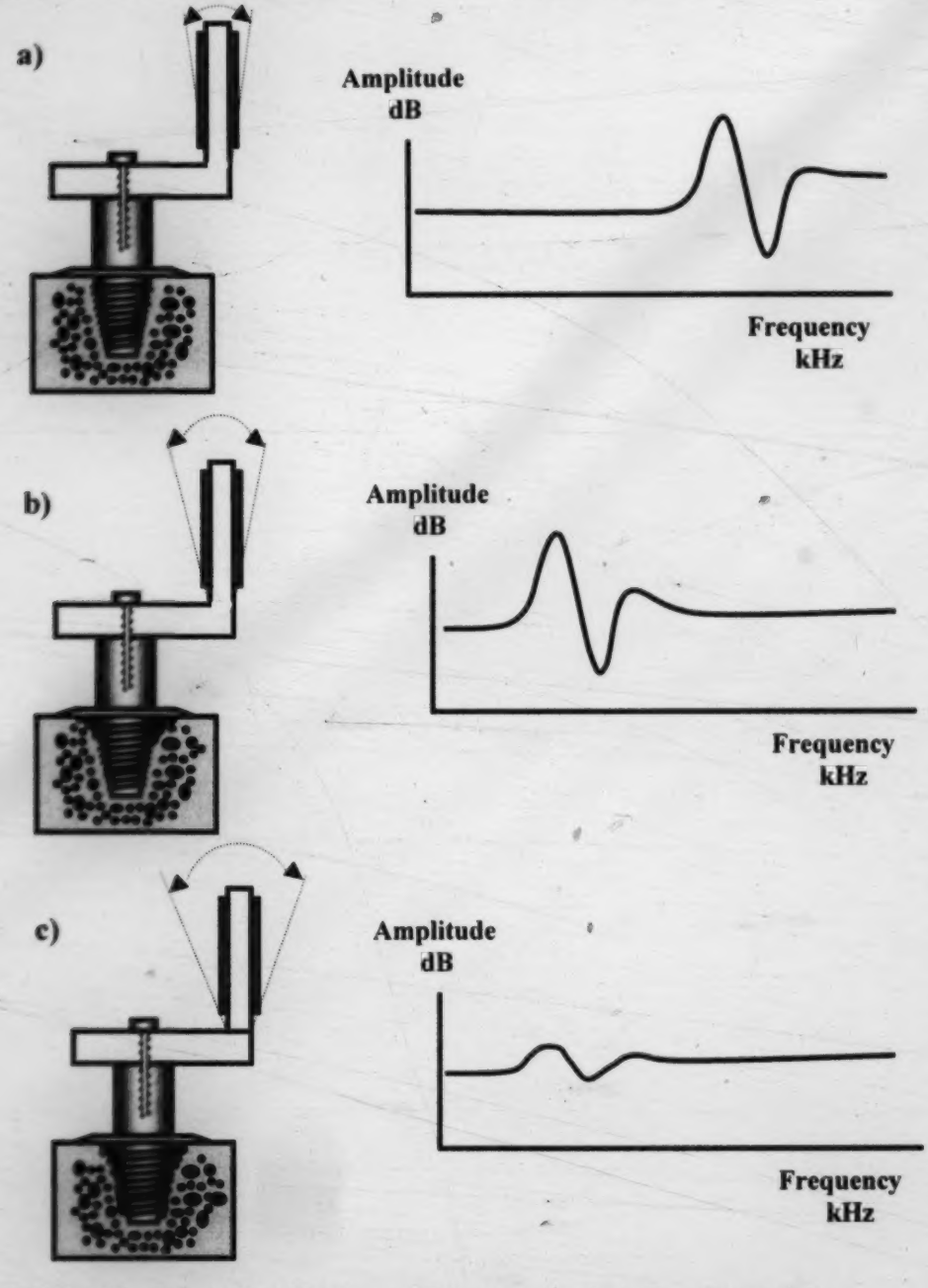

FIGURE 1-13: Schematic of Resonance Frequency Analysis Transducer and Response Curve for a) Osseointegrated Implant b) Osseointegrated Implant with Marginal Bone Resorption c) Implant Surrounded by Connective Tissue (Modified from Meredith 1997)

FIGURE 1-14: The Relative Size of the Resonance Frequency Analysis Transducer Compared with the Oral Cavity for Intraoral Testing

Chapter 2

Modeling the Periotest®/ Implant System

2.1 Introduction

In order to gain a better understanding of the phenomena of the Periotest® rod impacting the implant/abutment system, a new mathematical model is developed. This model will be used to explain how changes in various system variables could affect the dynamics of the system and ultimately the PTV.

When considering details of the physical problem, there are many variables or parameters that can complicate the model. The key is to incorporate only those parameters believed to have the major influence on the behavior of the system in hopes of attaining reasonable solutions. While over-simplifying the model can yield erroneous results, an appropriate balance between model complexity and realistic solutions makes modeling an engineering challenge.

Dynamical models of the Periotest®/implant system have been previously developed in order to better understand the mechanical behavioral response and output of the Periotest®. These dynamic models varied in complexity. Kaneko (1993) proposed a Periotest®/implant model, which was a single degree of freedom system, allowing for only one dimensional translation, and provided insight into the relationship between the contact time and the Periotest® value. However, this model lacked certain geometric and clinical parameters including tissue stiffness, damping and thickness, implant mass, and Periotest® variations in position of impact, all believed to have a major effect on the PTV. In order to address these topics, a more advanced model is required. A more complex model is developed in the present study and is based upon the physical system shown in Figure 2-1. This model is a planar one that combines both the rotational and translational degrees of freedom of the Periotest®/implant system from the models represented above.

2.2 Modeling Considerations

There are many parameters of Periotest® implant system to be considered when developing the dynamic model. The following is a discussion of the major parameters, their relevance and their incorporation into the model.

The key parameters considered important are the discrimination between bone tissues at the interface, the corresponding vertical stiffness and damping of the tissue, implant system (implant, abutment, abutment screw) stiffness, the mass and moment of inertia of the implant system, the mass of the Periotest® tapping rod, depths of the

implant into each type of bone, and the position at which the Periotest® tapping rod makes contact with the abutment of the implant system.

2.2.1 Interface Tissue

The type of tissue in which the implant is anchored has a large effect upon the response of the implant/abutment to the Periotest®. As mentioned in Chapter 1, bone in the human body can be made of a hard cortical outer layer or a more elastic spongy layer known as cancellous bone. Their relative proportions vary depending upon which bones are considered in the human body. The human skull consists of flat bones, which have both cortical and cancellous bone types. The relative thickness of flat bone can be deduced from the design of the effective thread lengths of the extraoral craniofacial implants used (Figure 2-3). There is also the consideration of the tissue, which forms around the implant. This tissue can be connective tissue (i.e. scar tissue), which is not desired and is considerably less stiff compared to an osseointegrated interface where there is a very solid connection between the bone and the implant.

The quality of bone tissue at the interface varies for each individual, as the bone can be new, old, remodeled, or even scar tissue for which the tissue stiffness can vary significantly. From a dynamics point of view, it is the tissue stiffness that is important. The higher stiffness suggests better interface bonding. Figure 2-2 models the bone stiffness at the interface of the implant as a series of springs. The springs are arranged in both the vertical (k^*) and horizontal (k) directions to represent the stiffness per unit length

of the bone in contact with the implant. In this way it is possible to include the thickness of contact between bone and implant.

Another mechanical property exhibited by bone tissue is its damping or the ability to dissipate energy. The damping behavior of bone is a result of the fact that it is a living tissue with cells making up its structure in addition to the mineral deposits of calcium and phosphates. Cells contain interstitial fluid (mostly water) and it is this that produces a viscous-like damping behavior of bone. The damping effects of bone are distributed throughout the thickness of each type of bone, and therefore, these damping effects were modeled as a viscous damping per unit length shown with dashpots in Figure 2-2. The damping per unit length of the tissue is denoted by the variable c with the vertical damping per unit length being c^*.

2.2.2 Implant System

Figure 2-3 illustrates the dimensions of a typical extra-oral craniofacial implant fixture. These implants are made from 99.75% commercially pure titanium, which is used for its superior corrosion resistance (Askeland 1990) and biocompatibility. However, it is relatively weak compared to titanium alloys (Askeland 1990) that have a tensile strength an order of magnitude larger. Table 2.1 compares the modulus of elasticity (Young's Modulus) of various materials relevant to the implant system.

Table 2-1: Material Properties

Material	Young's Modulus (GPa)	Reference
Commercially Pure Titanium	107	Dimarogonas 2001
Cortical Bone	13.7	Tricio et al. 1995
Soft Tissue	3.5	Del Valle 1995
Cancellous Bone	1.37	Tricio et al. 1995

Comparing the modulus of elasticity of titanium to that of cortical bone indicates that the titanium is considerably stiffer and as a result, the titanium components of the implant system will not deflect to the degree that the cortical bone might. Consequently, the model assumes the stiffness of the implant system can be neglected and thus can be modeled as a rigid body.

The modeling of the implant diameter has been incorporated so that the sensitivity of the Periotest® response to diameter can be examined. Figure 2-2 illustrates the effective diameter of the implant screw to be D.

The abutment is a tubular piece of commercially pure titanium to which the prosthesis is connected. The abutment is connected to the implant with an abutment screw. Figure 2-4 is a machine drawing of a typical abutment. Typically abutments range in length from 3mm to 10mm. The abutment is also assumed rigid in the model (Chavez 1993).

Figure 2-5 illustrates a machine drawing of a typical abutment screw. The abutment screw is used as a bolted connection between the implant and the abutment. Typically, when attaching the abutment, the abutment screw is given a torque in the range of 20Ncm to 45 Ncm to provide adequate preload in the bolted connection. A study done

by Faulkner et al. (1999) showed that the Periotest® could detect the loosening of the abutment screw. However, when tested with the Periotest® after being torqued to 20, 30, and 45Ncm with a torque controller, the output of the Periotest® would not change. This indicates that the stiffness of the bolted connection did not change after the torque reached 20 Ncm.

The implant system consists of an implant fixture, an abutment screw, and an abutment. From the information given above, the implant system is assumed to be a rigid body and is modeled as a uniform cylinder with centroidal moment of inertia of J_G and a mass of m_i.

2.2.3 Periotest® System

The Periotest® houses a stainless steel polished impacting rod within the hand-piece. When fired, the rod is guided towards the target along low friction bearings, which restrict the rod's motion along a linear path. As a result, when contact is made with the implant system, there is no rotational inertial influence from the rod. Therefore, the rod is modeled as a particle with mass m_p.

2.2.4 Datum Point

An arbitrary vertical datum level at point O is established on the longitudinal axis of the implant where the Periotest® makes contact and is shown in Figure 2-6. All vertical measurements such as striking height of Periotest®, distance to center of gravity of implant system, distance to bone tissue top layer, and distance to the lower bone tissue

layer are referenced from this point. The distance from the datum to the center of mass of the implant system is the variable b. The length of engagement between the supporting tissue layer and the implant is given as $\ell_2 - \ell_1$ (Figure 2-2) where ℓ_1 is the distance from the datum to the top of the tissue layer and ℓ_2 is measured from the datum to the bottom height of the tissue-implant interface. The distance from the datum level to an arbitrary point within the supporting tissue layer is given by ℓ'.

2.3 Free-Body Diagram vs Mass Acceleration Diagram

The motion of the Periotest®/implant system is described by a translation x and rotation θ about the datum point O (Figure 2-7). These two degrees of motion establish the generalized coordinate systems of the model. By applying the reaction forces and inertial forces due to the displacements in x and θ, the free-body (FBD) and mass acceleration (MAD) diagrams are created respectively (Figure 2-6). Newton's second law of motion yields the equations describing the motion of the Periotest®/implant system. The equation of motion in the horizontal direction is

$$\overset{+}{\leftarrow} \sum F_{x(FBD)} = ma_x \tag{2.1}$$

which reduces to

$$(m_i + m_p)\ddot{x} + m_i b\ddot{\theta}\cos\theta - m_i b\dot{\theta}^2 \sin\theta + k(\ell_2 - \ell_1)x + \frac{k}{2}(\ell_2^2 - \ell_1^2)\theta - c(\ell_2 - \ell_1)\dot{x} + \frac{c}{2}(\ell_2^2 - \ell_1^2)\dot{\theta} = 0. \tag{2.2}$$

The vertical equation of motion is identically satisfied as a_{G_y} is zero.

Equilibrium of the moments about O

$$\circlearrowleft + \sum M_{O\,(FBD)} = \sum M_{O\,(MAD)} \tag{2.3}$$

or

$$\begin{aligned} &- F_{vspring}(r\cos\theta + \ell'\sin\theta) - F_{vspring}(r\cos\theta + \ell'\sin\theta) \\ &- \frac{k}{2}[(\ell_2 - \ell_1)(\ell_2 + \ell_1)]x - \frac{k}{2}[(\ell_2 - \ell_1)(\ell_2 + \ell_1)\ell_1]\theta \\ &- \frac{k}{2}\left[(\ell_2 - \ell_1)^2\left(\frac{2}{3}(\ell_2 - \ell_1) + \ell_1\right)\right]\theta \\ &- \frac{c}{2}[(\ell_2 - \ell_1)(\ell_2 + \ell_1)]\dot{x} - \frac{c}{2}[(\ell_2 - \ell_1)(\ell_2 + \ell_1)\ell_1]\dot{\theta} \\ &- \frac{c}{2}\left[(\ell_2 - \ell_1)^2\left(\frac{2}{3}(\ell_2 - \ell_1) + \ell_1\right)\right]\dot{\theta} \\ &= J_G\ddot{\theta} + m_i\ddot{x}b\cos\theta + m_i b^2\ddot{\theta} \end{aligned} \tag{2.4}$$

where the force due to the vertical springs being loaded is:

$$F_{vspring} = k^*(\ell_2 - \ell_1)(r\sin\theta + \ell'[1 - \cos\theta]). \tag{2.5}$$

The resulting motion of the implant/abutment system is assumed to be small compared to the sizes shown and so the above equations can be simplified assuming small angles of rotation θ. Equations (2.2) and (2.4) reduce to

$$(m_i + m_p)\ddot{x} + (m_i b)\ddot{\theta} + k(\ell_2 - \ell_1)x + \frac{k}{2}(\ell_2^2 - \ell_1^2)\theta + c(\ell_2 - \ell_1)\dot{x} + \frac{c}{2}(\ell_2^2 - \ell_1^2)\dot{\theta} = 0 \tag{2.6}$$

$$(m_i b)\ddot{x} + (J_G + m_i b^2)\ddot{\theta} + \frac{k}{2}(\ell_2^2 - \ell_1^2)x + \frac{k}{3}(\ell_2^3 - \ell_1^3)\theta + k^*(\ell_2 - \ell_1)r^2\theta + \frac{c}{2}(\ell_2^2 - \ell_1^2)\dot{x} + \frac{c}{3}(\ell_2^3 - \ell_1^3)\dot{\theta} + c^*(\ell_2 - \ell_1)r^2\dot{\theta} = 0 \tag{2.7}$$

which can be written as

$$[m]\begin{Bmatrix}\ddot{\theta}\\ \ddot{x}\end{Bmatrix} + [c]\begin{Bmatrix}\dot{\theta}\\ \dot{x}\end{Bmatrix} + [k]\begin{Bmatrix}\theta\\ x\end{Bmatrix} = \begin{Bmatrix}0\\ 0\end{Bmatrix} \tag{2.8}$$

where the mass, stiffness and damping matrices are:

$$[m] = \begin{bmatrix} J_G + m_i b^2 & m_i b \\ m_i b & m_i + m_p \end{bmatrix}$$

$$[k]=\begin{bmatrix} \frac{k}{3}\left(\ell_2^3-\ell_1^3\right)+k^*r^2\left(\ell_2-\ell_1\right) & \frac{k}{2}\left(\ell_2^2-\ell_1^2\right) \\ \frac{k}{2}\left(\ell_2^2-\ell_1^2\right) & k\left(\ell_2-\ell_1\right) \end{bmatrix}$$

$$[c]=\alpha[k] \qquad [c^*]=\alpha[k^*] \qquad \alpha=\frac{c}{k}=\frac{c^*}{k^*}$$

It is important to note that proportional damping has been assumed and that α is the constant of proportionality. In other words, the damping matrix is expressed as a linear combination of the stiffness matrix only.

The model can be further simplified noting that a typical mass of the implant system (implant screw/abutment screw and abutment) m_i is 0.5 grams in contrast to the mass of the Periotest® rod m_p of 8.4 grams (Kaneko 1993). Consequently, the mass of the implant system can be neglected when compared to the mass of the Periotest® rod. The implication of this assumption is that the moment of inertia J_G, which depends directly on m_i, can also be neglected. These assumptions lead to the simplified equations of motion

$$\begin{bmatrix} 0 & 0 \\ 0 & m_p \end{bmatrix}\begin{Bmatrix} \ddot{\theta} \\ \ddot{x} \end{Bmatrix}+[c]\begin{Bmatrix} \dot{\theta} \\ \dot{x} \end{Bmatrix}+[k]\begin{Bmatrix} \theta \\ x \end{Bmatrix}=\begin{Bmatrix} 0 \\ 0 \end{Bmatrix}. \qquad (2.9)$$

This simplification yields a relationship between the coordinates

$$k_{11}\theta + k_{12}x = 0 \tag{2.10}$$

and a single equation of motion

$$m_p\ddot{x} + \frac{\left(k_{11}k_{22} - k_{12}^2\right)}{k_{11}}\left(x + \alpha\dot{x}\right) = 0. \tag{2.11}$$

Equation (2.11) can be rewritten in the following single degree of freedom form

$$m_p\ddot{x} + c_e\dot{x} + k_e x = 0,$$

where

$$k_e = \frac{k_{11}k_{22} - k_{12}^2}{k_{11}} \qquad \text{and} \qquad c_e = \alpha k_e$$

are the effective stiffness and damping respectively.

The solution to this single degree of freedom system has been previously given in Faulkner et al. (1999). The solution is given in the Appendix A and only the results are shown here. The position of the Periotest®/implant system for time t is:

$$x(t) = \frac{V}{\omega_n \sqrt{1-\zeta^2}} e^{-\zeta \omega_n t} \sin\left(\omega_n t \sqrt{1-\zeta^2}\right). \tag{2.12}$$

Here V is the velocity of the Periotest® impacting rod, ω_n is the undamped natural frequency of the system and ζ is the damping ratio given by

$$\omega_n = \sqrt{\frac{k_c}{m_p}} \qquad \text{and} \qquad \zeta = \frac{c_c}{c} = \frac{\alpha k_c}{2 m_p \omega_n} = \frac{\alpha}{2} \omega_n .$$

It is important to note that Equation (2.12) is only valid during the time t when there is contact between the Periotest® impacting rod and the implant system. The acceleration of the Periotest®/implant system is then

$$\ddot{x}(t) = \frac{-V \omega_n}{\sqrt{1-\zeta^2}} e^{-\zeta \omega_n t} \sin\left(\omega_n t + \phi\right) \tag{2.13}$$

while the period of contact is described by

$$\mathrm{CT} = \frac{1}{\omega_n \sqrt{1-\zeta^2}} \left[\pi - \tan^{-1} \frac{2\zeta \sqrt{1-\zeta^2}}{1-2\zeta^2} \right]. \tag{2.14}$$

The corresponding PTV can be compared with this contact time from either Equation (1.1) or (1.2). The results of this model will be compared to the measurements of a set of *in vitro* tests later.

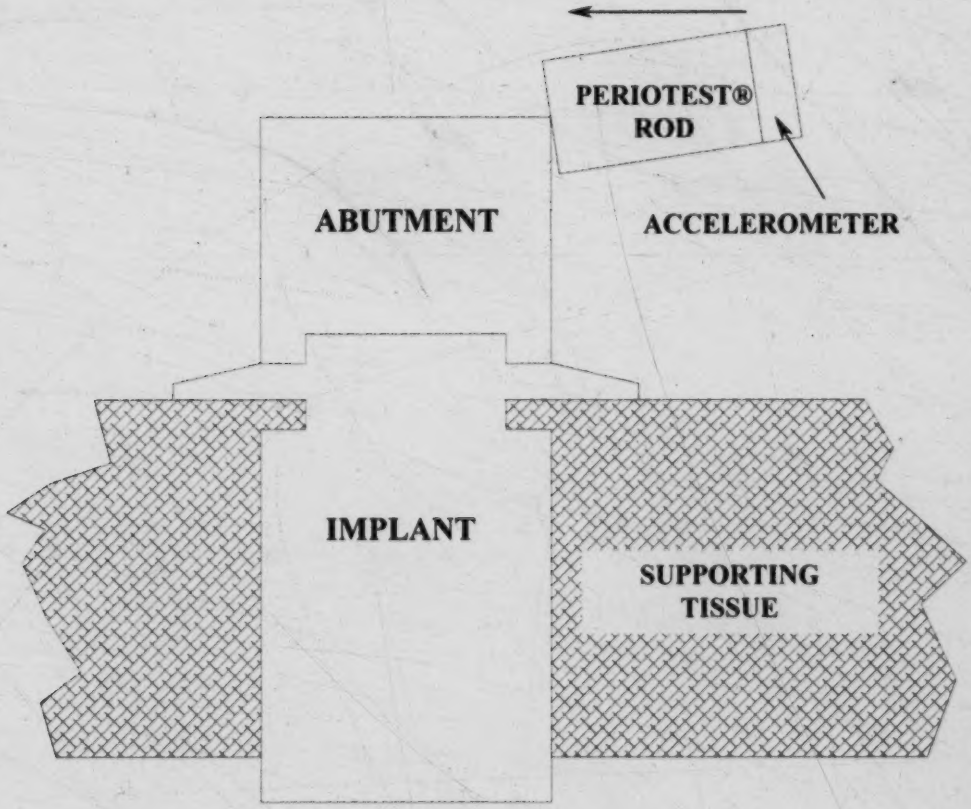

FIGURE 2-1: Schematic of Periotest® and Implant System

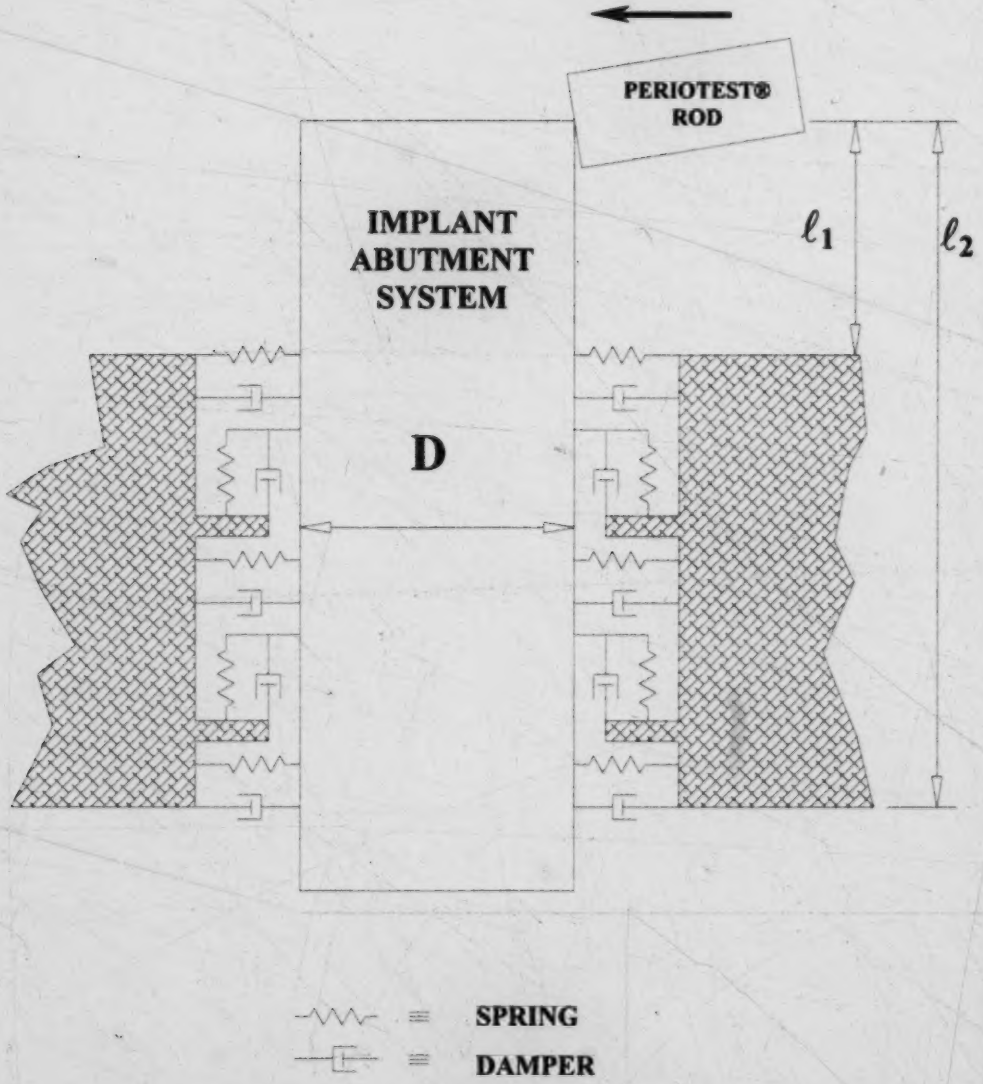

FIGURE 2-2: Proposed Mathematical Model of Periotest® and Implant System

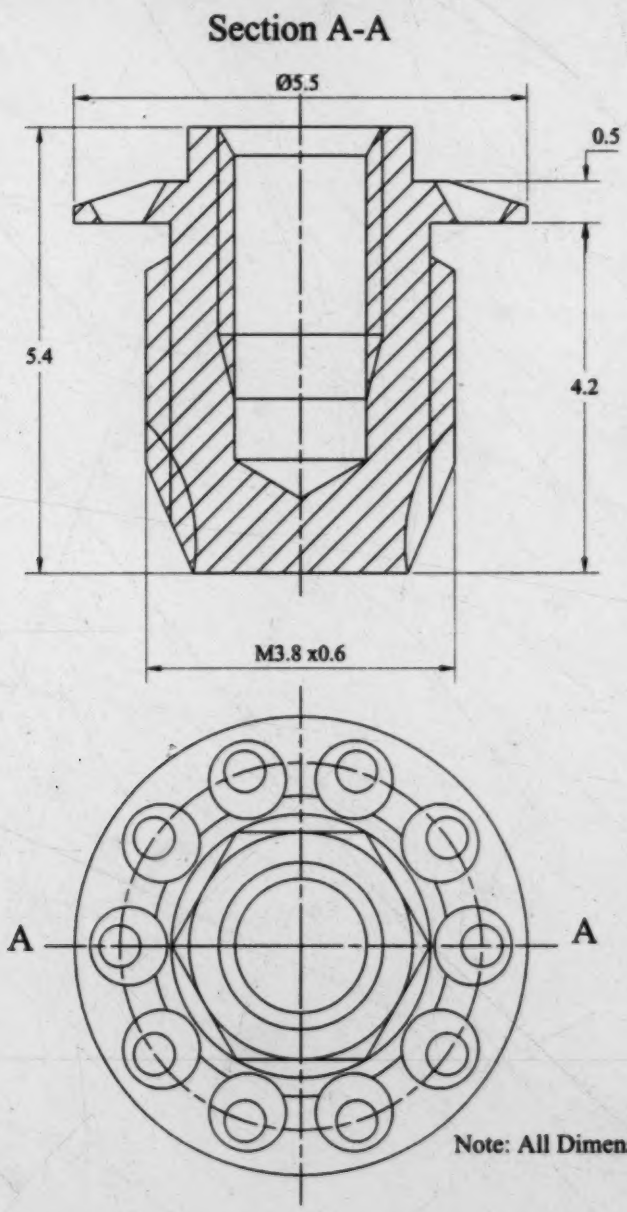

FIGURE 2-3: Typical 4mm Brånemark Flanged Implant Detail

Note: All dimensions in mm

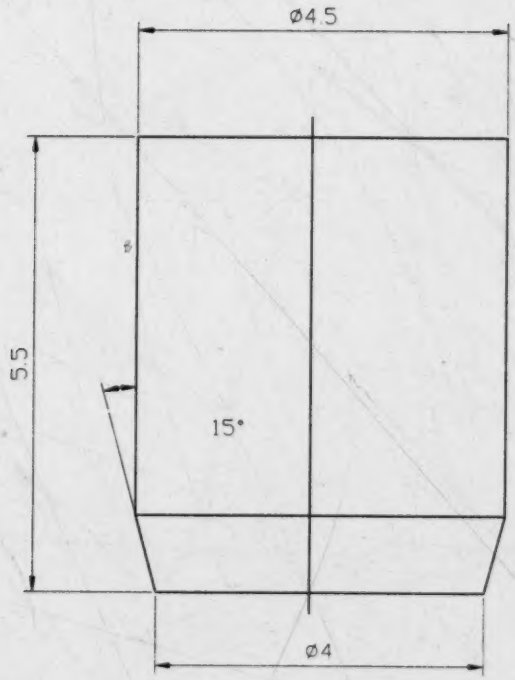

FIGURE 2-4: Typical 5.5mm Brånemark Abutment

Note: All dimensions in mm

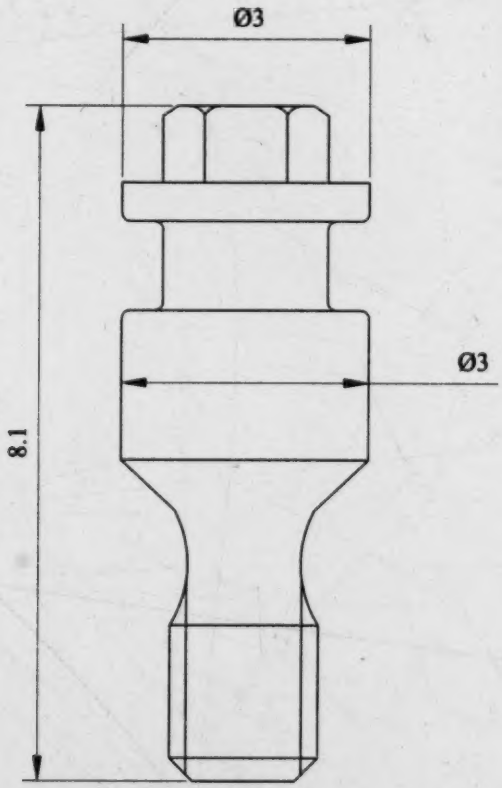

FIGURE 2-5: Typical Brånemark Abutment Screw

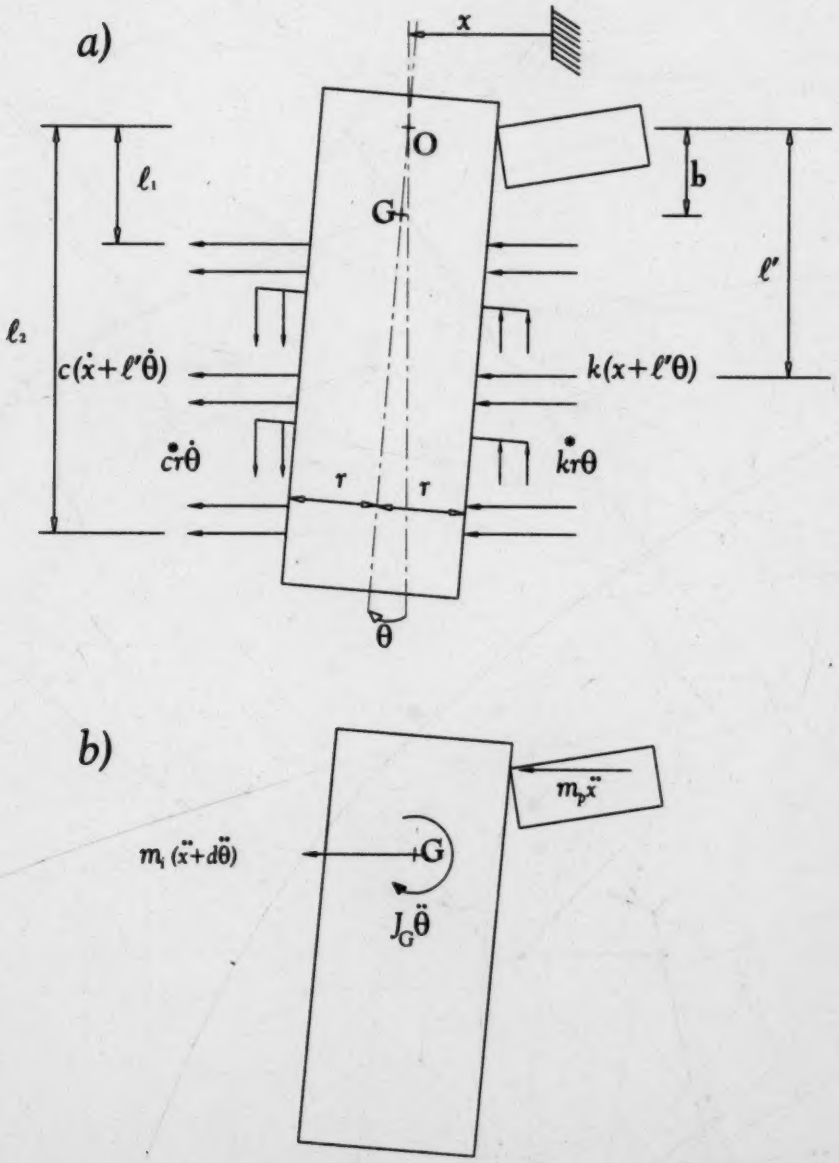

FIGURE 2-6: a) Free Body Diagram and b) Mass-Acceleration Diagram

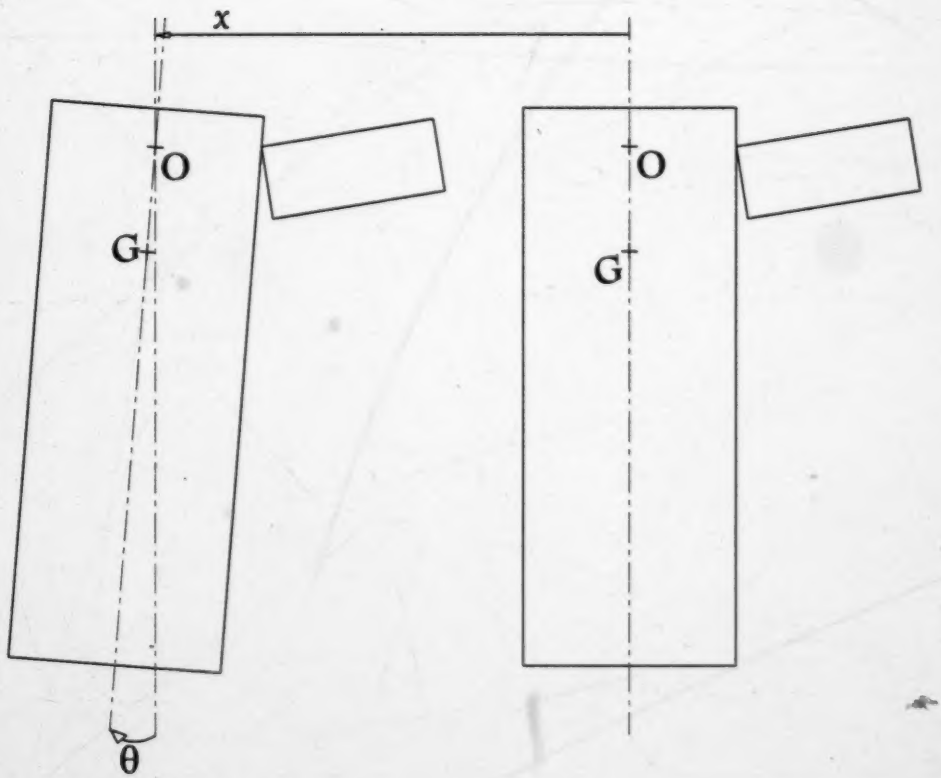

FIGURE 2-7: Generalized Co-ordinates of the System

Chapter 3

Testing Methods and Materials

3.1 Introduction

In the previous chapter, a dynamic model was developed to describe the Periotest®/implant system and ultimately predict the PTV. The system parameters required as input are the geometry of the implant, the length supporting tissue/implant osseointegration, as well as the relative stiffness and damping mechanical properties of the tissue in both the vertical and horizontal directions. While the geometry of the implant is known, and the effective length of osseointegration for only intraoral implants can be estimated from radiography or at time of surgical implantation, the stiffness and damping properties are difficult to obtain.

In this chapter, both an *in vitro* study and an *in vivo* study are described. The aim of the *in vitro* study is to measure the effect of changing system parameters on the PTV

and to compare these with the predictions of the dynamic model. An *in vitro* study allows for the testing of the implant/Periotest® system under controlled circumstances by considering the response of the system to changes in only one particular variable at a time. The results should provide a clearer understanding of the significant parameters affecting the PTV to provide guidance for clinical application of the instrument. The *in vivo* study was a longitudinal study of 11 patients over the course of approximately one year. The intention of this phase was to detect any changes in PTV and relate them to changes in the status of the implant osseointegration.

3.2 Materials and Methods

3.2.1 Modified Periotest®

A standard Periotest® unit was modified so that the resolution of the output could be increased from ±1PTV. To this end, the Periotest® accelerometer signal was measured directly from pin #1 of the M8930 Lf 442CN integrated circuit inside the Periotest® unit (Figure 3-1) and monitored using a digital data acquisition system. This analog accelerometer signal was used to calculate the PTV external to the Periotest® software. The intent here is to utilize the accelerometer signal directly before any signal processing or conditioning is done.

3.2.2 Data Acquisition System

The data acquisition system digitized the analog output signal of the Periotest® accelerometer for each of the 16 strikes of the Periotest® impacting rod and calculated the PTV with higher precision.

For this purpose, an instruNet ultra high accuracy, high-speed data acquisition system was used in conjunction with a Pentium II 300MHz laptop. Custom-made software for the user interface was developed according to the data collection requirements. This software was developed to allow the user to rapidly set up the system for quick easy testing and displaying of Periotest® accelerometer signal.

Properly capturing the Periotest® accelerometer signal with the instruNet A-D converter required knowledge of the typical range of signal frequencies produced by the Periotest®/implant system. According to sampling theorem (Proakis & Manolakis 1996), the sampling rate F_s of the instruNet must be set for a given analog signal and this rate is set by knowing the maximum frequency (minimum contact time) of the signal. The minimum contact time CT that the Periotest® measures in terms of PTV is -8 PTV. Recall Equation (1.1), which relates contact time to PTV

$$PTV = 50 \times CT - 21.3 \qquad (1.1)$$

So that a PTV of –8 corresponds to a CT of 0.266 milliseconds. This in turn corresponds to a period of vibration of 0.532 ms and a frequency of 1879 Hz. In order to properly reconstruct the analog signal of the Periotest® while avoiding the problems of aliasing,

the sampling rate must be greater than twice the maximum frequency present in the analog signal. As a result, in order to capture the Periotest® signal without aliasing, the sampling rate should be set to 4 kHz or more. Attaining a 4 kHz sampling rate was not a problem for the instruNet system, which can sample at 167 kHz. In fact, the sampling rate was set to this maximum in order to capture the signal as precisely as possible. The data was collected in a strip chart style resulting in 666,664 points for the 4 second test. In order to capture the one scan when the Periotest® handpiece is activated, a software trigger is set to start the recording when a threshold voltage of –0.05 volts DC is detected with a negative slope. The digitization is stopped when all 666,664 points have been recorded.

Figure 3-2 is an image of the Periotest® output captured using the custom made user interface software. The top signal shows the voltage recording from the accelerometer for all 16 impacts over a 4 second interval. Here voltage and time are plotted on the y-axis and x-axis respectively. The lower signal is an enlargement of one of the 16 impulses. It is important to note that the contact time is very short, in the order of a tenth of a millisecond. From this signal, an algorithm was developed to calculate the PTV from the 16 impacts recorded during a single test. The algorithm would initially sweep through the data from a test and determine how many impacts occurred by detecting the large amplitudes. Once the value of each amplitude was known, the algorithm detects the voltage value, which would correspond to Point A in Figure 3-3 and record the time. The algorithm would then step forward from the original detected amplitude and record the time for Point C. Knowing these two times, the contact time is

determined and the PTV calculated using Equation (3.1) for that particular impact. The algorithm would repeat this procedure until the PTV for all impacts of that test session were calculated. The PTV for a specified test was calculated by averaging the PTV of all detected impulses.

3.2.3 Testing Discs

To simulate supporting tissue that might be found in the craniofacial area, it was desirable that the testing material have a modulus of elasticity of the same order of magnitude as cortical bone. Typically, an implant completely integrated into cortical bone would represent the stiffest system. The material chosen was Photoelastic FRB-10 plastic (Measurements Group Inc., P.O. Box 27777, Raleigh North Carolina, USA, 27611) with an elastic modulus of 9.3 GPa (the approximate value for cortical bone is 14.0 GPa). While the FRB-10 has a Young's modulus similar to cortical bone no attempt was made to simulate the characteristics of damping. Four 41.25mm diameter discs were made from FRB-10 as shown in Figure 3-4. The thickness of each disc was 1.87mm, 2.78mm, 3.83mm, and 4.78mm. A hole was drilled through the center of each disk and then tapped appropriately. A 4mm flanged extraoral craniofacial implant (SEC 002) of the Brånemark system (Entific Medical Systems, North York, Canada) was inserted into each of the previously tapped holes (Figure 3-5) using a Torque Controller (Nobel Biocare, Götenborg, Sweden) set at 45 Ncm. Finally, a 10mm abutment (SDCA 043, Nobel Biocare, Götenborg, Sweden) was secured to each implant with an abutment screw, which was preloaded to a 20 Ncm torque with the torque controller. The 10mm

abutment was an intraoral abutment. The abutment screw of the intraoral abutment was shortened to allow the abutment to be connected to an extraoral flange implant. The testing of the discs was conducted by securing each disc in turn into a holding plate (Part A of Figure 3-6) using two screws and washers. This plate, in turn, was clamped down to the testing table (Part B of Figure 3-6).

3.2.4 Testing Apparatus

The testing table, shown in Figure 3-6 (Part B), is the same one used by Derhami et al. (1995) along with the remainder of the testing apparatus. The testing table is connected to the metallic base via a ball joint (Part C, Figure 3-6) that can be locked to ensure parallel positioning of the testing table with the floor. The large base (Part D, Figure 3-6) of the testing table functions as a flat metallic surface for anchoring the magnetic dial indicator (Part E, Figure 3-6), and the Periotest® handpiece holding unit (Part F, Figure 3-6). The Periotest® holding unit allows for both coarse vertical and angular positioning of the handpiece. In addition, a fine adjustment screw located on the Periotest® holding unit allows for fine vertical position adjustment of the Periotest® handpiece. The pitch of the fine adjustment screw allows for vertical displacements of 0.5mm/revolution. However, the use of a dial indicator, with a resolution of 0.0254mm (0.001inch), provided a more precise method for measuring the vertical displacement of the Periotest®. The dial indicator was attached to a magnetic based post that allowed for easy positioning around the testing table as well as quick anchoring onto the testing table. The dial indicator was placed onto the Periotest® holding unit.

The Periotest® handpiece was secured to the holding unit by means of a friction fit. The front of the handpiece was inclined at approximately 5 degrees below the horizontal to ensure only one point of contact between the Periotest® and the implant system during impact. This incline is well within the range (±11 degrees to the horizontal) for the proper operation of the Periotest® unit A (Lukas & Schulte 1990). This angulation is important for consistent PTV results and will be considered further in what follows.

The Periotest® handpiece was then positioned so that the impacting rod would make lateral contact with the abutment. The horizontal distance between the tip of the Periotest® handpiece and the abutment was kept within the 0.5 to 2.5mm range specified in the Periotest® operating instructions.

The vertical position of the Periotest® rod impact was measured with respect to the surface of the anchoring material. The initial testing position was established so that the upper tip of the Periotest® impacting rod would make contact with the top edge of the 10mm abutment. It is important to note that the flanged component of the implant protrudes 0.5mm from the surface of the anchoring tissue and the abutment connects flush to this surface. As a result, the upper end of the abutment is 10.5mm above the surface of the disc. A cathetometer (Griffin & George Ltd, Great Britain) (Figure 3-7) was used to verify that the impact of the Periotest® rod just below the coronal platform edge of the abutment (Teerlinck et al. 1991).

3.2.5 Testing

The Periotest® was calibrated before and after each testing session with the standard calibration sleeve (at a PTV of 12) to ensure that the output of the Periotest® had not drifted during the course of the testing. According to the Periotest® operating instructions, deviations greater than ± 2 PTV may indicate a malfunction.

The Periotest® was set at a vertical height of 10.5mm (crown of the abutment) above the surface of the anchoring disc. A total of 4 tests (4x16=64 impacts) were completed for each position along the longitudinal axis of the abutment. The PTV was calculated using the algorithm developed. In addition, the PTV from the Periotest® unit was recorded for each test and then averaged for each position. After each test the Periotest® would be repositioned 0.25mm lower using the adjustment screw located on the handpiece holding unit. The testing would continue until the Periotest® reached a height of 4.5mm. It was not possible to take Periotest® measurements below this height as the thickness of the sheath of the impacting rod has a diameter of 5mm.

3.2.6 Strain Gauged Abutment

To confirm that the output of the Periotest® accelerometer was actually monitoring the motion of the Periotest®/implant system, a 10mm abutment (SDCA 043, Nobel Biocare, Götenborg, Sweden) was instrumented with 2 precision strain gauges (EA-06-015EH-120, Micro-Measurements Division, Measurements Group Inc. Raleigh, North Carolina, USA). This allowed a measurement of both the motion of the Periotest®/implant system when in contact and the free vibration of the implant system

after separation. The output from the gauges corresponds to a measurement of the strain at a particular point on the abutment and is independent from the accelerometer signal of the Periotest®.

Figure 3-8 shows the lead wires of the 2 precision strain gauges connected to the bottom surface of the 10mm abutment. The placement of the gauges near the root of the abutment allows the maximum strain in the abutment to be measured. The two gauges are arranged in a half bridge circuit used for measuring the bending of a beam. The strain gauge leads were connected to a Vishay 2100 series strain conditioner and amplifier system and from there the signal was fed into a Tektronics TDS H10A digital oscilloscope for sampling and viewing the signal. The sampling rate was set to 500 000 samples/sec. After attaching the gauges, the abutment was screwed into the 2.78mm testing disc and then into the testing apparatus described before in Section 3.2.2. The Periotest® was then used to cause a single impact on the abutment near the crown of the abutment. The signal from the Periotest® accelerometer and strain gauged abutment were captured and displayed using the same equipment.

3.2.7 *In Vivo* Testing

A longitudinal *in vivo* study was conducted with the aid of COMPRU (Craniofacial Osseointegration And Maxilliofacial Prosthetic Rehabilitation Unit, Misericordia Hospital, Edmonton, Alberta, Canada) to assess the ability of the Periotest® to detect any trends in patient implant healing. The study consisted of 11 patients requiring a Bone Anchored Hearing Aid (BAHA®, Entific Medical Systems, North

York, Canada). Each patient had one 4mm flanged extraoral craniofacial implant (SEC 002, Entific Medical Systems, North York, Canada) surgically implanted into the mastoid portion of the temporal bone (Figure 3-9). A BAHA® abutment (SHCC 034, Entific Medical Systems, North York, Canada) is attached. Testing of the implant systems with the Periotest® was conducted at 4 intervals beginning at surgical implantation and continuing at 3 months, 6 months and 1 year. The Periotest® used is the same system outlined in Section 3.2 for the *in vitro* testing. Typically, 4 tests were taken with the handpiece held parallel to the floor and perpendicular to the long axis of the abutment so that impact could be made at the rim of the BAHA® abutment. A second set of 4 tests was conducted, which assessed the axial health/stiffness of the peri-implant tissue, with the handpiece held along the long axis of the implant system. Due to the geometric restrictions of both the BAHA® abutment and the handpiece housing, the axial tests were not perfectly along the axis, but at the outer edge of the BAHA® abutment rim.

3.3 Results

The results from both the *in vitro* and *in vivo* studies are provided in Chapter 4. A comprehensive comparison of these results with the numerical model developed in Chapter 2 is aimed at providing a better understanding of the parameters influencing PTV.

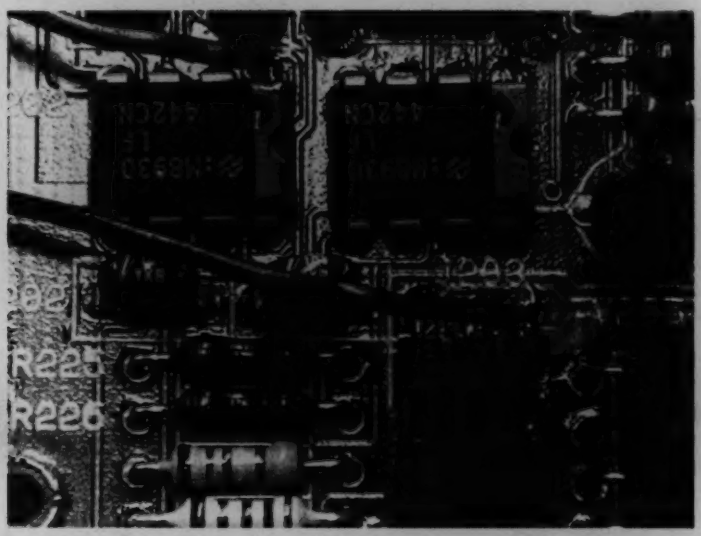

FIGURE 3-1: Periotest® Modification for Data Acquisition System Connection

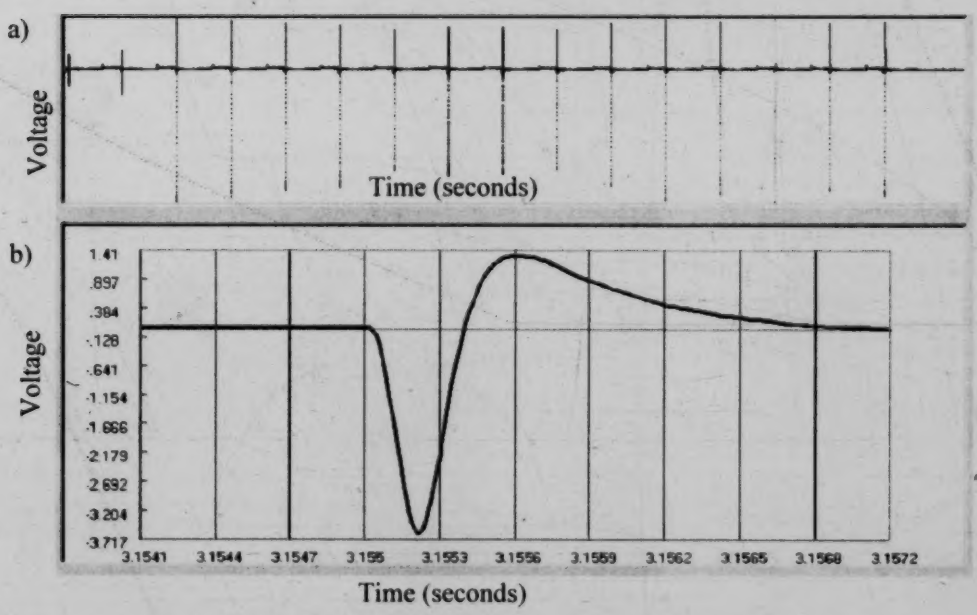

FIGURE 3-2: Periotest® Accelerometer Signal Displayed
a) All Sixteen Impacts
b) One impact shown with an expanded time scale

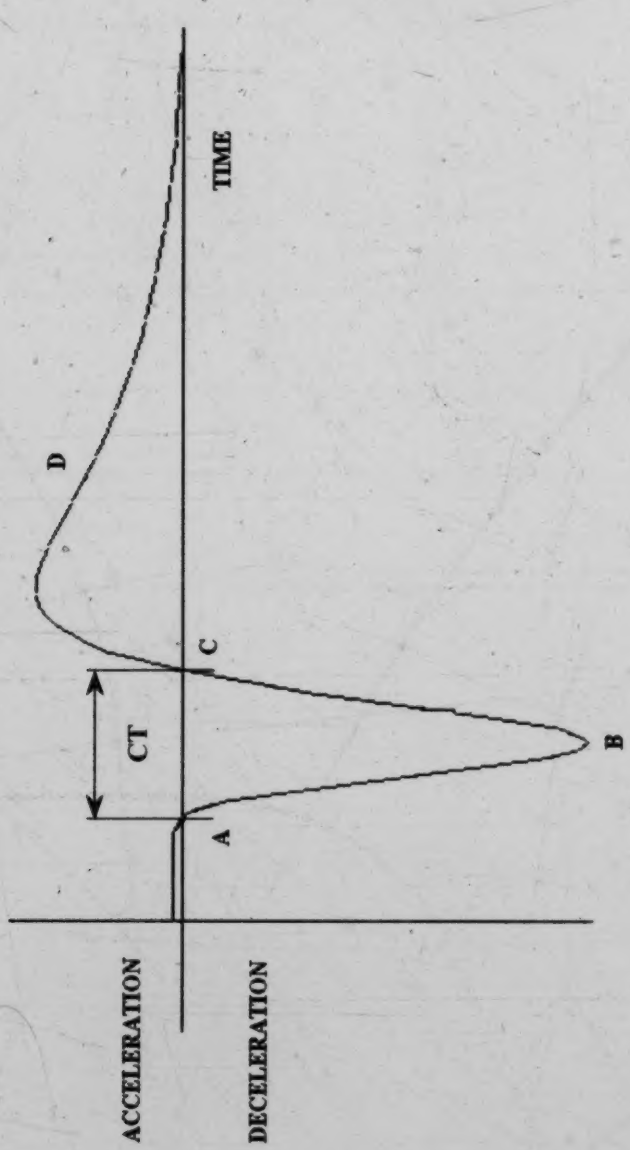

FIGURE 3-3: Typical Periotest® Accelerometer Signal

Tolerance: ± 0.025mm
Material: Photoelastic Plastic FRB-10

A
1.87 mm
2.78 mm
3.83 mm
4.78 mm

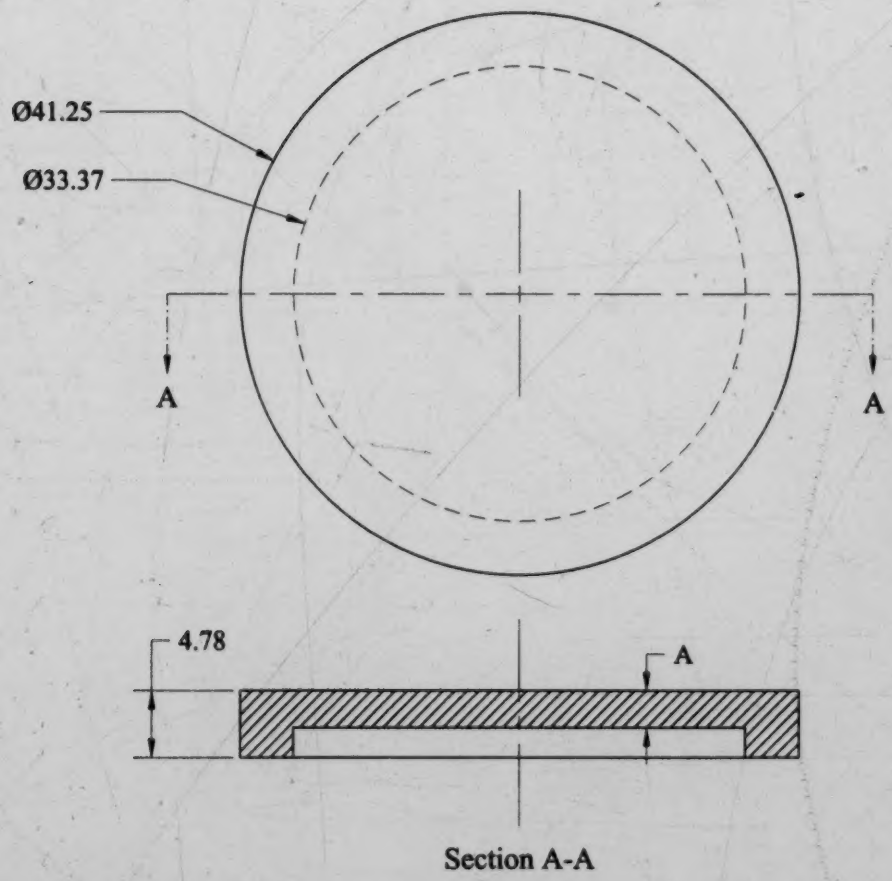

FIGURE 3-4: Machine Drawing of the *In Vitro* Testing Discs

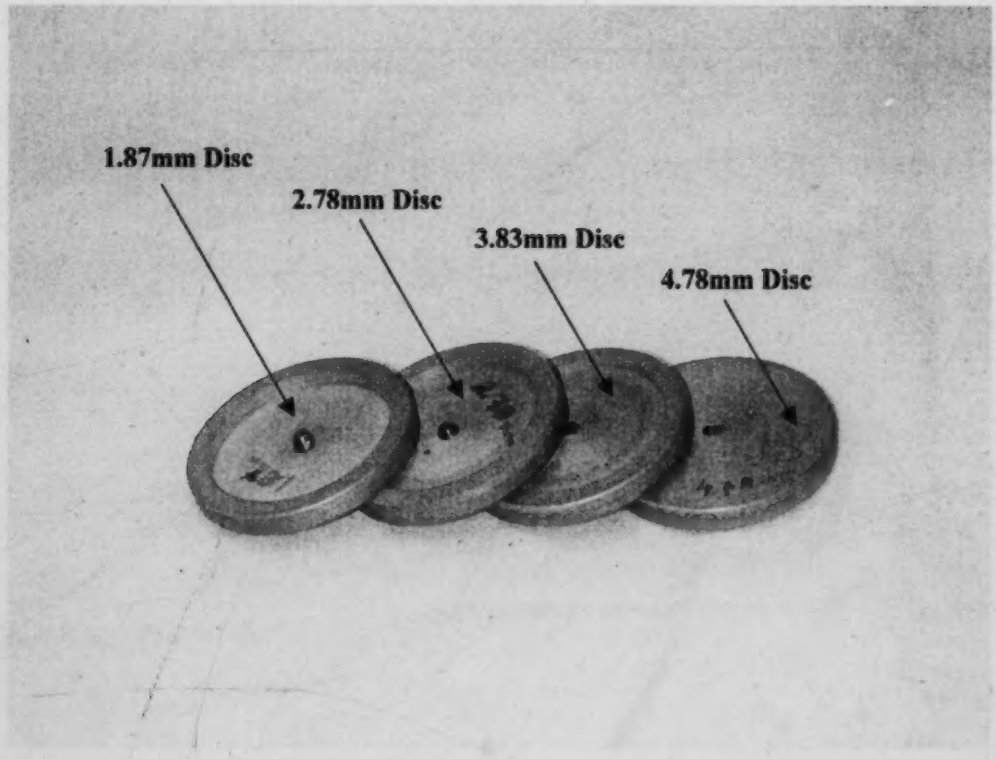

FIGURE 3-5: *In Vitro* Testing Discs

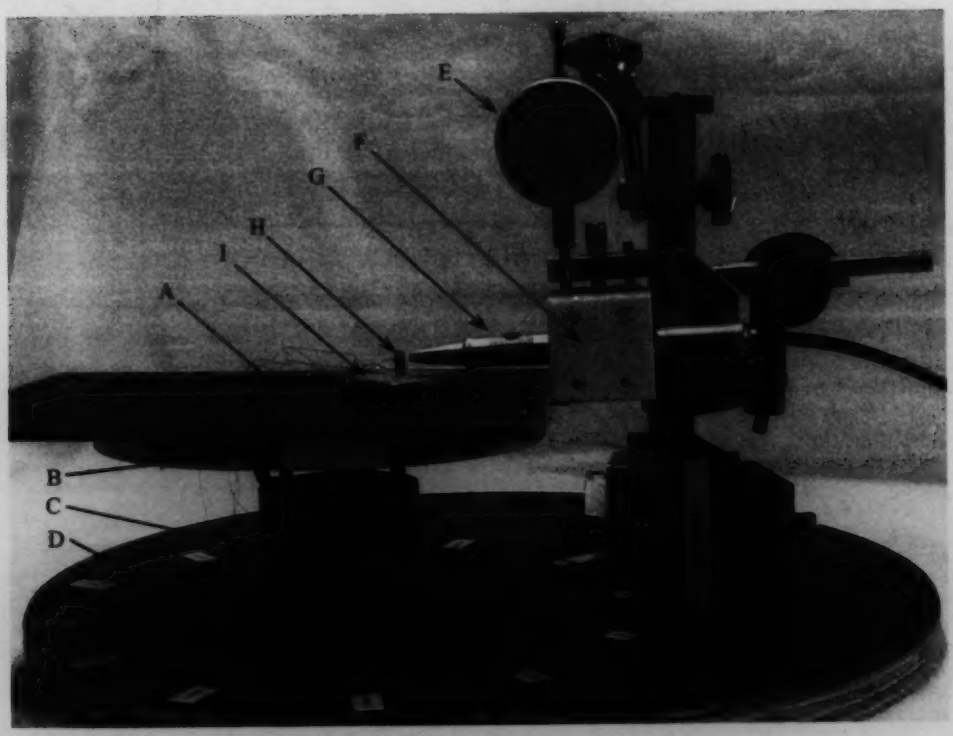

FIGURE 3-6: *In Vitro* Testing Equipment

A) Holding Plate for *In Vitro* Disc
B) Testing Table
C) Ball Joint
D) Metallic Base
E) Dial Indicator with Magnetic Base
F) Periotest® Handpiece Holding Unit
G) Periotest® Handpiece
H) 10mm Abutment
I) *InVitro* Disc

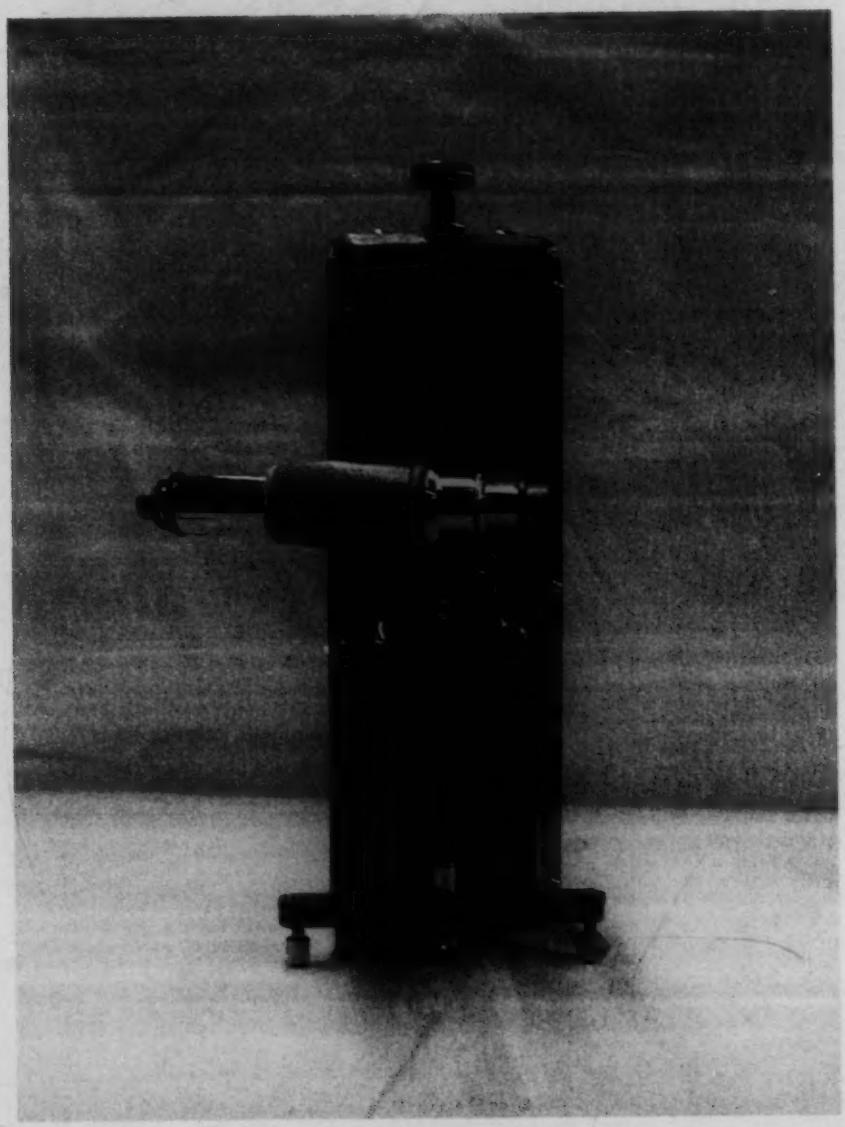

FIGURE 3-7: Cathetometer (Griffin & George Ltd.)

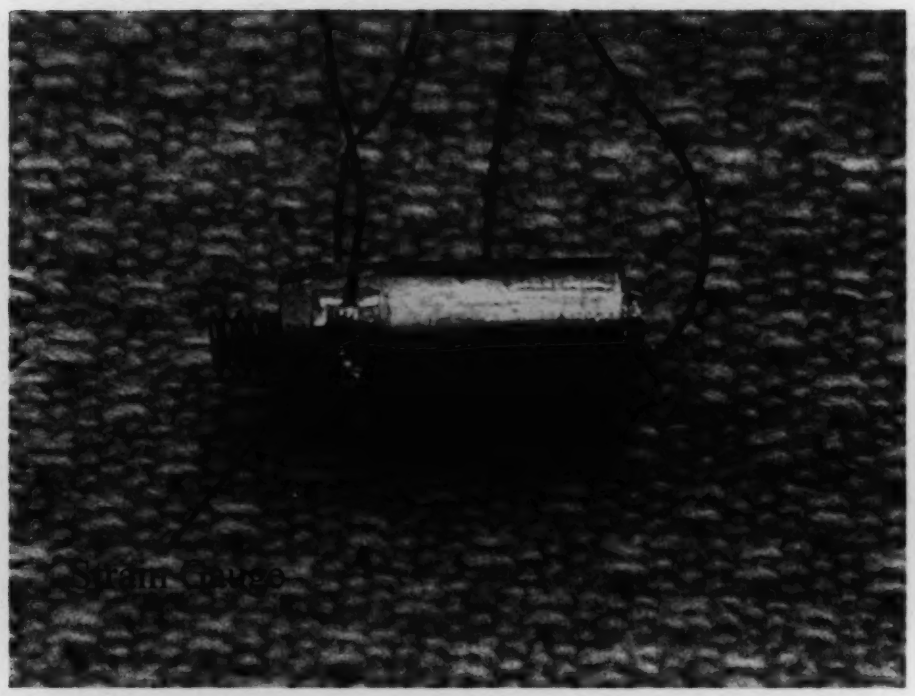

FIGURE 3-8: Strain Gauged 10mm Abutment

FIGURE 3-9: Surgical Location for BAHA® Implant Placement

Chapter 4

Results & Discussion

The aim of this thesis is to provide an analysis of the Periotest® by developing a 2 degree of freedom model which explains the dynamical interaction between the Periotest® and the implant system and validate this model with an *in vitro* study. Both the model and *in vitro* study account for variation in Periotest®/implant system parameters such as implant length and diameter, supporting tissue mechanical properties, and striking height, which have been considered to have an influence on the PTV. In addition, a longitudinal *in vivo* study using the Periotest® was conducted on 11 BAHA® (bone anchored hearing aid) patients with the aim of assessing the mechanical performance of craniofacial implants over the short term and possibly detecting any healing trends. The results and findings from the theoretical model as well as both the *in vitro* and *in vivo* studies have been collected and are presented in this chapter.

4.1 Strain Gauge Results

4.1.1 Contact Time Validation

One component of the *in vitro* study was the testing of an abutment instrumented with strain gauges. The intent of this experiment was to simultaneously monitor the independent output of both the Periotest® and the strain gauges as a check on the assumption that the impacting rod and abutment are actually in contact during the time in which the contact time is measured. The results of a typical impact test are given in Figure 4-1 showing both the strain gauged abutment signal and the corresponding Periotest® accelerometer signal. The large amplitude of the abutment strain gauge signal occurs at precisely the same time as the Periotest® signal (Point A), indicating that the rod has made contact with the implant system and has begun to decelerate. It is important to note that the duration of both signals is identical, indicating that the rod remains in contact with the abutment until both signals become positive. This result suggests that the contact time used for determining the PTV is truly the time for which the rod is in contact with the implant system and thus confirming the findings of Lukas and Schulte (1990).

4.1.2 Damping Behaviour of FRB-10

The strain gauged abutment test also provides an indication of the very low damping in the FBR-10 discs. After the Periotest® rod and the implant have separated (Point C Figure 4-1), the strain gauges continue to detect the motion of the implant

system due to free vibration. It is important to note that the amplitude of each successive period of vibration is only slightly less than the previous and that the signal requires many periods of vibration before the system is back at rest. This is an indication of very small damping. This type of damping may or may not be typical *in vivo* and therefore a similar test *in vivo* to assess the damping properties of the supporting tissue would be desirable.

4.2 *In Vitro* Testing Results

One aspect of the *in vitro* study was to investigate the effect of changing system parameters such as length of supporting tissue/implant engagement and impacting position have on the PTV. The results of the *in vitro* testing are shown in Figure 4-2. The thinnest disc (1.87mm), which simulates the least amount of tissue anchorage, is the most sensitive to changes in striking position. For example, assuming a starting striking position is 6mm with an associated PTV of 0.5 and the position is then set at 8mm above the tissue level, which provides a 4.5 PTV. This is an increase of 4 PTV for a change in striking position of 2mm. This trend indicates that for a given thickness of supporting tissue, the PTV will decrease as the striking height decreases. It is important to note that the sensitivity to striking height for the longer lengths of tissue anchorage is not as prominent as it is for the thinnest disc. Another trend indicates that for a constant striking height the PTV will decrease with an increase in supporting tissue thickness.

4.3 Validation of the Dynamic Model using *In Vitro* Testing

4.3.1 The *In Vitro* Theoretical Model

Another aspect of the *in vitro* testing was the validation of the numerical model potential to assess the PTV as a result of changing striking position and the height of tissue/implant engagement. However, before the theoretical model can be applied, simplification of the model is required to better represent the more specific *in vitro* scenario. It has been determined that the FRB-10 supporting tissue has very low damping and therefore by assuming that the model has negligible damping the equations of motion reduce to

$$\begin{bmatrix} 0 & 0 \\ 0 & m_p \end{bmatrix} \begin{Bmatrix} \ddot{\theta} \\ \ddot{x} \end{Bmatrix} + \begin{bmatrix} \frac{k}{3}\left(\ell_2^3 - \ell_1^3\right) + k * r^2\left(\ell_2 - \ell_1\right) & \frac{k}{2}\left(\ell_2^2 - \ell_1^2\right) \\ \frac{k}{2}\left(\ell_2^2 - \ell_1^2\right) & k\left(\ell_2 - \ell_1\right) \end{bmatrix} \begin{Bmatrix} \theta \\ x \end{Bmatrix} = \begin{Bmatrix} 0 \\ 0 \end{Bmatrix}. \qquad (4.1)$$

While the geometric variables of the system such as the height of impact above the tissue level and the height of tissue/implant anchorage are known, the relative vertical to horizontal stiffness is unknown. The stiffnesses were determined by fitting the model to the experimental data at two points. The first point was at a striking height (ℓ_1) of 7.5mm for the 1.87mm disc while the second point was selected at the same striking height but for the 2.78mm disc. The remainder of the theoretical results were then calculated using these values (Figure 4-2). The numerical predictions match the *in vitro*

results quite well for the larger lengths of supporting tissue/implant engagement but are still acceptable for the thinner discs.

4.3.2 Discussion of Supporting Tissue Quality

4.3.2.1 Sensitivity to Supporting Tissue Type /Stiffness

The developed model incorporates supporting tissue type by varying the magnitude of the stiffnesses, k and k^*, at the interface (Equation 4-1). These stiffnesses are related to the modulus of elasticity (E) of the supporting tissue and as a result, a cortical layer of supporting tissue with an E of 13.7 GPa would have a higher stiffness than that of a cancellous layer (E = 1.37 GPa). While only one layer of supporting tissue was tested *in vitro*, the model indicates that as the stiffness of the tissue increases, the natural frequency will also increase. This produces a lower period of oscillation (contact time), which ultimately lowers the PTV. This trend is shown in Figure 4-3 where the magnitude of the horizontal and vertical stiffnesses doubled while the ratio between the two stiffnesses is maintained.

The model predicts that by changing the ratio of the two stiffnesses result in a change in PTV (Figure 4-4). For each successive curve there is a doubling of the stiffness ratios. The upper curve (Case 1) exhibits the lowest stiffness ratio and illustrates how PTV is more sensitive to slight changes in striking height. As the stiffness ratio increases the PTV becomes less sensitive to changing striking height. These results show that there

is a dependence of PTV on the type of supporting tissue, which has been shown in clinical studies (Olivé and Aparicio 1990; Salonen et al. 1993; Salonén et al. 1997).

4.3.2.2 Sensitivity to Supporting Tissue Length of Engagement

The relationship of the tissue/implant engagement is shown in Figure 4-2 where the lowest curve represents the longest length of engagement (4.16mm) and the upper curve the least (1.87mm). While for the most part experimental and theoretical results show good agreement, the model does not appear to predict the response in the thinnest disc at the upper and lower extremes of striking height. This result could be due to the fact that there are a limited number of threads in actual contact with the supporting material. As there is a 0.5mm gap between the flange and the first thread of a 4mm Brånemark flanged implant (Figure 2-3), and as there is a pitch of 0.6mm, this results in only 2 threads in contact with the remaining 1.37mm of FRB-10. Usually *in vivo*, there are few situations where only 2mm of bone exist. Typically, the flat bones of the skull, into which these short implants are placed, have two cortical layers with intervening cancellous bone and are at least 3mm to 5mm thick. Although there is a change of only 1mm thickness between the 2.78mm engagement and that of the previous disc, it is really a change of 50% of the 1.87mm disc's thickness. This is evident when looking at the two curves and noting the 3 PTV negative shift for the 2.78mm disc. Correspondingly, the percentage change in thickness of the 2.78mm disc to the 3.83mm disc is around 33% and the drop in PTV is 2.5. As the thickness of the disc increases, which represents the

engagement length, the percentage change in increase is less than for the previous disk and thus the shift in PTV is less. Eventually, the curves for larger lengths of implant engagement will flatten and show little effect due to height variation. The results indicate that it is important to realise that it is the length of engagement between the supporting tissue and the implant and not just the implant length that influences the PTV.

To further illustrate the effect from long engagement lengths, consider the example of long intraoral implants. Typically, these implants have supporting lengths of 8 – 20mm while the abutments, with artificial tooth covering, are typically no longer than 5.5mm. Using the model developed and assuming that there is 10mm and 20 mm of tissue/implant engagement, yielded the lower two curves in Figure 4-5. It is important to note for the 20mm case that there is only a change of 1PTV for a 2mm change in height. This agrees with the study by Salonen et al. (1997) where 118 implants with lengths varying from 11mm to 21mm were placed in the lower jaw of human patients. Their results showed no variation in PTV for these implants.

It is noteworthy that the thickest disc in the *in vitro* study was 4.78mm but the maximum length of the implant is 4.16mm. As a result, the supporting material extended beyond of the implant. The effective length of engagement was 4.16mm, which was used in the dynamic model and from Figure 4-2 the theory from the model correlates quite well with the data from the *in vitro* study of this particular disc. As the Periotest® detected a change in the apical tissue/implant engagement length of as little as 0.33mm, which is the change in engagement length for implants in the 3.83mm and 4.78mm discs (4.16mm

engagement), this would mean that the Periotest® has the potential for detecting marginal bone losses of 0.5 - 1mm in the first year (Adell et al. 1986). Consider the example where there is a loss of 0.5mm of marginal bone shown in Figure 4-6. The loss of marginal bone decreases the length of engagement, which increases the striking height above the supporting tissue. Both effects will increase the PTV (Figure 4-7). For example, consider a 5mm abutment attached to an implant anchored in 3.83mm of supporting tissue (Point A). For a marginal loss of 0.5mm the striking height will increase to 5.5mm and the length of tissue anchorage will decrease to 3.33mm (Point B) and results in a PTV change of 1.5. Therefore, marginal bone loss around the periphery of the implant can significantly affect the PTV.

4.3.3 Sensitivity to Implant Diameter

Although the *in vitro* testing did not incorporate any variation in implant diameter, the model did. Equation (4.1) shows how the stiffness of the supporting tissue is dependent upon the radius squared of the implant r^2. As the radius r of the implant increases, the stiffness of the system will increase which results in a lower PTV. Figure 4-8 shows the numerical results of the model when considering the affect from changing the diameter of the implant from 3.75mm to 5mm for a given thickness of tissue anchorage. The trend shows that for the 5mm diameter implant the change in PTV is less sensitive to changes in striking height than for the 3.75mm diameter implant. As a result, any indication of a change in PTV will correspond to a large change in the supporting

tissue structure at the interface for a larger diameter implant. The curves show that the overall PTV values for the 5mm diameter implant are lower than the PTV of the 3.75mm diameter implant. Therefore, the theoretical model confirms the hypothesis that Drago (2000) had with regard to implant diameter affecting the PTV.

4.3.4 Discussion of Testing Protocol

4.3.4.1 Sensitivity to Striking Height

Both the model and *in vitro* testing show that the striking height along the abutment has a major affect on the PTV. As the striking height above the coronal platform of the implant is increased, the lower the PTV (Figure 4-2). This trend is in good agreement with other studies (Teerlinck et al. 1991; Derhami et al. 1995; Meredith et al. 1998; Haas et al. 1999; Drago 2000).

4.3.4.2 Sensitivity to Handpiece Angulation

In Chapter 3, the testing procedure required the Periotest® handpiece to be positioned with a negative incline of approximately 5 degrees from the horizontal to ensure only one point of contact between the Periotest® and the implant system during impact. It is important to note that the surface of the impacting head is a 2mm diameter circular flat surface. In addition, the surface of the implant is relatively flat which makes it difficult for the two surfaces to mate perfectly, especially if there is a slight amount of angulation of the handpiece. If the impacting rod were to strike the surface of the implant

with a slight angle either upwards or downwards there could be a height variation of 2mm as shown in Figure 4-9. The effect of a 2mm variation in striking height can be seen directly from Figure 4-2. These variations are greater than 3 PTV for the thinnest disc and approximately 1.5 PTV for the thickest. Therefore it is extremely important to have a consistent way of using the Periotest® instrument with consistent angulation.

4.3.4.3 Comparing Kaneko Rotational Model (1994) with *In Vitro* Data

An early Periotest® model by Kaneko (1994) was introduced in Chapter 1 which showed the dependence of PTV on the striking height h, the length of engagement h' and the stiffness of the supporting tissue using the effective stiffness Equation (1.4).

$$k_{eff} = k\left[\frac{h'}{h+h'}\right]^2 \tag{1.4}$$

Applying the same procedure that was used to validate the model from Chapter 2 yields the results shown in Figure 4-10. There is poor correlation between the *in vitro* data and Kaneko's model. The slopes of the model curves are greater than those of the *in vitro* testing. This indicates that there is a more drastic change in PTV for a change in height, which was not the case *in vitro*. For example, consider a craniofacial implant of 4.16mm engagement length and consider the possibility of a change in striking height of 2mm. The Kaneko's model would detect a change in PTV of about 5 compared with the experimentally determined variations of 1.5. Also consider the sensitivity of the model to

a 2mm change in engagement length. From Kaneko's model, there should again be a change in PTV of 5. It is felt that the more accurate two degree of freedom model developed in this thesis gives a better match to measured data.

4.4 Periotest® Calibration and Resolution

4.4.1 Calibration

The calibration procedure for the Periotest®, which was explained earlier in Chapter 3, was intended to test the mobility of natural dentition. Judging by the Miller Index in Table 4-1 [Lukas D. & Schulte W. (1990)], which has been used to evaluate mobility of teeth, there is a range of 4 levels indicating different degrees of tooth mobility. A stable tooth would be assessed a 0 where as at the other extreme, a level III would be given for a tooth with a high degree of mobility. This range corresponds to a PTV range of 0 to 30 respectively. Logically, the manufacturers of the Periotest® device set the calibration of the Periotest® to be 12 PTV, which is near the mean of the mobility range for normal dentition. Unfortunately, this is not the typical Periotest® output range of -2 to -6 PTV for both intra- and extraoral implants. It is important to note that this range is relatively very small compared to the range for natural dentition. Therefore, in order to practically apply the Periotest® for testing craniofacial implants, the device should be calibrated within this smaller range of PTVs.

Table 4-1: The Relationship Between Contact Time, Periotest® Value and Degrees of Mobility

Contact time (ms)	Periotest® Value	Degree of Mobility (Miller Index)
1.21	30	III can be moved with labial pressure
0.86	20	II mobility can be see
0.626	10	I mobility can be felt
0.506	4	0 stably anchored
0.426	0	Ankylosis (without periodontium)
0.266	-8	

Another issue which is of concern when calibrating the Periotest® device is the acceptable deviation of PTVs about the calibration PTV of 12. From the Periotest® operating instructions manual, the Periotest® can be considered calibrated if the PTV from using the calibration sleeve is with ±2 PTV. This is a range of 4 PTV, which is near the range expected for craniofacial implants. This lack of sensitivity is due primarily to the limited resolution of the Periotest® output.

4.4.2 Resolution of the Periotest®

The output of the Periotest® is displayed on the instrument's liquid crystal display as an integer value, with a resolution of ±1PTV. This resolution is too coarse in the operating range for implants and thus limits the usefulness of the instrument. This coarse resolution can account for the lack of correlation between parameters and PTV noted by previous investigators. The problem is accentuated for the longer implants as there is relatively little change in PTV for changes in implant/tissue engagement or striking height. This can be seen in Figure 4-11, which shows *in vitro* testing results of the

Periotest® output LCD compared with the theory for changes in tissue thickness and striking height.

4.5 *In Vivo* Results

A longitudinal *in vivo* study was conducted in conjunction with COMPRU to assess the ability of the modified Periotest®, to detect any trends in healing of the patients with new implant placements. In the study, 11 patients requiring Bone Anchored Hearing Aids (BAHA®) were to be tested at implantation, 3months, 6 months and 1 year intervals with the Periotest®.

The PTV values for the lateral tests at surgical implantation ranged from –5 to 1 PTV, which according to Schulte & Lukas (1993) is an indication of good bone anchorage. They considered an osseointegrated intraoral implant to fall within the range of –8 to +5 PTV. Over the duration of 1 year, the lateral test PTVs for the entire testing group remained within the –5 to 1 range. Both the *in vivo* results as well as the lack of implant failures indicate good level of osseointegration for all implants.

The indication of a healing trend is not apparent from any of the data on the 11 patients (Appendix B). As an example consider the trend for patient #00895 (Figure 4-12), where the PTV at day 0 is -2 then substantially drops to -3.75 at 3 months, then to -4 at 6 months and then jumps to -1.5 at 1 year. This trend would seem to indicate that the stiffness of the supporting tissue increased over the first 6 months but only to decrease in the second half of the study. Another contradiction in the *in vivo* results for patient

#00895 was lack of consistency between the lateral and axial testing. The lower curve on Figure (4-12) indicates that the vertical stiffness of the supporting tissue is progressively increasing over the year of testing. This would imply that the last data taken at 12 months is not a true indication of the supporting tissue stiffness. Unfortunately, there was no way of comparing the data from the Periotest® unit with the data from the data acquisition system because of the accidental addition of a low pass filter to the Periotest® unit. In effect, this filter allowed only signal having a PTV of -2 to be recorded. Any signal with a PTV lower that -2 would be recorded as a -2PTV signal. This filter was later removed (June 2000) so that actual accelerometer signal could be captured.

The lack of a rigorous clinical testing protocol may also have contributed to the lack of a trend in the *in vivo* data. At the start of this clinical study an appreciation of the effects of the variations in striking height, striking position, handpiece angulation were not realized. The clinical staff taking the measurements did not maintain a uniform technique and therefore it is difficult to compare PTV values taken at different dates. A recommended revised protocol is presented in Appendix C.

The calibration of the Periotest® should also be considered. The large variation allowed by the manufacturer could easily mask the changes being sought.

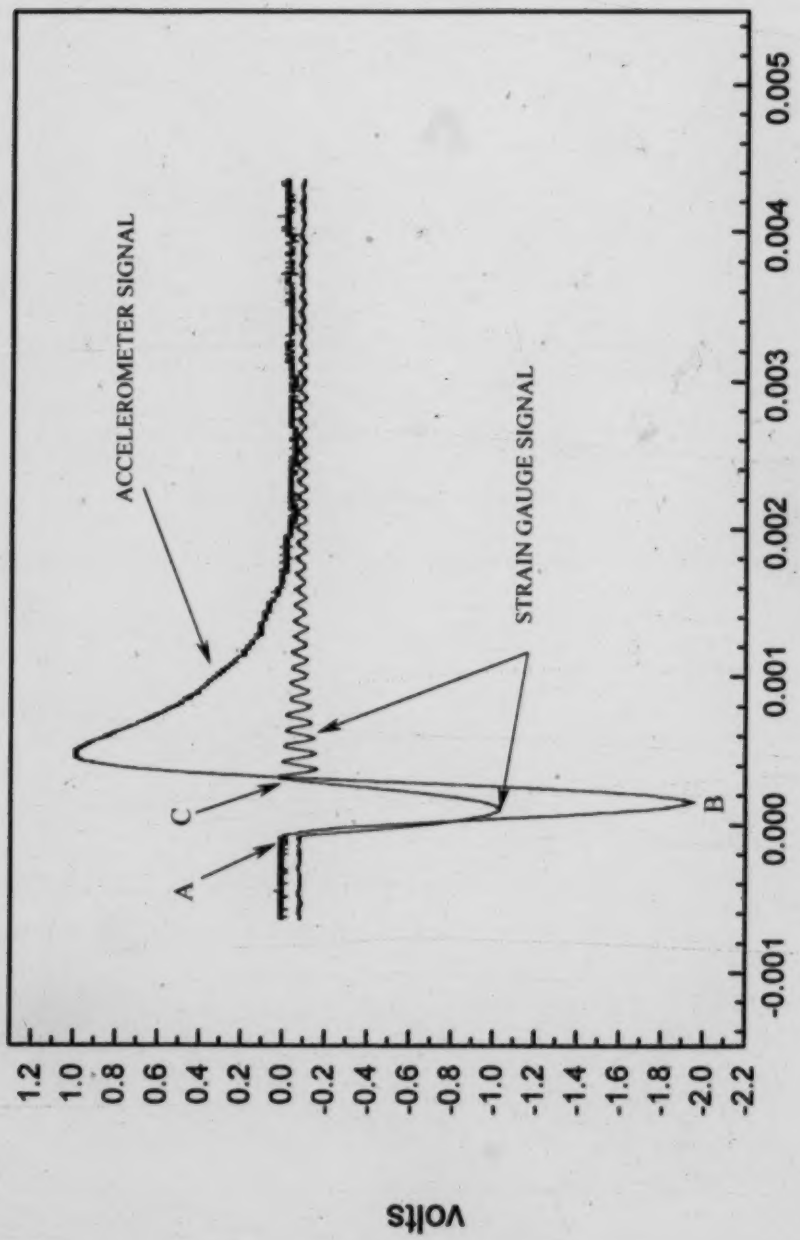

FIGURE 4-1: Comparison of the Periotest® Accelerometer Signal with the Strain Gauged Abutment Signal for One Impact.

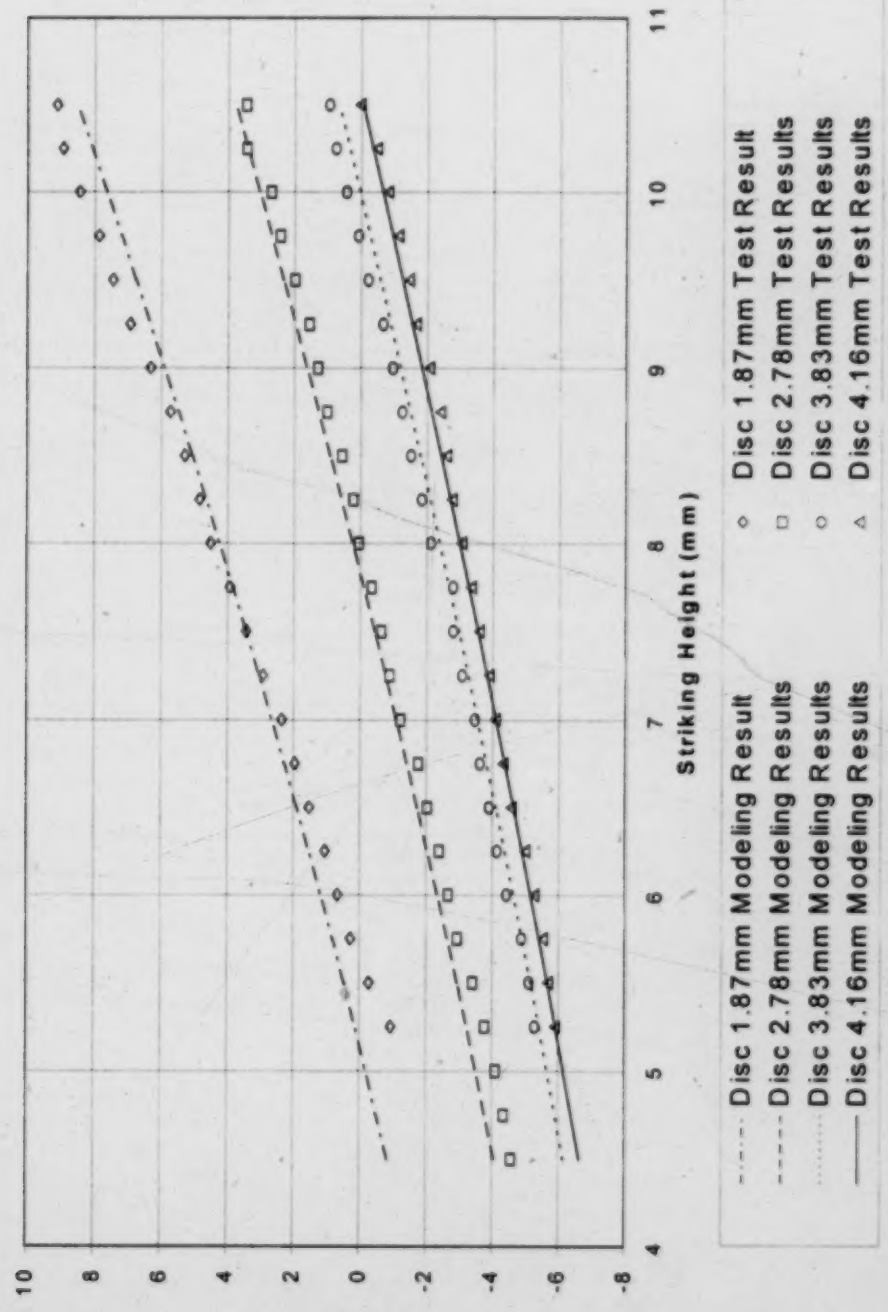

FIGURE 4-2: Numerical Modeling and *In Vitro* Results for Changing Tissue/Implant Anchorage and Striking Height

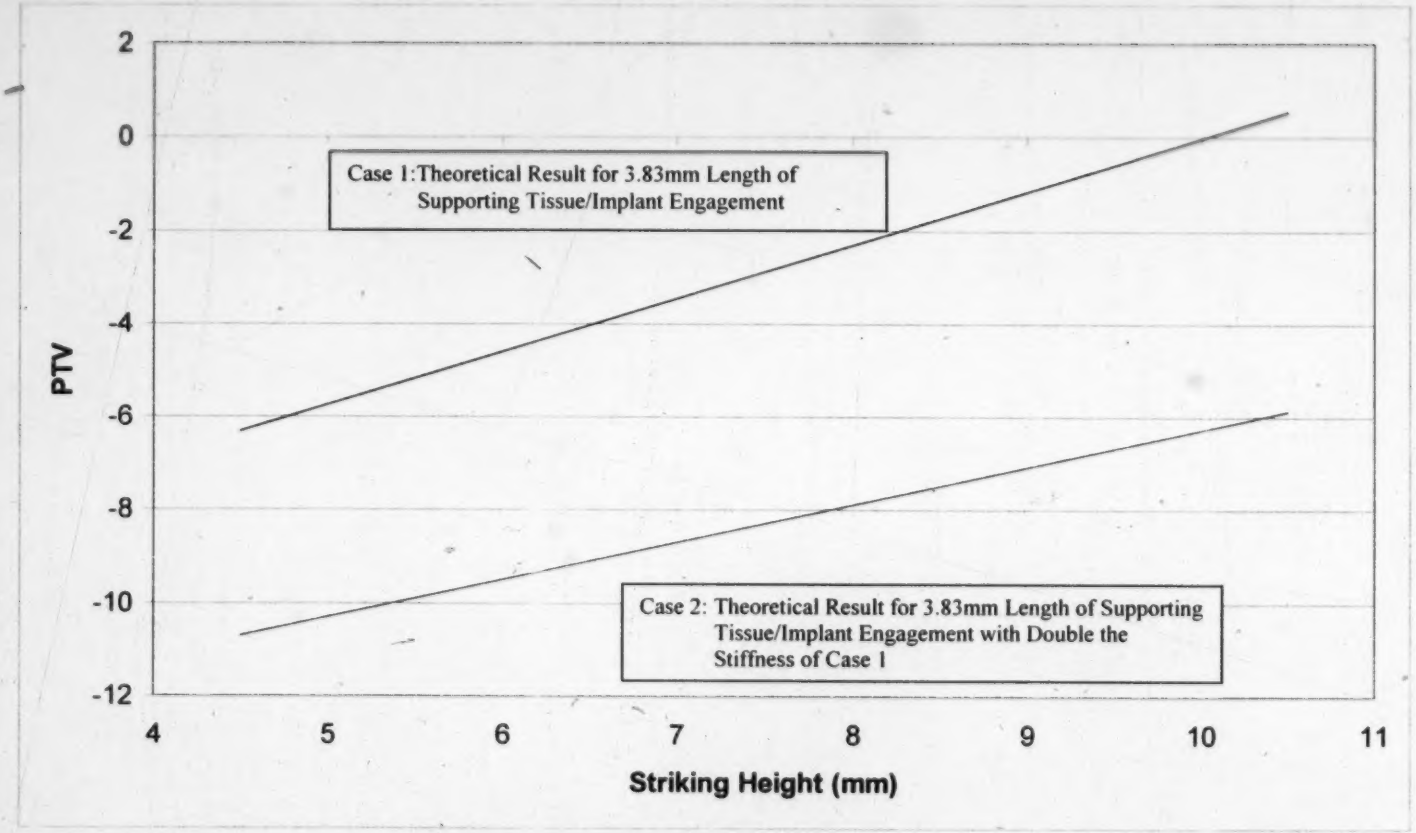

FIGURE 4-3: The Numerical Model Predicting the PTV Response for a Doubling of the Supporting Tissue Stiffness for an Implant with 3.83mm of Anchorage

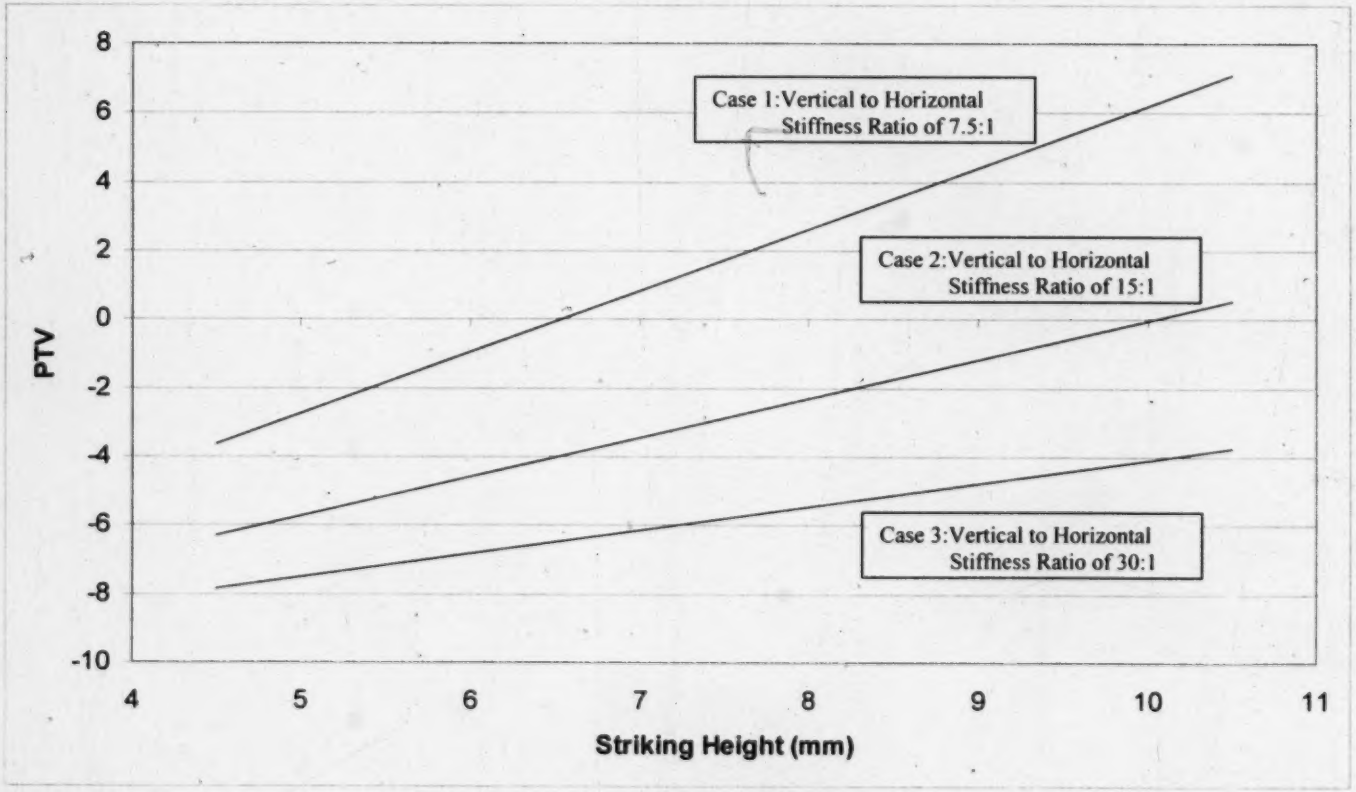

FIGURE 4-4: The Numerical Model Predicting the PTV Response due to a Change in the Ratio of Vertical to Horizontal Supporting Tissue Stiffnesses for an Implant with 3.83mm of Anchorage

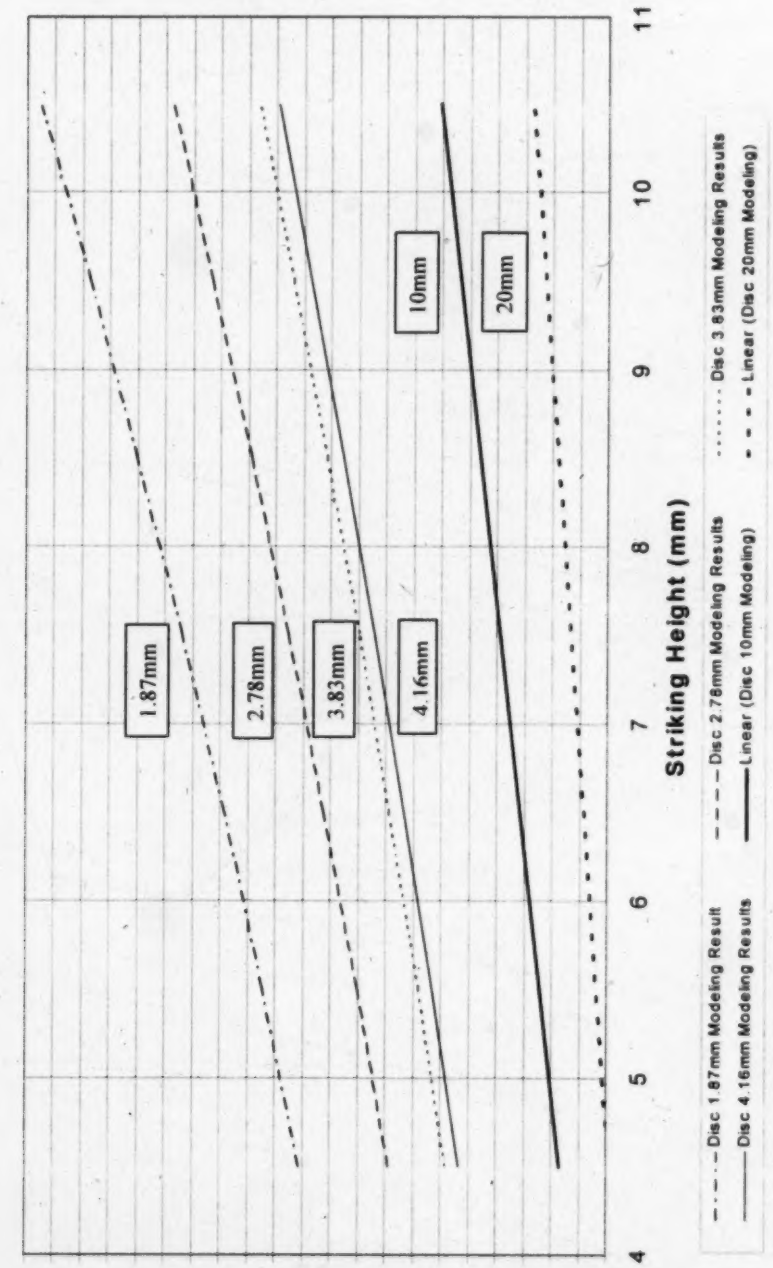

FIGURE 4-5: The Numerical Model Predicting the PTV Response for Longer Tissue/Implant Engagement Levels

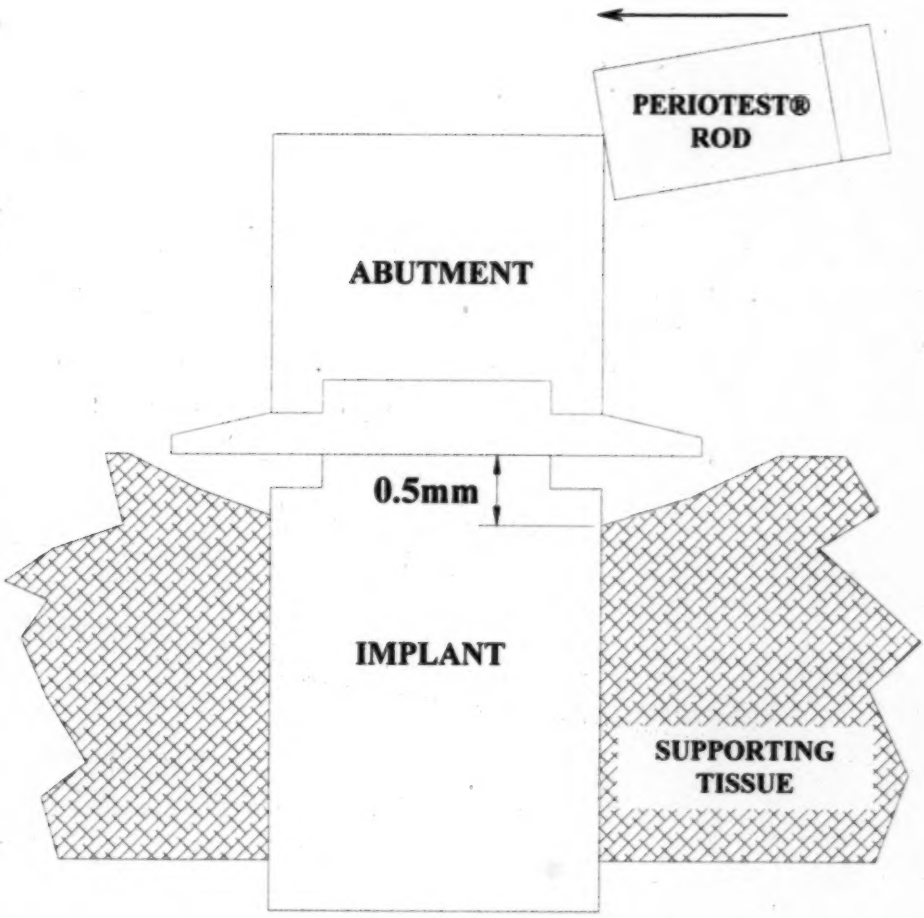

FIGURE 4-6: Change in Length of Tissue/Implant Engagement and Striking Height due to Marginal Loss of Supporting Tissue

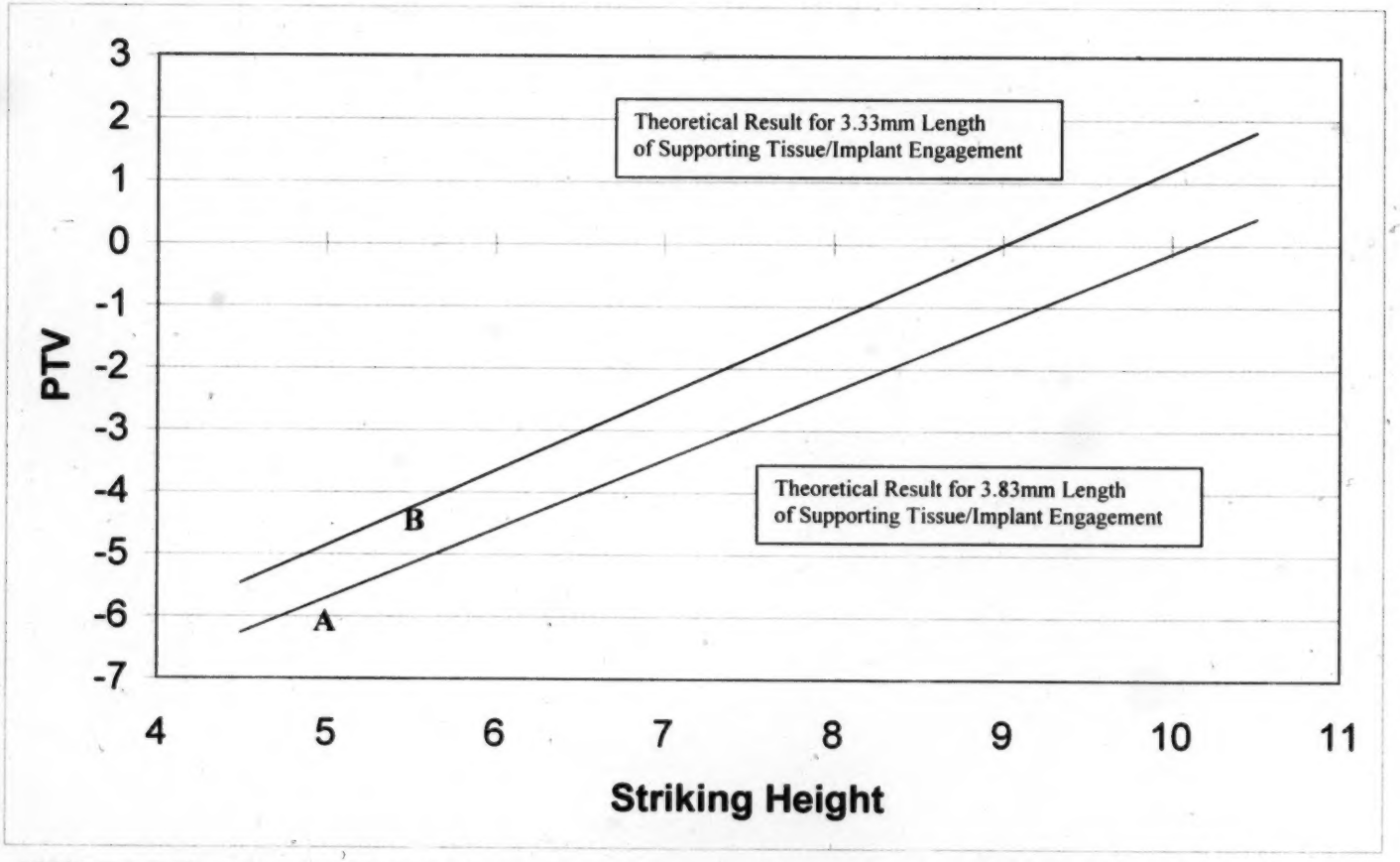

FIGURE 4-7: The Numerical Model Predicting the PTV Response for a 0.5mm Marginal Loss of Supporting Tissue

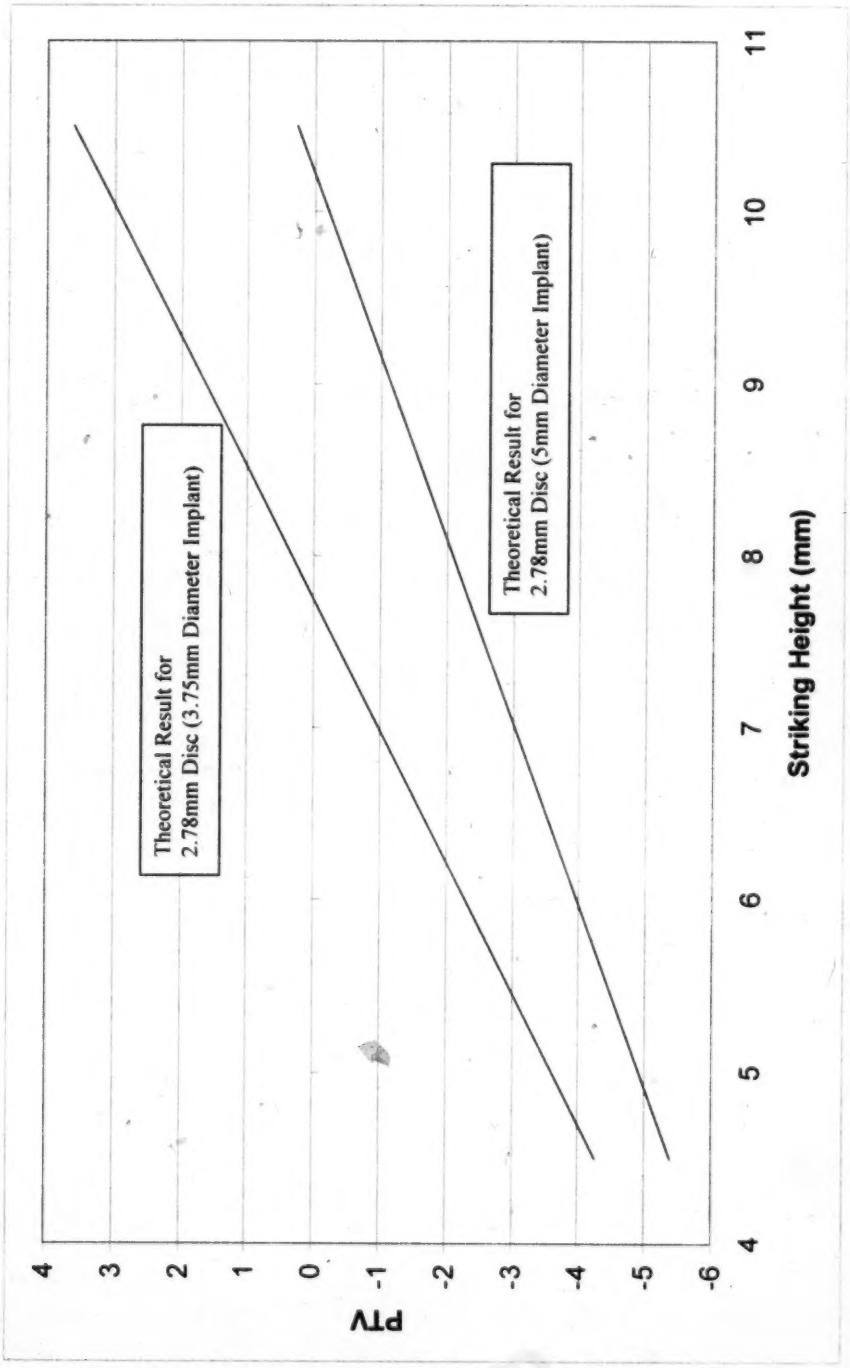

FIGURE 4-8: The Numerical Model Predicting the PTV Response for Both 3.75mm and 5mm Diameter Implants with an Anchorage Length of 2.78mm

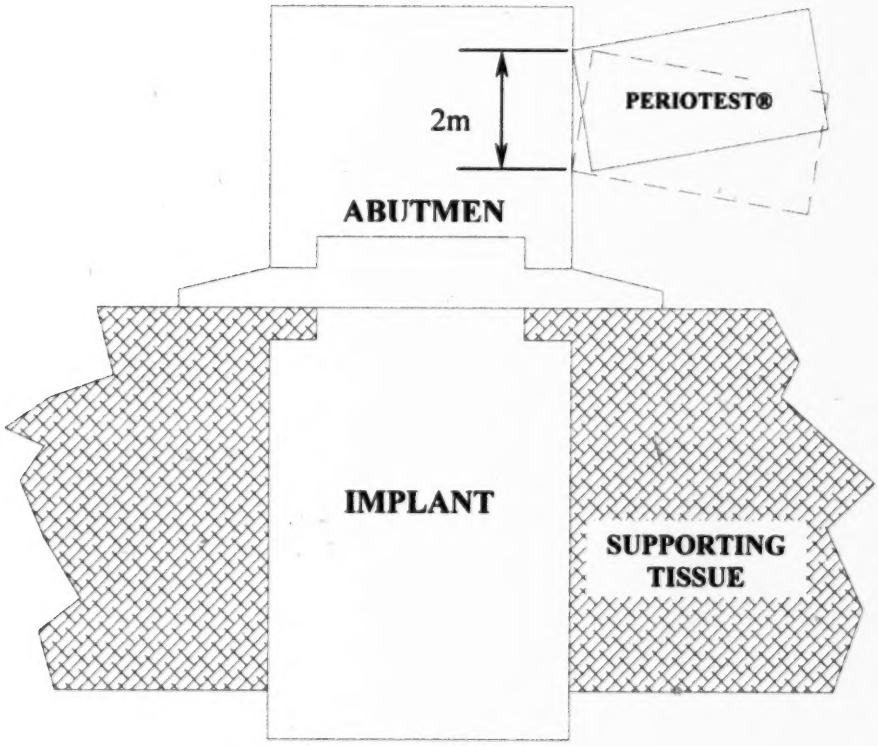

FIGURE 4-9: Effect of Angulation of the Periotest® on Striking Height

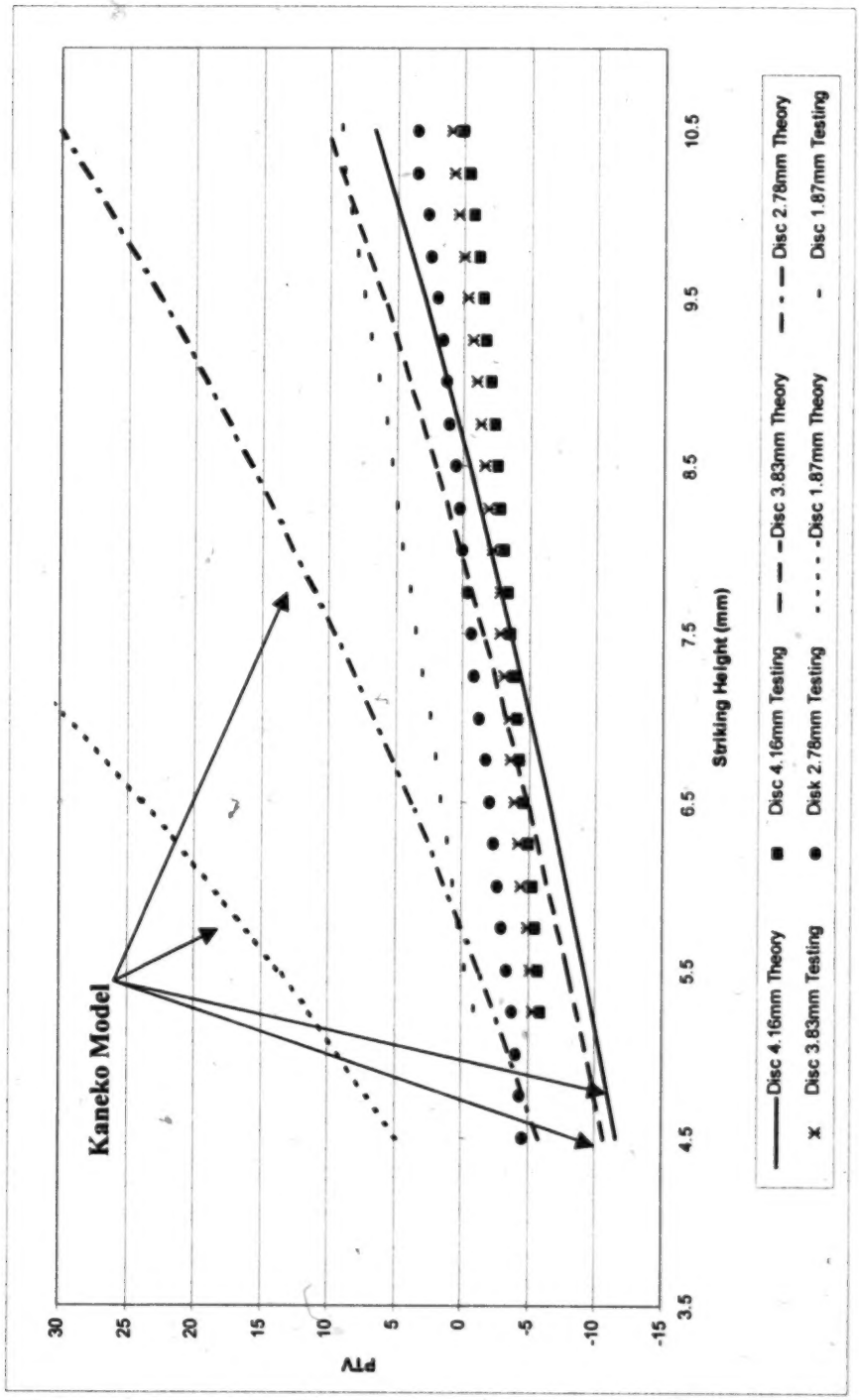

FIGURE 4-10: *In Vitro* Testing Results Compared with the Rotational Kaneko Model (1994)

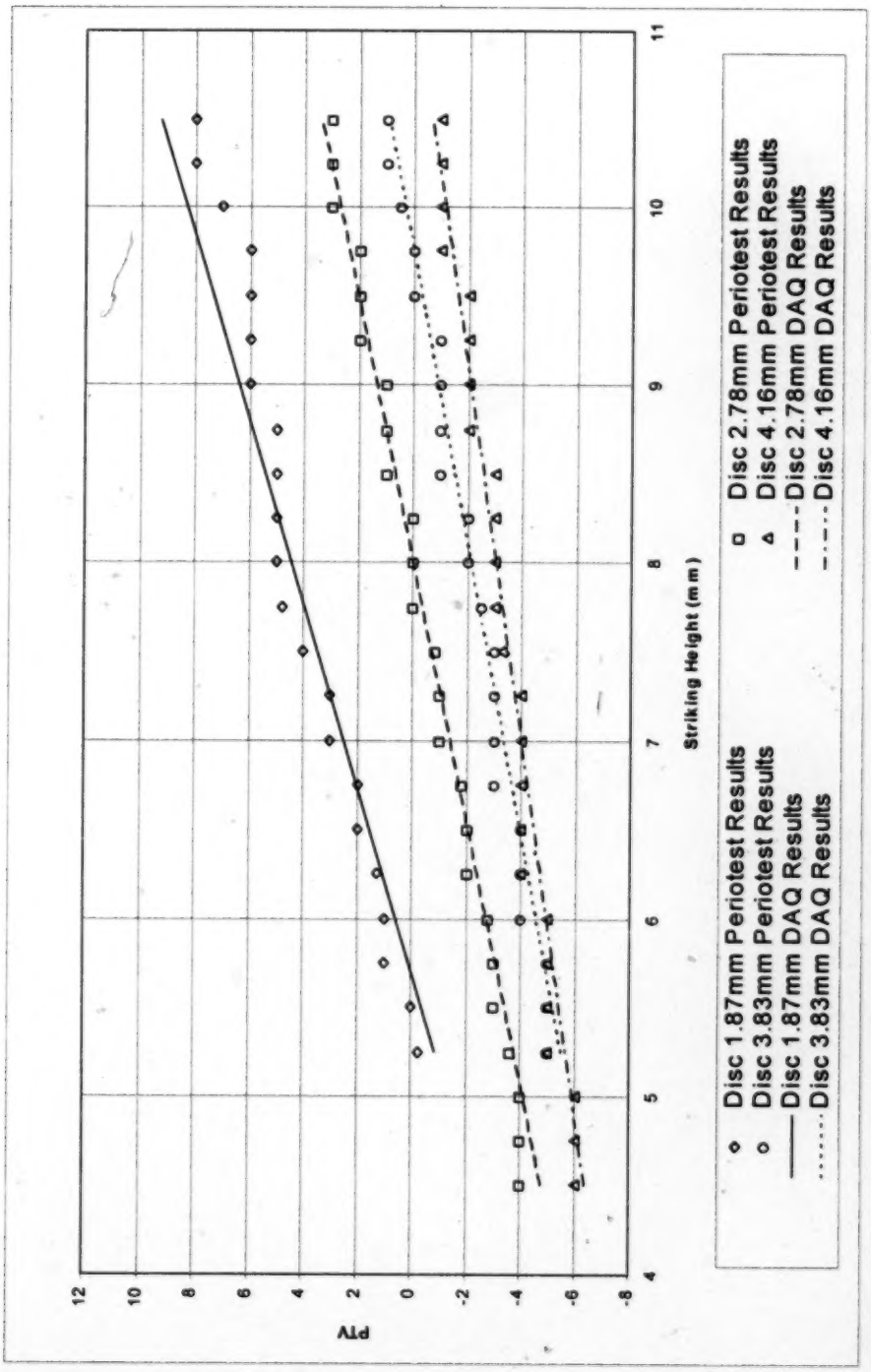

FIGURE 4-11: Comparison of the Standard Periotest® Output with the Digitally Acquired Periotest® Output

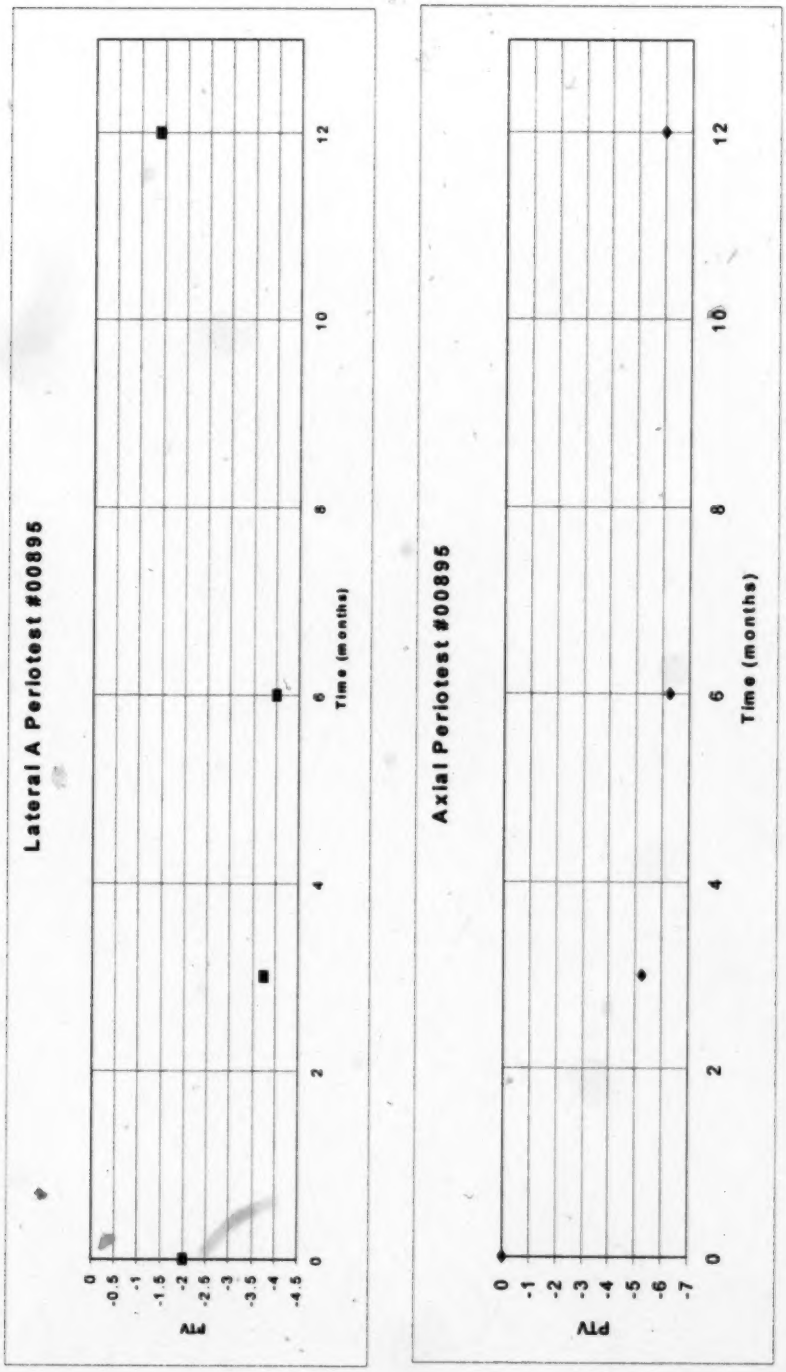

FIGURE 4-12: *In Vivo* Testing Data for Patient #00895

Chapter 5

Conclusions

5.1 Summary

The objective of the present study was to provide a better understanding of the Periotest®/implant system dynamics by assessing the influence of certain geometric parameters such as implant length, diameter, abutment length as well as supporting tissue properties such as density of bone, the length of supporting tissue, and implant engagement have on the PTV. These parameters have been noted in extensive clinical studies unfortunately with little understanding of how they affect the PTV.

To investigate this, a two degree of freedom model of the Periotest®/implant system was developed in Chapter 2. This model is the first to incorporate both translational and rotational motion of the Periotest®/implant system, as well as the influence from the vertical stiffness of the supporting tissue. The modeling results show that an increase in striking height above the supporting tissue surface results in a decrease

in PTV for a given length of engagement between the supporting tissue and implant. As the length of engagement between the supporting tissue/implant increases, the PTV will decrease for a given striking height. In addition, the PTV has been shown to depend on changes in the stiffness (Young's Modulus) of supporting tissue as well as the vertical to horizontal stiffness ratio. Finally, the model showed that larger diameter implants provide less Periotest®/implant system mobility, which results in lower PTV.

As a means for validating the numerical approach, an *in vitro* study was conducted. The results of the *in vitro* study matched quite well with the numerical method. The application of a strain gauged abutment was the first known attempt to validate the contact time measured by the Periotest® and to directly monitor the damping behavior of the supporting material. The *in vitro* study also showed that striking height had an effect on the PTV, which complements the findings of other studies. The trends showed that as the striking height increased, the PTV would increase and thus indicating a lower effective stiffness of the supporting tissue. Another result of the study correlated the PTV with the supporting tissue/implant length of engagement and not with simple implant length, which has been considered by researchers to affect PTV. The trend showed that longer the lengths of tissue/implant engagement resulted in a lower PTV and the reduction in sensitivity to striking height. The *in vitro* data also shows that the Periotest® can detect a change in tissue/implant engagement length of as little as 0.33mm, which is the change in disc thickness from the 3.83mm to the 4.78mm disc. As a result, the Periotest® should detect the marginal bone loss around the periphery of an implant.

The study also showed how clinical misuse of the Periotest® can lead to problems. The geometry of the impacting head is such that for any deviation in angulation from the horizontal of the handpiece results in a 2mm change in striking height and therefore cause a dramatic change in PTV. This effect is more predominant for the craniofacial implant systems, which typically have a ratio of the striking height to engagement length of 1 or greater. As a result, clinicians must take great care when positioning the impacting rod so that only one point of contact is made with the coronal portion of the abutment. For longitudinal studies on one patient over time a consistent protocol needs to be followed.

The calibration procedure for the Periotest® has been found ineffective due to the operating range of PTVs for implants compared to normal dentition.

The *in vivo* results were inconclusive which could be attributed to an initial poor understanding from the effects of the many of the parameters considered above including a lack of rigorous clinical testing protocol. As a result, a recommended revised testing protocol was developed.

5.2 Future Considerations

5.2.1 Model with Multi-Layered Supporting Tissue

Typically, bone as a supporting tissue rarely exists as a single layer of cortical, cancellous, or fibrous tissue. It is more commonly found in some combination of the three (e.g. bicortical). Therefore, the model developed in Chapter 2 could not assess the

response of the Periotest®/implant system for a supporting tissue consisting of multiple layers with varying stiffness and damping properties. As a result, what is required is an extension of the model that can incorporate multiple layers of supporting tissue. This is a simple process of adding as many layers with differing stiffness and damping per unit length below the existing set of stiffness and damping system and measuring the new depths from the datum point O appropriately.

5.2.2 Calibration Device

It has been shown that the existing calibration method has been designed with the intention of assessing the mobility of teeth and not implants which show ankylosis (fusion) in a lower more narrow range than for teeth. Therefore, what is required for proper calibration of the Periotest® is device design so that the geometry produces a predefined PTV. Such a system could be a set of cantilever beams that calibrate the Periotest® at -1, -3, -5, -7 PTV or even a set of implant/abutments which have been rigidly placed in a block of material FRB-10 for example and would have a range of known PTVs when struck at the crown of each abutment. In this way, the calibration of the Periotest® will be within the testing range of the implant systems. This method will also offer another means of checking the interoperator variability using the Periotest® and as a result it would serve as an educational tool.

5.2.3 Increase the Precision of the Periotest® Output

The comparison of the *in vitro* data recorded with the data acquisition system to the basic Periotest® unit has shown that by providing one more significant figure to the PTV output can substantially increase the operating range and resolution of the Periotest®. Therefore, if the manufacturer of the Periotest® could provide at least one significant figure to the liquid crystal display then the Periotest® could become a more effective tool when assessing the mobility of implants.

5.2.4 Investigating of the Damping of Bone *In Vivo*

The damping behaviour of the *in vitro* supporting material exhibited low damping when tested with a strain-gauged abutment. This may not be the case for natural bone. Further investigation into the damping properties of bone could be performed with the same instrumentation. Studies by Elias et al. (1996) and Meredith (1997) have taken steps towards quantifying the damping of the supporting tissue.

5.2.5 Assessment of Bone Height During Surgery or CT Scan

Prior knowledge of the thickness of bone at time of implantation can be advantageous from the modeling point of view. Recording the thickness can be performed after the pilot hole is drilled or from a CT scan taken prior to the operation. By knowing the length of engagement of the implant, the effective stiffness of the

supporting tissue can be determined from the model. In addition, with this information, the model should predict the PTV and thus validating the model again.

References

Adell R., U. Lekholm, and B. Rockler (1986). Marginal tissue reactions to osseointegrated titanium fixtures(I). A 3-year longitudinal prospective study. Int J Oral Maxillofac Surg 15, 39-52.

Aparicio C., and P. Orozco (1998). Use of 5mm-diameter implants: Periotest® values Related to a clinical and radiographic evaluation. Clin Oral Impl Res 9, 398-406

Askeland, D.R. (1990). The Science and Engineering of Materials (Second Edition), Chapman & Hall.

Branemark P-I, G. Zarb, and T. Albrektsson (1985). Tissue-Integrated Prosthesis. Osseointegration in clinical dentistry. Chicago, Quintessence Publ Co.

Carr A.B., E. Papazoglou, and P.E. Larsen (1995). The relationship of Periotest® values, biomaterial, and torque to failure in adult baboons. Int J Prosthodontics 8, 15-20.

Chai, J.Y., J. Yamada, and I.C. Pang (1993). In vitro consistency of the Periotest® instrument. J Prosthodont 2, 9-12.

Chavez H, L.F. Ortman, R.L. DeFranco, and J. Medige (1993). Assessment of oral implant mobility. J Prosthet Dent 70,421-426.

Cranin A.N., J. Degrado, M. Kaufman, M. Baraoidan, R. DiGregorio, G. Batgits, and Z. Lee Z. (1998). Evaluation of the Periotest® as a diagnostic tool for dental implants. Journal of Oral Implantology 24,139-146.

del Valle, V.R. (1995). Loading and Strain Distribution from Osseointegrated Craniofacial Implants. M.Sc. thesis. University of Alberta, Alberta, Canada

Derhami K., J.F. Wolfaardt, G. Faulkner, and M. Grace (1995). Assessment of the Periotest® device in baseline mobility measurements of craniofacial implants. Int J Oral Maxillofac Implants 10, 221-229

Dimarogonas A.D. (2001). Machine design a CAD approach. Wiley-Interscience\ Publiciation. John Wiley & Sons, INC.

Drago C.J. (2000). A prospective study to assess osseointegration of dental endosseous implants with the Periotest® instrument. Int J Oral Maxillofac Implants 15, 389-395.

Elias J.J., J.B. Brunski, and H.A. Scarton (1996). A dynamic modal testing technique for noninvasive assessment of bone-dental implant interfaces. Int J Oral Maxillofac Implants 11, 728-734.

Faulkner, M.G., J.F. Wolfaardt, and A. Chan (1999). Measuring abutment/joint integrity using the Periotest® instrument. Int J Oral Maxillofac Implants 14, 681-688.

Haas R., M. Saba, N. Mensdorff-Pouilly, and G. Mailath (1995). Examination of the damping behaviour of IMZ implants. Int J Oral Maxillofac Implants 4, 410-414.

Haas R., T. Bernhart, O. Dortbudak, and G. Mailath (1999). Experimental study of the damping behaviour of IMZ implants. Journal of Oral Rehabilitation 26:19-24.

Ichikawa T., M. Miyamoto, Y. Horisaka, and N. Matsumoto (1994). Clinical evaluation of Periotest® for two-piece apatite implants. Int J Oral Maxillofac Implants 9, 461-467

Isidor F. (1998). Mobility assessment with the Periotest® system in relation to histological findings of oral implants. Int J Oral Maxillofac Implants 13, 377-383.

Kaneko, T.M. (1993). Dynamics of the Periotest method for diagnosing the dental implant-bone interface. Journal of Materials Science: Materials Medicine 4, 256-259.

Kaneko, T.M. (1994). Relationship between the stiffness of the dental implant-bone system and the duration of the implant-tapping rod contact. Med. Eng. Phys. 16,310-315

Lukas D., and W. Schulte (1990). Periotest - A dynamic procedure for the diagnosis of the human periodontium. Clin. Phys. Physiol. Meas. 11(1), 65 - 75.

Manz M.C., H.F. Morris, and S. Ochi (1992). An evaluation of the Periotest® system part(II). Implant Dent 1, 221-226.

Meredith N. (1997). On the clinical measurement of implant stability and osseointegration. Ph.D. thesis. Dept of Biomaterials/Handicap Research, Institute for Surgical Sciences, Göteborg University, Göteborg, Sweden and Dept. of Oral and Dental Science, Bristol Dental Hospital, Lower Maudlin Street, Bristol, U K

Meredith N., B. Friberg, L. Sennerby, and C. Apricio (1998). Relationship between contact time measurements and PTV values when using the Periotest® to measure implant stability. Int J Prosthodont 11, 269-275.

Nishimura K., T. Itoh , K. Takaki, R. Hosokawa, T. Naito, and M. Yokota (1997). Periodontal parameters of osseointegration dental implants. A 4-year controlled follow-up study. Clin Oral Implants Res 8, 272-278.

Ochi S., H.F. Morris, and S. Winkler (1994). The influence of implant type, material, coating, diameter, and length on Periotest values at second-stage surgery: Dicrg interm report No. 4. Implant Dent 3(3), 159-162

Olivé J., and C. Aparicio (1990). The Periotest® method as a measure of osseointegrated oral implant stability. Int J Oral Maxillofac Implants 5, 390-400.

Proakis, J.G., and D.G. Manolakis (1996). Digital Signal Processing Principles, Algorithms, and Applications (third ed.). Prentice Hall.

Salonen M.A.M., K. Oikarinen, K. Virtanen, and H. Pernu (1993). Failures in the osseointegration of endosseous implants. Int J Oral Maxillofac Implants 8, 92-97.

Salonen M.A.M., A.M. Raustia, V. Kainulainen, and K.S. Oikarinen (1997). Factors related to Periotest® values in endosseal implants: a 9-year follow-up. J. Clin Periodontol 24, 272 -277.

Schulte W., D. Lukas (1993). Periotest® to monitor osseointegration and to check the occlusion in oral implantology. J Oral Implantol 19, 23-32

Teerlinck J, M., Quirynen, P. Darius, and D. van Steenberghe (1991). Periotest®: An objective, clinical diagnosis of bone apposition toward implants. Int J Oral Maxillofac Implants 6(1), 55-60.

Tricio J., P. Laohapand, D. van Steenberghe, M. Quirynen, and I. Naert (1995). Mechanical state assessment of the implant-bone continuum: a better understanding of the Periotest® method. Int J Oral Maxillofac Implants 10, 43-49.

van Steenberghe D., and M. Quirynen (1993). Reproducibility and detection threshold of peri-implant diagnostics. Adv Dent Res 7(2), 191-195.

van Steenberghe D., J. Tricio, I. Naert, and M. Nys (1995). Damping characteristics of bone-to-implant interfaces. A clinical study with the Periotest® device. Clin Oral Impl Res 6, 31-39.

Wilkes G.H., and J.F. Wolfaardt (1998). Chapter 3, Craniofacial Osseointegrated Prosthetic Reconstruction Advances in Plastic & Reconstructive Surgery® (vol. 15), Mosby Inc.

Wolfaardt J.F., G.H. Wilkes, S.M. Parel, and A. Tjellström (1993). Craniofacial osseointegration: the Canadian experience. Int J Oral Maxillofac Implants 8,197.

Appendix A

Analytical Model of the Periotest® Method

The complete analytical solution to the Periotest®/implant system model outlined in Chapter 2 is presented in this appendix.

Consider the Periotest®/implant system in Figure A-1 displaced from its equilibrium position with a an assume positive displacement and rotation x and θ respectively as

$$x > 0 \qquad \dot{x} > 0 \qquad \ddot{x} > 0$$

$$\theta > 0 \qquad \dot{\theta} > 0 \qquad \ddot{\theta} > 0.$$

By equating the forces in free body diagram to the mass x accelerations in the x-direction of the mass-acceleration diagram, the equation of motion in the horizontal direction is

$$\overleftarrow{+} \sum F_{x(FBD)} = ma_x \tag{A.1}$$

$$(m_t + m_p)\ddot{x} + m_t b\ddot{\theta}\cos\theta + m_t b\dot{\theta}^2 \sin\theta + F_{hspring} + F_{hdamper} = 0 \tag{A.2}$$

where the spring force is given by

$$F_{hspring} = k(\ell_2 - \ell_1)x + k(\ell_2 - \ell_1)\ell_1\theta + \frac{k}{2}(\ell_2 - \ell_1)(\ell_2 - \ell_1)\theta \tag{A.3}$$

$$= k(\ell_2 - \ell_1)x + \frac{k}{2}[2\ell_1\ell_2 - 2\ell_1^{\,2} + \ell_2^2 - 2\ell_1\ell_2 + \ell_1^{\,2}]\theta$$

$$= k(\ell_2 - \ell_1)x + \frac{k}{2}[\ell_2^2 - \ell_1^{\,2}]\theta$$

Similarily the force in the damper

$$F_{hdamper} = c(\ell_2 - \ell_1)\dot{x} + \frac{c}{2}[\ell_2^2 - \ell_1^{\,2}]\dot{\theta}. \tag{A.4}$$

The resulting equation of motion in the x-direction is

$$(m_t + m_p)\ddot{x} + m_t b\ddot{\theta}\cos\theta + m_t b\dot{\theta}^2 \sin\theta + k(\ell_2 - \ell_1)x$$
$$+ \frac{k}{2}[\ell_2^2 - \ell_1^{\,2}]\theta + c(\ell_2 - \ell_1)\dot{x} + \frac{c}{2}[\ell_2^2 - \ell_1^{\,2}]\dot{\theta} = 0 \tag{A.5}$$

The vertical equation of motion is identically satisfied as a_{Gy} is zero.

Equilibrium of the moments about O

$$\circlearrowleft \sum M_{O\,(FBD)} = \sum M_{O\,(MAD)} \tag{A.6}$$

$$
\begin{aligned}
&-F_{vspring}(r\cos\theta+\ell'\sin\theta)-F_{vspring}(r\cos\theta-\ell'\sin\theta)\\
&-\frac{k}{2}[(\ell_2-\ell_1)(\ell_2+\ell_1)]\ddot{x}-\frac{k}{2}[(\ell_2-\ell_1)(\ell_2+\ell_1)\ell_1]\ddot{\theta}\\
&-\frac{k}{2}\left[(\ell_2-\ell_1)^2\left(\frac{2}{3}(\ell_2-\ell_1)+\ell_1\right)\right]\theta\\
&-\frac{c}{2}[(\ell_2-\ell_1)(\ell_2+\ell_1)]\dot{x}-\frac{c}{2}[(\ell_2-\ell_1)(\ell_2+\ell_1)\ell_1]\dot{\theta}\\
&-\frac{c}{2}\left[(\ell_2-\ell_1)^2\left(\frac{2}{3}(\ell_2-\ell_1)+\ell_1\right)\right]\dot{\theta}\\
&=J_G\ddot{\theta}+m_t\ddot{x}b\cos\theta+m_tb^2\ddot{\theta}
\end{aligned}
\tag{A.7}
$$

The displacement of the vertical stiffnesses and damping components (Figure A-2) is

$$\text{displacement} = r\sin\theta+\ell'(1-\cos\theta)\,. \tag{A.8}$$

The force in the vertical springs due to the displacement (A.8) is

$$F_{vspring} = k^*(\ell_2-\ell_1)(r\sin\theta+\ell'(1-\cos\theta)) \tag{A.9}$$

where k^* is the stiffness per unit length of supporting tissue in contact with the implant.

With this expression, the rotational equation of motion is

$$
\begin{aligned}
&-\tfrac{1}{2}k^*(\ell_2-\ell_1)(r\sin\theta+\ell'(1-\cos\theta))(r\cos\theta-\ell'\sin\theta)\\
&-\tfrac{1}{2}k^*(\ell_2-\ell_1)(r\sin\theta+\ell'(1-\cos\theta))(r\cos\theta+\ell'\sin\theta)\\
&-\tfrac{1}{2}c^*(\ell_2-\ell_1)(r\sin\dot{\theta}+\ell'(1-\cos\dot{\theta}))(r\cos\dot{\theta}-\ell'\sin\dot{\theta})\\
&-\tfrac{1}{2}c^*(\ell_2-\ell_1)(r\sin\dot{\theta}+\ell'(1-\cos\dot{\theta}))(r\cos\dot{\theta}+\ell'\sin\dot{\theta})\\
&-\frac{k}{2}[(\ell_2-\ell_1)(\ell_2+\ell_1)]\ddot{x}-\frac{k}{2}[(\ell_2-\ell_1)(\ell_2+\ell_1)\ell_1]\ddot{\theta}\\
&-\frac{k}{2}\left[(\ell_2-\ell_1)^2\left(\frac{2}{3}(\ell_2-\ell_1)+\ell_1\right)\right]\theta\\
&-\frac{c}{2}[(\ell_2-\ell_1)(\ell_2+\ell_1)]\dot{x}-\frac{c}{2}[(\ell_2-\ell_1)(\ell_2+\ell_1)\ell_1]\dot{\theta}\\
&-\frac{c}{2}\left[(\ell_2-\ell_1)^2\left(\frac{2}{3}(\ell_2-\ell_1)+\ell_1\right)\right]\dot{\theta}\\
&=J_G\ddot{\theta}+m_t\ddot{x}b\cos\theta+m_tb^2\ddot{\theta}
\end{aligned}
\tag{A.10}
$$

The resulting motion of the implant/abutment system is assumed to be small compared to the sizes shown and so the above equations can be simplified assuming small angles of rotation θ. Therefore $\sin\theta \approx \theta$ and $\cos\theta \approx 1$ reduces (A.10) to

$$\begin{aligned}
&-\tfrac{1}{2}k^*(\ell_2-\ell_1)(r\theta)(r-\ell'\theta)-\tfrac{1}{2}k^*(\ell_2-\ell_1)(r\theta)(r+\ell'\theta)\\
&-\tfrac{1}{2}c^*(\ell_2-\ell_1)(r\dot\theta)(r-\ell'\dot\theta)-\tfrac{1}{2}c^*(\ell_2-\ell_1)(r\dot\theta)(r+\ell'\dot\theta)\\
&-\frac{k}{2}\left[\left(\ell_2^2-\ell_1^2\right)\right]x-\frac{k}{2}\left[\left(\ell_2^2-\ell_1^2\right)\ell_1\right]\theta-\frac{k}{2}\left[(\ell_2-\ell_1)^2\left(\frac{2}{3}(\ell_2-\ell_1)+\ell_1\right)\right]\theta\\
&-\frac{c}{2}\left[\ell_2^2-\ell_1^2\right]\dot x-\frac{c}{2}\left[\left(\ell_2^2-\ell_1^2\right)\ell_1\right]\dot\theta-\frac{c}{2}\left[(\ell_2-\ell_1)^2\left(\frac{2}{3}(\ell_2-\ell_1)+\ell_1\right)\right]\dot\theta\\
&=J_G\ddot\theta+m_t\ddot x b+m_t b^2\ddot\theta
\end{aligned}\tag{A.11}$$

and by gathering similar terms and simplifying yields

$$\begin{aligned}
&J_G\ddot\theta+m_t\ddot x b+m_t b^2\ddot\theta+k^*(\ell_2-\ell_1)(r^2\theta)+c^*(\ell_2-\ell_1)(r^2\dot\theta)\\
&+\frac{k}{2}\left[\left(\ell_2^2-\ell_1^2\right)\right]x+\frac{k}{2}\left[\left(\ell_1\ell_2^2-\ell_1^3\right)+\frac{1}{3}\left((\ell_2-\ell_1)^2\left(2(\ell_2-\ell_1)+3\ell_1\right)\right)\right]\theta\\
&+\frac{c}{2}\left[\ell_2^2-\ell_1^2\right]\dot x+\frac{c}{2}\left[\left(\ell_1\ell_2^2-\ell_1^3\right)+\frac{1}{3}\left((\ell_2-\ell_1)^2\left(2(\ell_2-\ell_1)+3\ell_1\right)\right)\right]\dot\theta=0
\end{aligned}\tag{A.12}$$

and further simplification finally yields

$$\begin{aligned}
&(m_t b)\ddot x+(J_G+m_t b^2)\ddot\theta+k^*(\ell_2-\ell_1)r^2\theta+c^*(\ell_2-\ell_1)r^2\dot\theta\\
&+\frac{k}{2}(\ell_2^2-\ell_1^2)x+\frac{k}{3}(\ell_2^3-\ell_1^3)\theta+\frac{c}{2}(\ell_2^2-\ell_1^2)\dot x+\frac{c}{3}(\ell_2^3-\ell_1^3)\dot\theta=0
\end{aligned}\tag{A.13}$$

Equations (A.5) and (A.13) can be written as

$$[m]\begin{Bmatrix}\ddot\theta\\ \ddot x\end{Bmatrix}+[c]\begin{Bmatrix}\dot\theta\\ \dot x\end{Bmatrix}+[k]\begin{Bmatrix}\theta\\ x\end{Bmatrix}=\begin{Bmatrix}0\\ 0\end{Bmatrix}\tag{A.14}$$

where the mass, stiffness and damping matrices are:

$$[m]=\begin{bmatrix} J_G + m_i b^2 & m_i b \\ m_i b & m_i + m_p \end{bmatrix} \tag{A.15}$$

$$[k]=\begin{bmatrix} \frac{k}{3}\left(\ell_2^3 - \ell_1^3\right) + k^* r^2 \left(\ell_2 - \ell_1\right) & \frac{k}{2}\left(\ell_2^2 - \ell_1^2\right) \\ \frac{k}{2}\left(\ell_2^2 - \ell_1^2\right) & k\left(\ell_2 - \ell_1\right) \end{bmatrix} \tag{A.16}$$

$$[c]=\alpha[k] \qquad [c^*]=\alpha[k^*] \qquad \alpha=\frac{c}{k}=\frac{c^*}{k^*}$$

The mass of the implant was considered to be negligible when compared to the mass of the Periotest®. Consequently, the rotational inertia of the implant is also negligible and thus neglected resulting in the following form of the matrix

$$\begin{bmatrix} 0 & 0 \\ 0 & m_p \end{bmatrix}\begin{Bmatrix} \ddot{\theta} \\ \ddot{x} \end{Bmatrix} + [c]\begin{Bmatrix} \dot{\theta} \\ \dot{x} \end{Bmatrix} + [k]\begin{Bmatrix} \theta \\ x \end{Bmatrix} = \begin{Bmatrix} 0 \\ 0 \end{Bmatrix} \tag{A.17}$$

$$k_{11}\theta + k_{12}x = 0 \tag{A.18}$$

$$m_p\ddot{x} + \frac{\left(k_{11}k_{22} - k_{12}^2\right)}{k_{11}}\left(x + \alpha\dot{x}\right) = 0 \tag{A.19}$$

$$m_p\ddot{x} + c_e\dot{x} + k_e x = 0 \tag{A.20}$$

$$k_e = \frac{k_{11}k_{22} - k_{12}^2}{k_{11}} \qquad c_e = \alpha k_e$$

This is a second order differential equation of motion and a solution is assume to be in the following form,

$$x = e^{st} \tag{A.21}$$

where $\dot{x} = se^{st}$ (A.22)

$$\ddot{x} = s^2 e^{st}. \tag{A.23}$$

Substituting (A.21), (A.22), and (A.23) into (A.20) yields

$$s^2 e^{st} + \left(\frac{c_e}{m_p}\right) s e^{st} + \left(\frac{k_e}{m_p}\right) e^{st} = 0 \tag{A.24}$$

which simplifies to

$$\left[s^2 + \left(\frac{c_e}{m_p}\right) s + \left(\frac{k_e}{m_p}\right)\right] e^{st} = 0. \tag{A.25}$$

However, $e^{st} \neq 0$ and therefore (A.25) becomes an algebraic equation for s

$$s^2 + \left(\frac{c_e}{m_p}\right) s + \left(\frac{k_e}{m_p}\right) = 0 \tag{A.26}$$

which can be solved for s

$$s = -\frac{c_e}{2m_p} \pm \frac{1}{2}\sqrt{\frac{c_e^2}{m_p^2} - \frac{4k_e}{m_p}} \tag{A.27}$$

by applying the solution for a quadratic equation. Therefore the equation describing the displacement of the Periotest®/implant system is

$$x(t) = A_1 e^{\left\{-\frac{c_e}{2m_p}+\frac{1}{2}\sqrt{\frac{c_e^2}{m_p^2}-\frac{4k_e}{m_p}}\right\}t} + A_2 e^{\left\{-\frac{c_e}{2m_p}-\frac{1}{2}\sqrt{\frac{c_e^2}{m_p^2}-\frac{4k_e}{m_p}}\right\}t} \tag{A.28}$$

$$\omega_n = \sqrt{\frac{k_e}{m_p}} \qquad \zeta = \frac{c_e}{c} = \frac{\alpha k_e}{2m_p\omega_n} = \frac{\alpha}{2}\omega$$

$$x(t) = e^{-\zeta\omega_n t}\left[A_1 e^{\omega_n t\sqrt{\zeta^2-1}} + A_2 e^{-\omega_n t\sqrt{\zeta^2-1}}\right] \tag{A.29}$$

$\zeta = 0$ leads to undamped vibrations, $\zeta > 1$ leads to over damped, so consider the case where $\zeta < 1$ for under damped system therefore (A.29) can be rewritten as

$$x(t) = e^{-\zeta\omega_n t}\left[A_1 e^{\omega_n t i\sqrt{1-\zeta^2}} + A_2 e^{-\omega_n t i\sqrt{1-\zeta^2}}\right] \tag{A.30}$$

where

$$e^{i\theta} = \cos\theta + i\sin\theta \tag{A.31}$$

$$x(t) = e^{-\zeta\omega_n t}\begin{Bmatrix} A_1\cos t\omega_n\sqrt{1-\zeta^2} + A_1 i\sin t\omega_n\sqrt{1-\zeta^2} \\ + A_2\cos(-t)\omega_n\sqrt{1-\zeta^2} + A_2 i\sin(-t)\omega_n\sqrt{1-\zeta^2} \end{Bmatrix} \tag{A.32}$$

$$x(t) = e^{-\zeta\omega_n t}\left\{(A_1 + A_2)\cos t\omega_n\sqrt{1-\zeta^2} + (A_1 - A_2)i\sin t\omega_n\sqrt{1-\zeta^2}\right\} \tag{A.33}$$

A_1 & A_2 are complex conjugates where

$A_1 = A + iB$
$A_2 = A - iB$

$$x(t) = e^{-\zeta\omega_n t}\left\{A\cos t\omega_n\sqrt{1-\zeta^2} + B\sin t\omega_n\sqrt{1-\zeta^2}\right\} \quad \text{(A.34)}$$

Now consider the initial conditions for which the initial displacement of the Periotest®/implant system is zero and the initial velocity is V shown

$$x(0) = 0$$
$$\dot{x}(0) = V \quad \text{(A.35)\&(A.36)}$$

respectively. By applying the (A.35) to (A.34) result in A=0 and (A.34) reduces to

$$x(t) = e^{-\zeta\omega_n t}\left\{B\sin t\omega_n\sqrt{1-\zeta^2}\right\}. \quad \text{(A.37)}$$

The equation describing the velocity of the Periotest®/implant system can be found by taking the time derivative of (A.37) which yields

$$\dot{x}(t) = B\left[-\zeta\omega_n e^{-\zeta\omega_n t}\sin\omega_n t\sqrt{1-\zeta^2} + e^{-\zeta\omega_n t}\cos\omega_n t\sqrt{1-\zeta^2}\left(\omega_n\sqrt{1-\zeta^2}\right)\right] \quad \text{(A.38)}$$

$$\dot{x}(0) = V = B\left[\zeta\omega_n(0) + \omega_n\sqrt{1-\zeta^2}\right] \quad \text{(A.39)}$$

$$B = \frac{V}{\omega_n\sqrt{1-\zeta^2}} \quad \text{(A.40)}$$

$$x(t) = \frac{V}{\omega_n\sqrt{1-\zeta^2}}e^{-\zeta\omega_n t}\sin\left(\omega_n t\sqrt{1-\zeta^2}\right) \quad \text{(A.41)}$$

$$\dot{x}(t) = \frac{V}{\sqrt{1-\zeta^2}}e^{-\zeta\omega_n t}\left[\cos\left(\omega_n t\sqrt{1-\zeta^2}\right)\left(\sqrt{1-\zeta^2}\right) - \zeta\sin\left(\omega_n t\sqrt{1-\zeta^2}\right)\right] \quad \text{(A.42)}$$

$$\ddot{x}(t) = \frac{-V\omega_n}{\sqrt{1-\zeta^2}}e^{-\zeta\omega_n t}\left[(1-2\zeta)\sin\left(\omega_n t\sqrt{1-\zeta^2}\right) - 2\zeta\left(\sqrt{1-\zeta^2}\right)\cos\left(\omega_n t\sqrt{1-\zeta^2}\right)\right] \quad \text{(A.43)}$$

Let

$$\cos\phi = 1 - 2\zeta$$
$$\sin\phi = 2\zeta\sqrt{1-\zeta^2} \qquad \text{(A.44) \& (A.45)}$$

$$\omega = \omega_n\sqrt{1-\zeta^2} \qquad \text{(A.46)}$$

$$\ddot{x}(t) = \frac{-V\omega_n}{\sqrt{1-\zeta^2}} e^{-\zeta\omega_n t}\sin(\omega_n t + \phi) \qquad \text{(A.47)}$$

Equating (A.44) & (A.45) yields

$$(\cos\phi)2\zeta\sqrt{1-\zeta^2} = 1 - 2\zeta(\sin\phi) \qquad \text{(A.48)}$$

$$\tan\phi = \frac{2\zeta\sqrt{1-\zeta^2}}{1-2\zeta} \qquad \text{(A.49)}$$

Consider the contact time where $\ddot{x}m_p = 0$ (just after separation) for (A.47)

$$\ddot{x}(t) = 0 = \frac{-V\omega_n}{\sqrt{1-\zeta^2}} e^{-\zeta\omega_n t}\sin(\omega_n t + \phi) \qquad \text{(A.50)}$$

In order for (A.50) to be satisfied

$$\sin(\omega t + \phi) = 0 \qquad \text{(A.51)}$$

$$t = \frac{n\pi}{\omega} - \frac{\phi}{\omega} \qquad \text{(A.52)}$$

Substituting (A.46) and (A.49) into (A.52) yields the equation for contact time

$$CT = \frac{1}{\omega_n\sqrt{1-\zeta^2}}\left[\pi - \tan^{-1}\frac{2\zeta\sqrt{1-\zeta^2}}{1-2\zeta^2}\right] \qquad \text{(A.53)}$$

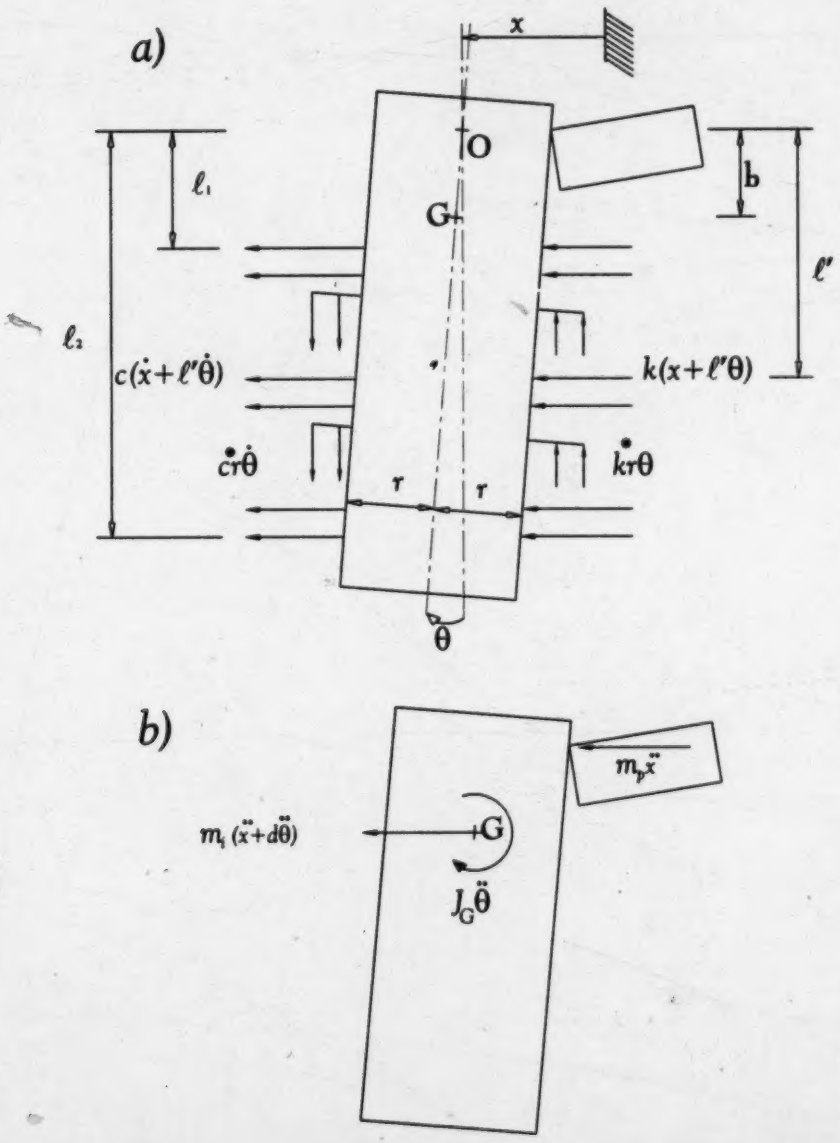

FIGURE A-1: a) Free Body Diagram and b) Mass Acceleration Diagram

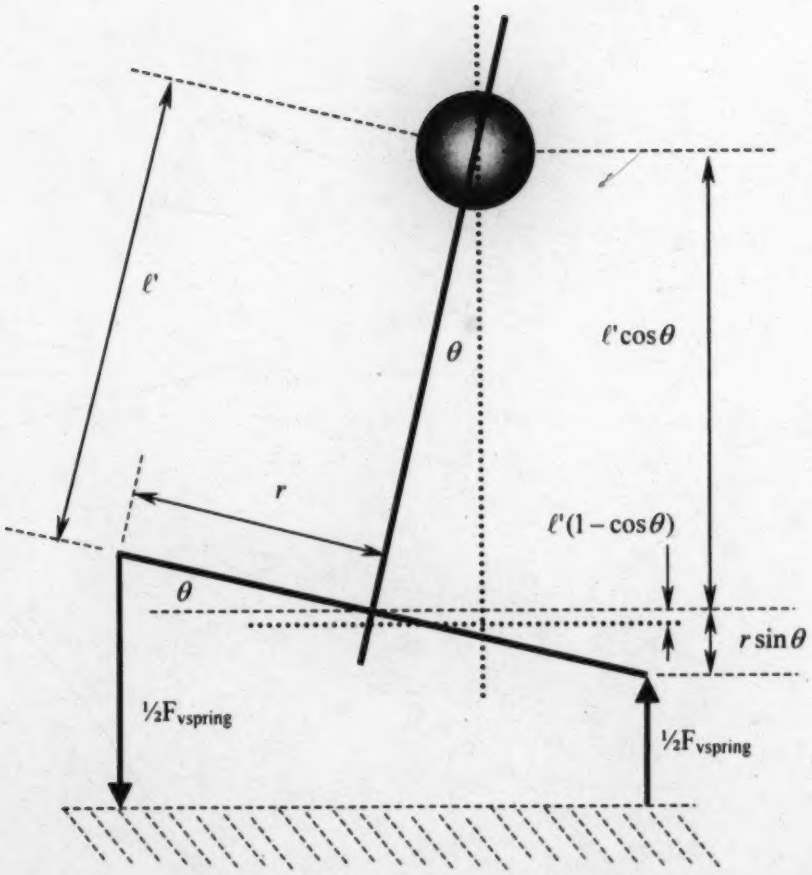

FIGURE A-2: Deflection of the System for Determining the Force in the Vertical Springs

Appendix B

In Vivo Data

This appendix contains the Periotest® data from the 11 BAHA® patients taking part in the *in vivo* study. Both the lateral and axial tests are shown for each patient over the course of the year long study.

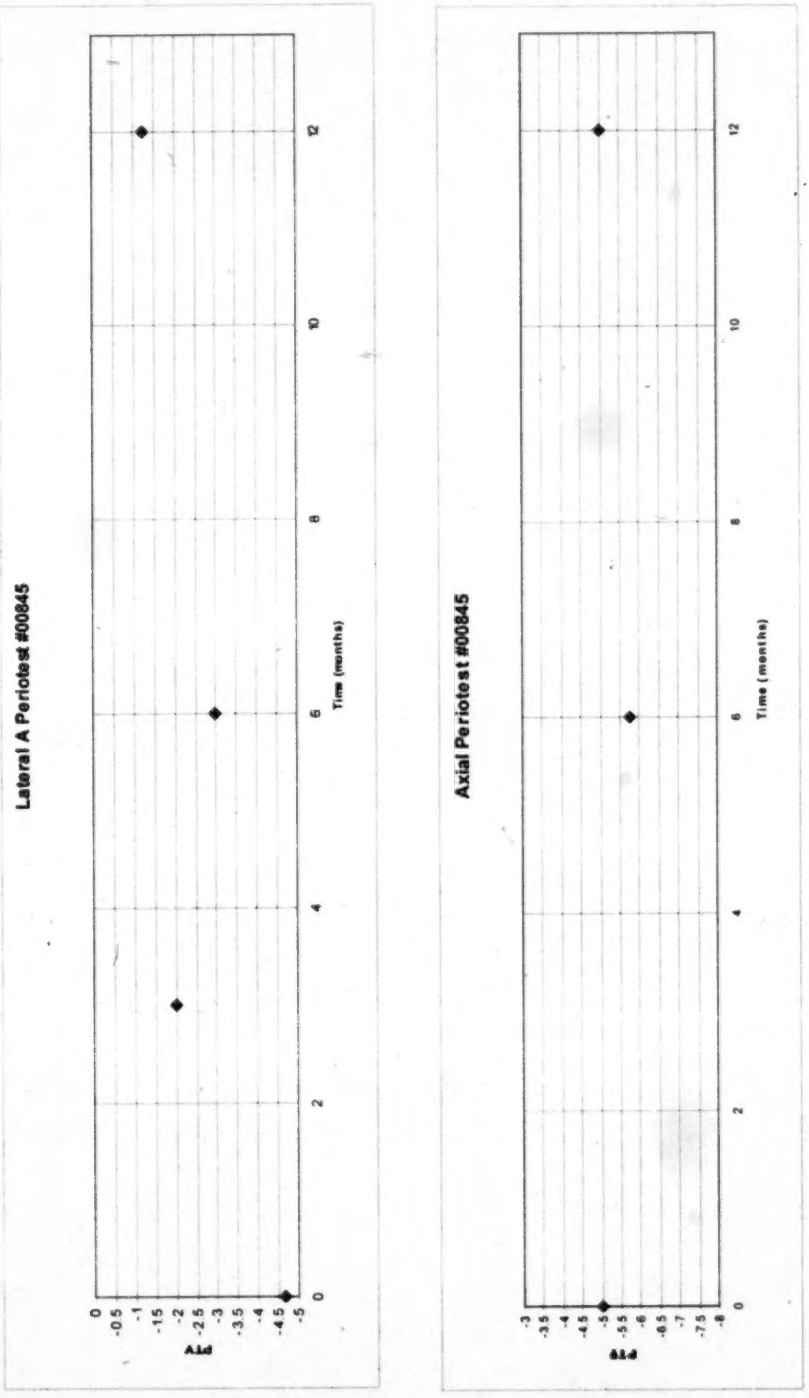

FIGURE B-1: *In Vivo* Testing Data for Patient #00845

FIGURE B-2: *In Vivo* Testing Data for Patient #00874

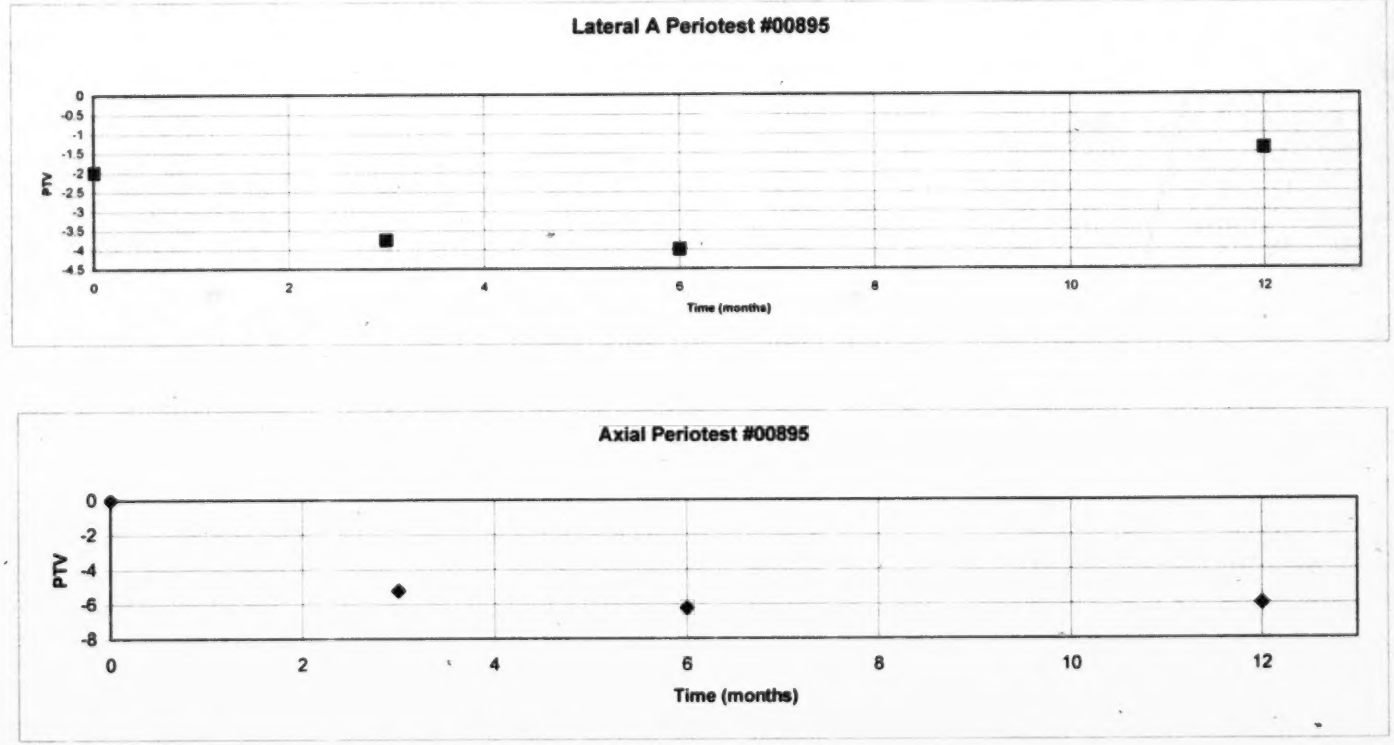

FIGURE B-3: *In Vivo* Testing Data for Patient #00895

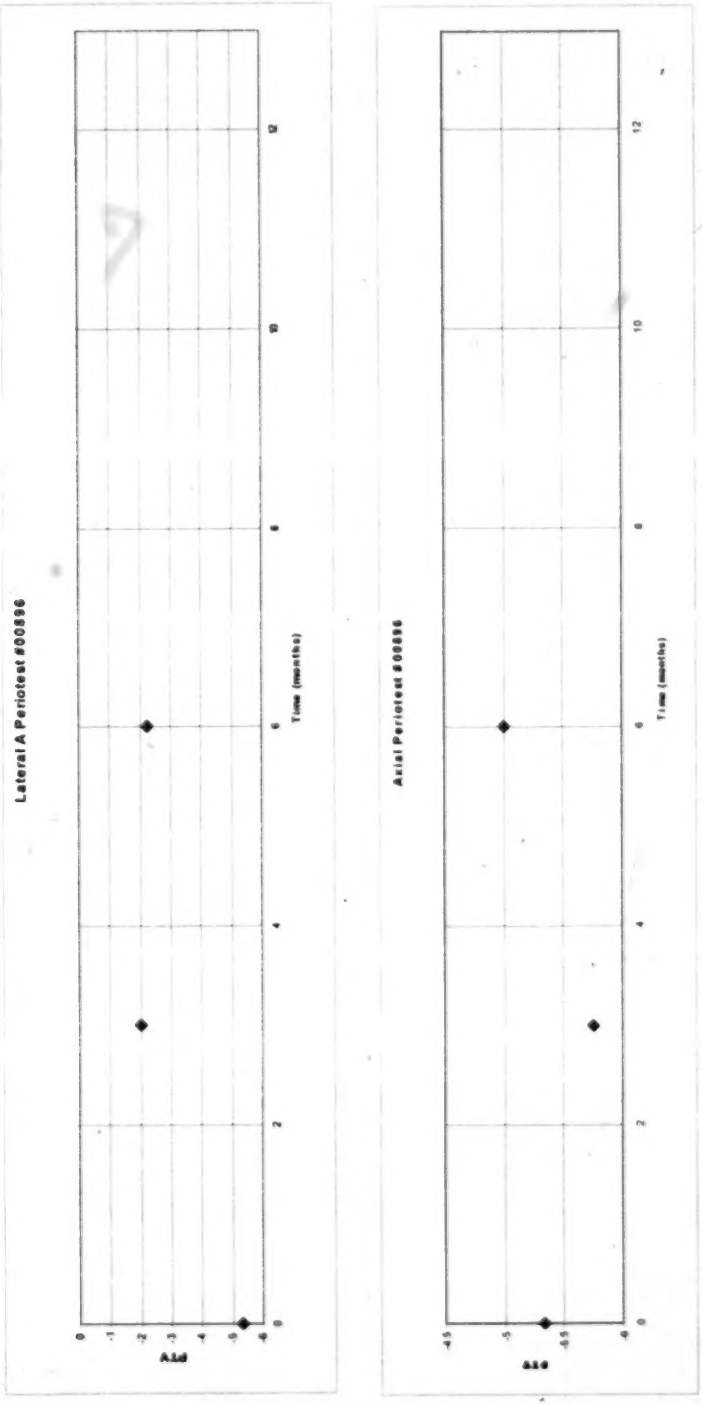

FIGURE B-4: *In Vivo* Testing Data for Patient #00896

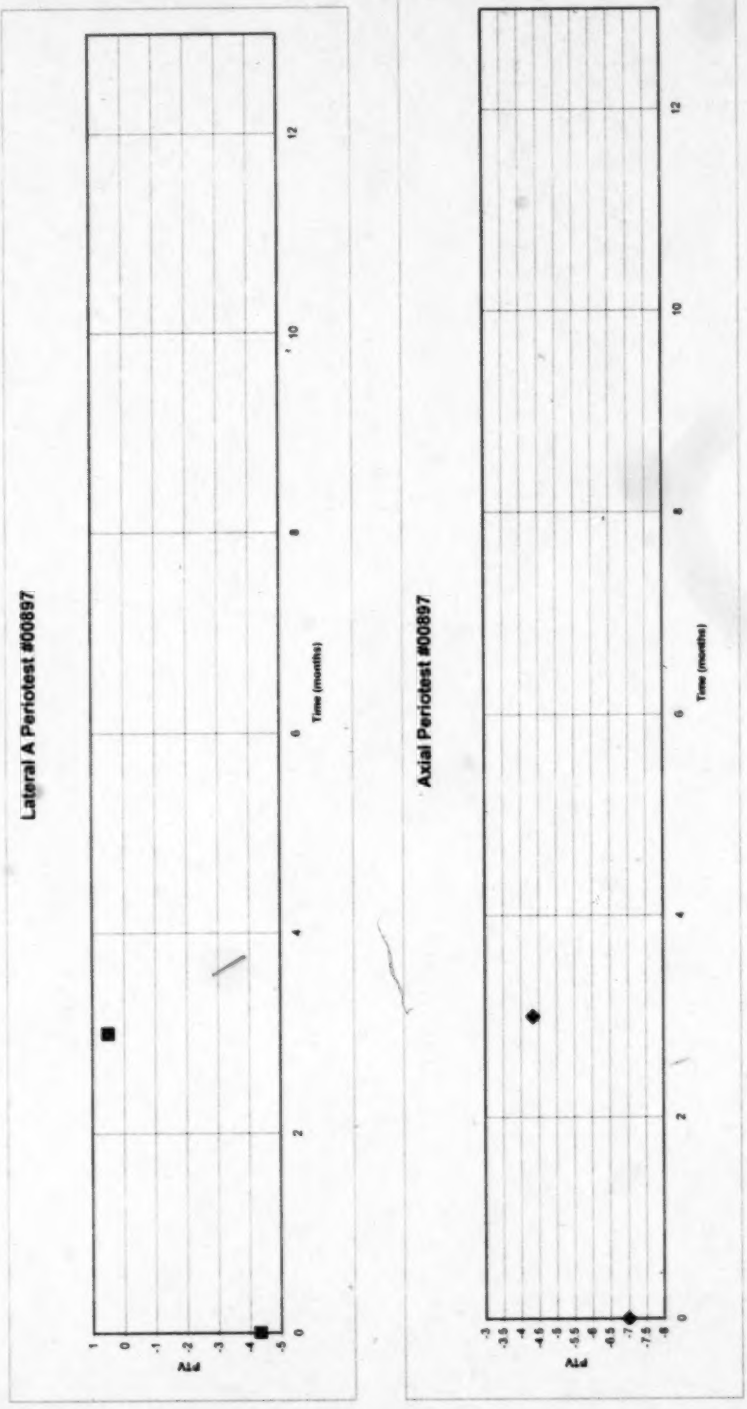

FIGURE B-5: *In Vivo* Testing Data for Patient #00897

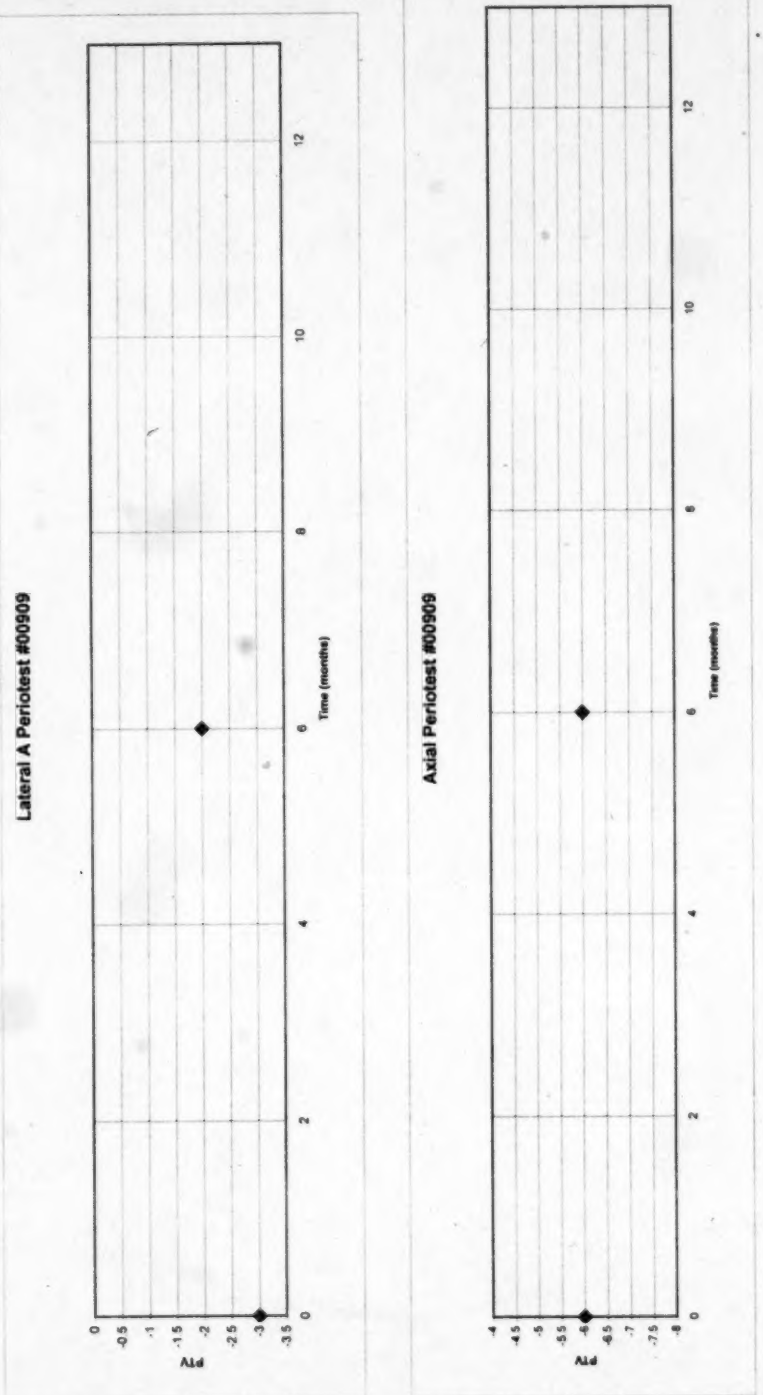

FIGURE B-6: *In Vivo* Testing Data for Patient #00909

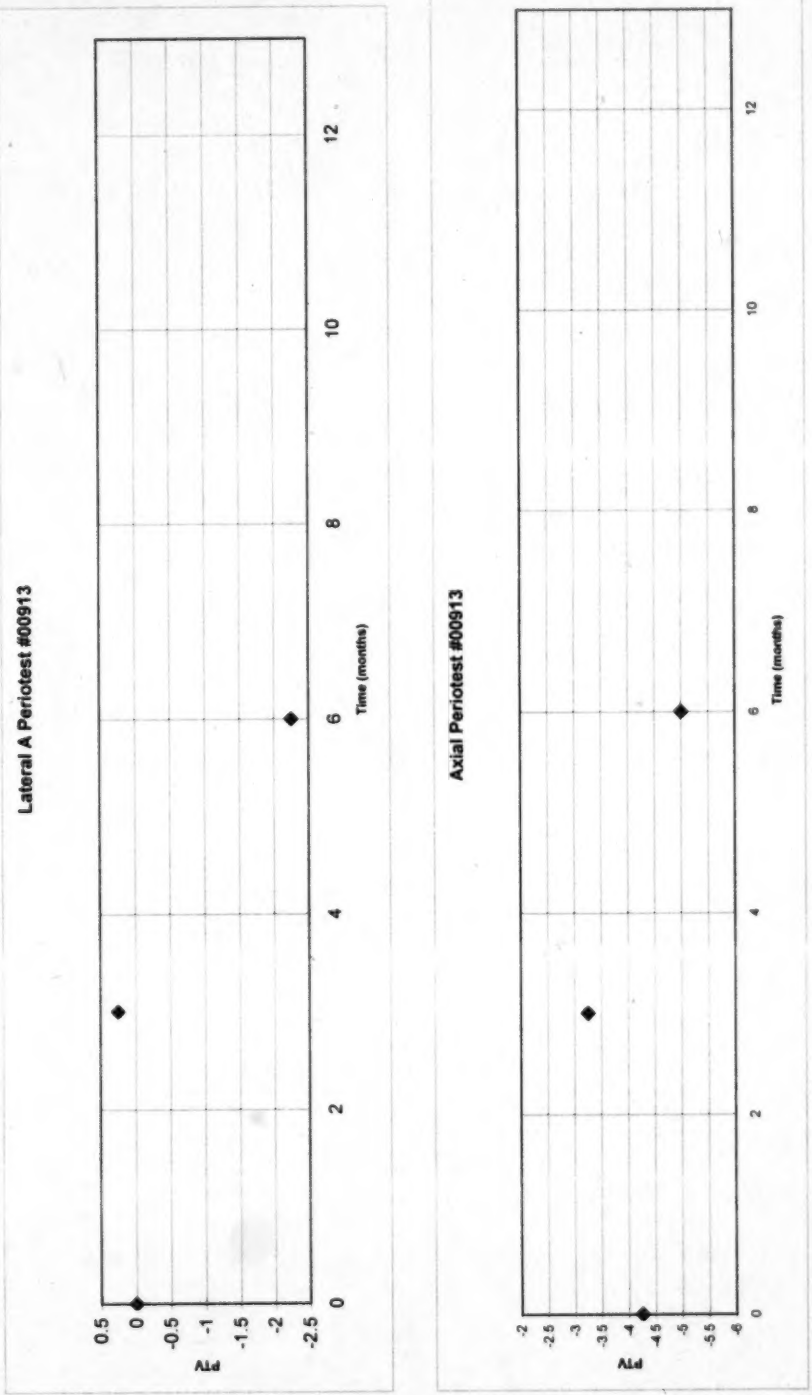

FIGURE B-7: *In Vivo* Testing Data for Patient #00913

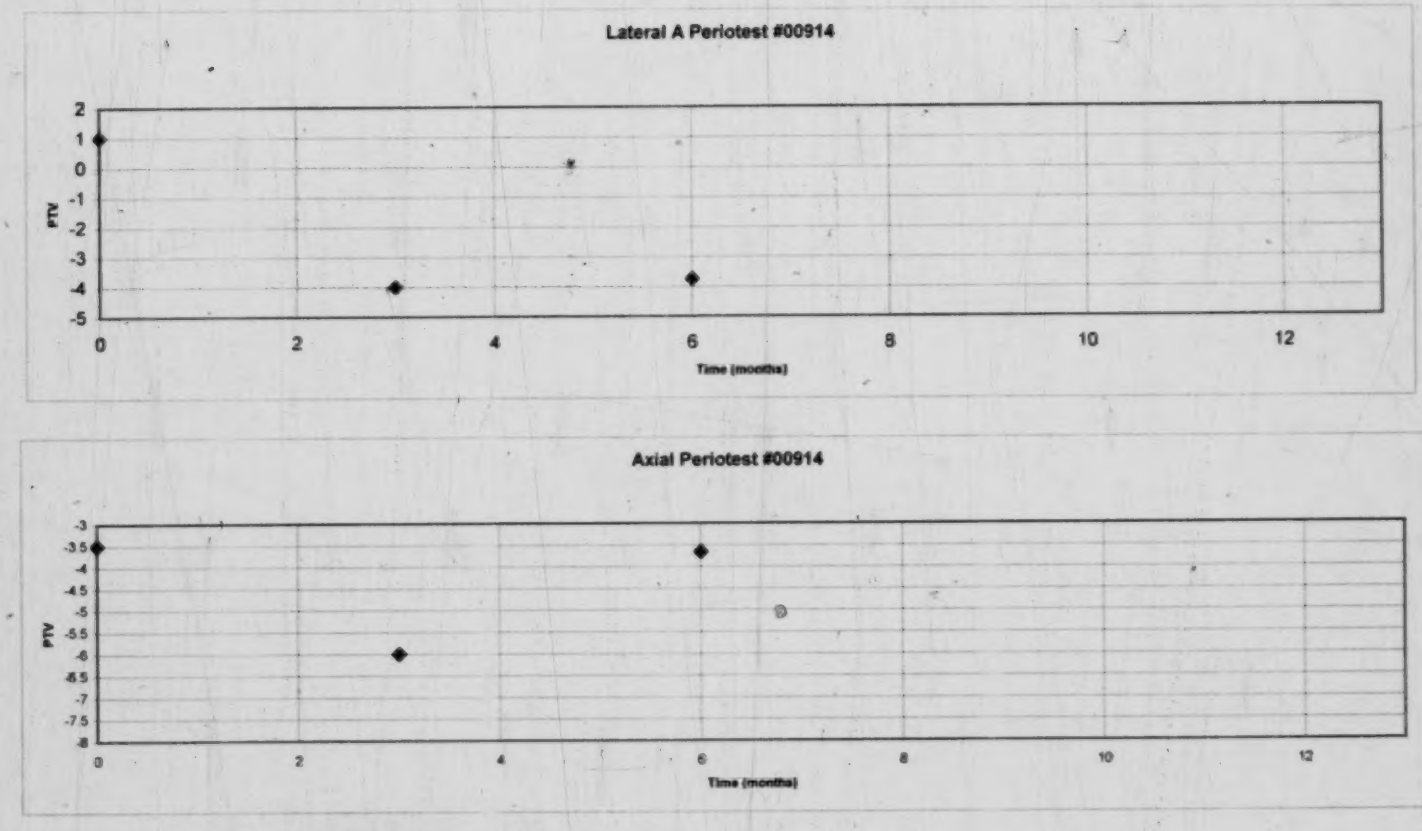

FIGURE B-8: *In Vivo* Testing Data for Patient #00914

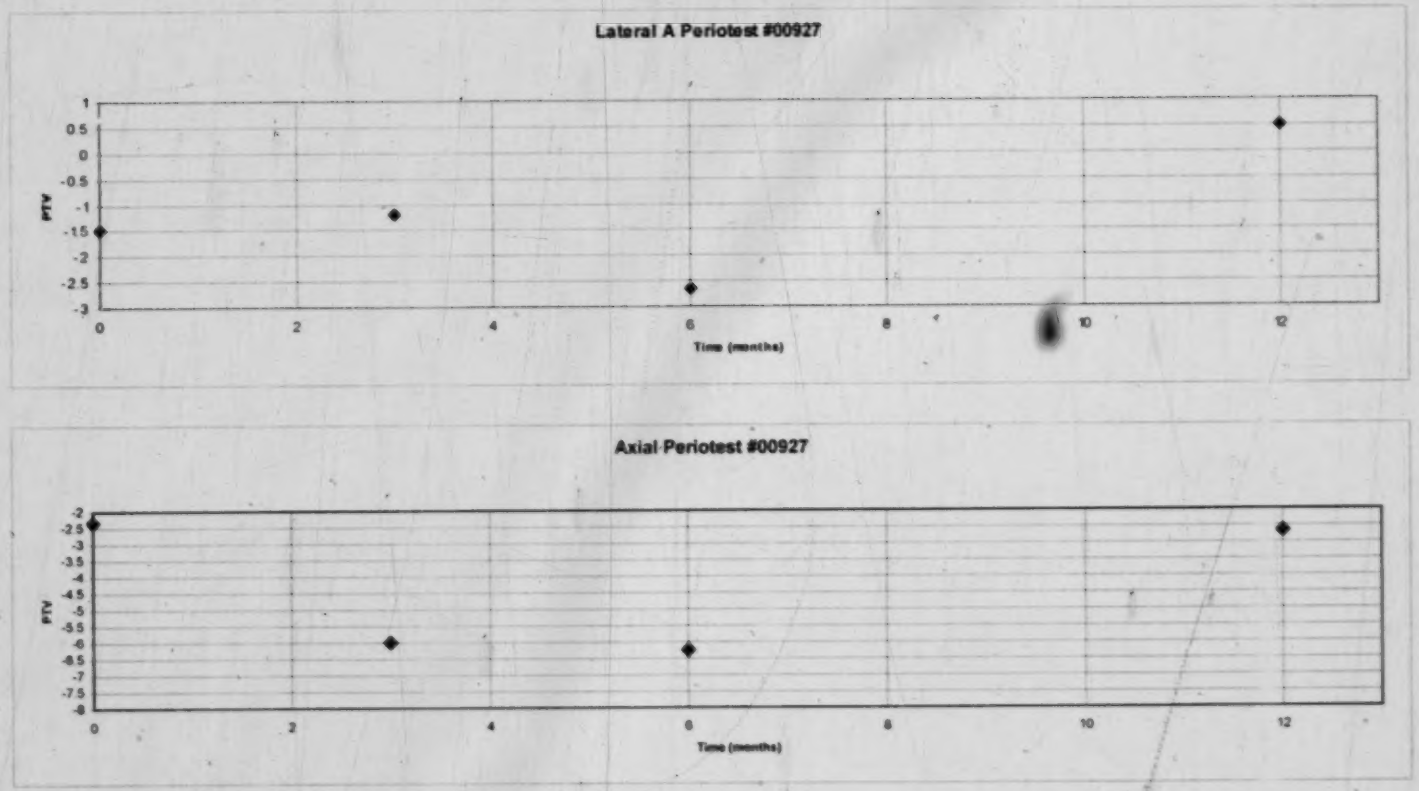

FIGURE B-9: *In Vivo* Testing Data for Patient #00927

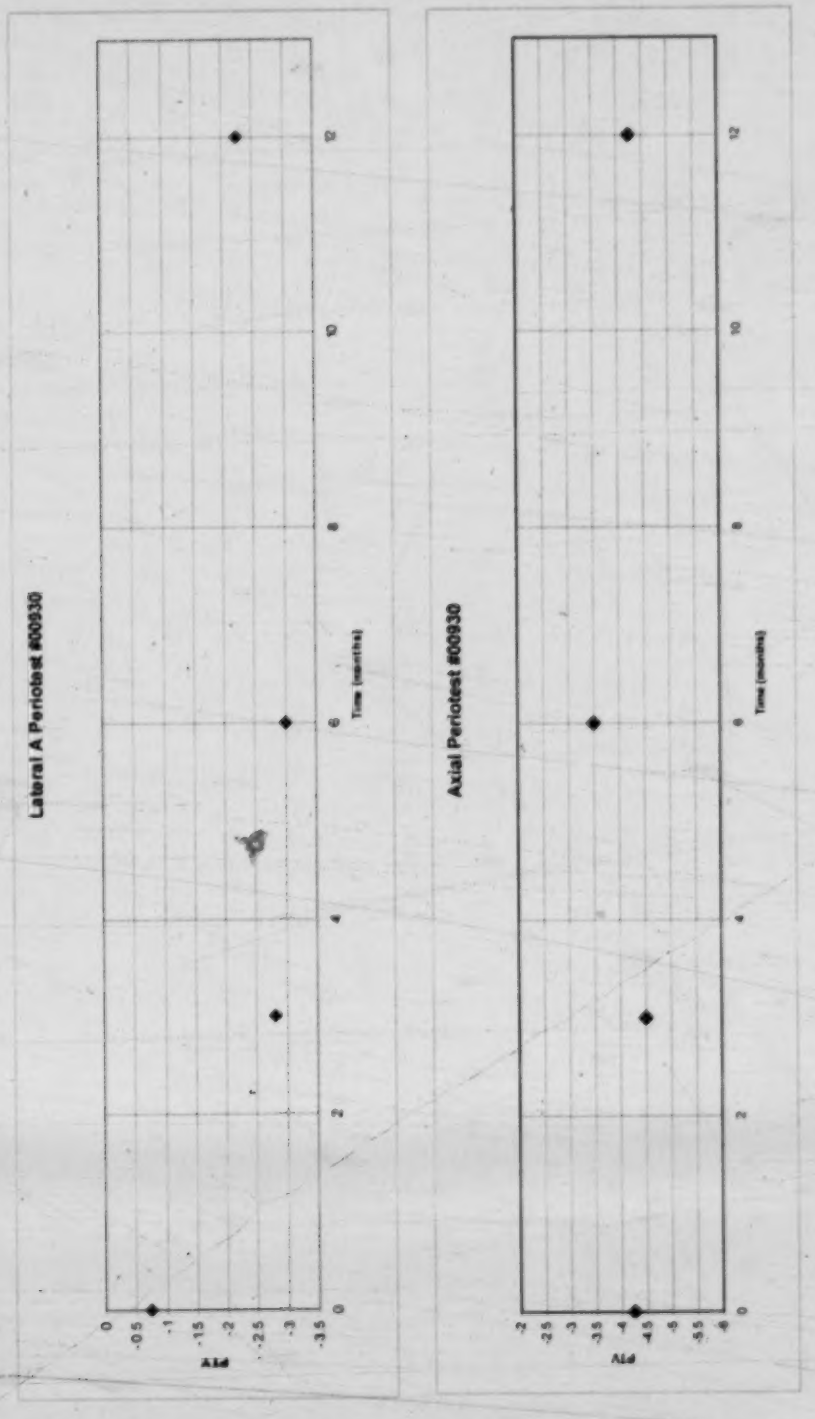

FIGURE B-10: *In Vivo* Testing Data for Patient #00930

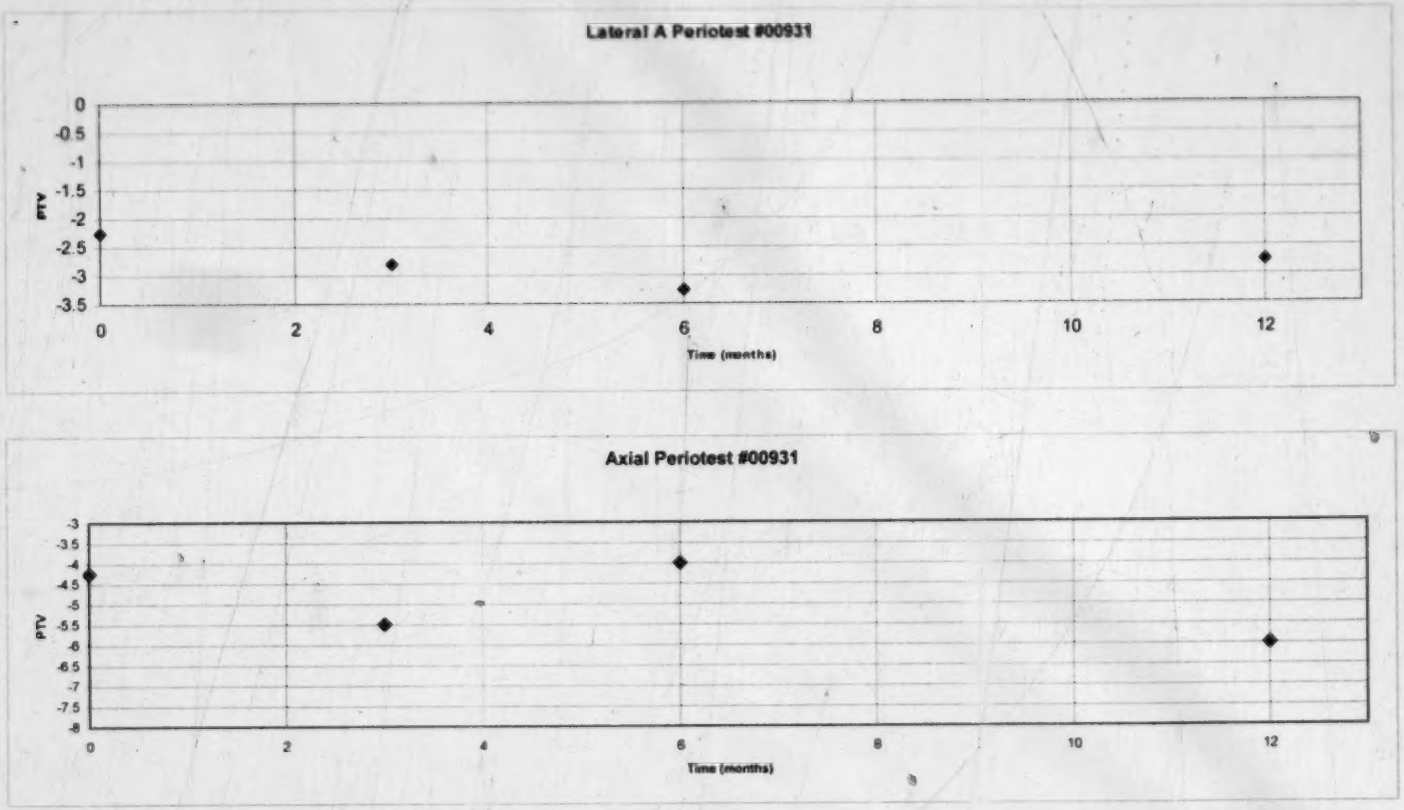

FIGURE B-11: *In Vivo* Testing Data for Patient #00931

Appendix C

Clinical Protocol for Periotest® Testing

It has been shown that slight variation in impact height can have a significant effect on the PTV due to the difficulty of impacting the same location. In addition, length of tissue/bone engagement has been shown to affect PTV especially when there is a variation around the periphery of the implant leading to different PTV for different striking positions. As a result, a clinical testing protocol for using the Periotest® device has been developed to produce repeatable results.

1) Torque abutment screws to the appropriate preload value.

2) The coronal rim of the abutment serves as the location of impact.

3) The Periotest® handpiece is to be held perpendicular to the long axis of the abutment with a slight angle (~5°).

4) The striking direction is maintained throughout the course of study.

5) The same abutment length used for Periotest® testing is maintained throughout the study.

6) If possible, measurements in an alternate striking direction may be taken as well as testing with the handpiece held in line with the long axis of the abutment.